2012

Quantifying Near-Bank Turbulence Through a Storm Event

Charles Z. Walburn
West Virginia University

Quantifying Near-Bank Turbulence Through a Storm Event

By

Charles Z. Walburn

Thesis submitted to the
Benjamin M. Statler College of Engineering and Mineral Resources
at
West Virginia University
in partial fulfillment of the requirements
for the degree of

Master of Science
in
Civil and Environmental Engineering

Dr. Leslie C. Hopkinson, Ph.D.
Dr. Donald D. Gray, Ph.D.
Dr. Nicolas P. Zegre, Ph.D.

Department of Civil and Environmental Engineering

Morgantown, West Virginia
2012

Keywords: Reynolds stress, streambank erosion, turbulence, acoustic Doppler velocimeter, acoustic Doppler current profiler

Abstract

Quantifying Near-Streambank Turbulence Through a Storm Event

Charles Z. Walburn

Sediment is a leading cause of water quality impairment for streams and rivers. Streambank erosion is a dominant source contributing to sediment pollution and there is a growing need for adopting management practices to reduce it. Bank retreat occurs from a combination of fluvial erosion, subaerial processes, and mass failure. Fluvial entrainment, initiated by near-boundary turbulence, is one of the main drivers of streambank retreat as it leads to unstable streambank geometries. This research characterized the turbulent structure of flow near the toe of a streambank throughout a storm event, at times of high shear stress. The specific objectives included designing and building a field mount to support in-stream velocimeters during high flow events, quantifying the distribution of Reynolds stresses and turbulent kinetic energy (TKE) through a storm hydrograph, and identifying the relationship between hydraulic radius and turbulent stresses.

Three-dimensional velocity was measured using a Sontek 16-MHz ADV (Field) and two-dimensional velocity was measured using a Sontek SL3000 (ADCP) at baseflow and through a storm hydrograph at an experimental cross-section (West Run in Morgantown, WV). Velocity was measured (2 min sample time at 25 Hz) and stream stage was recorded every seven minutes with the ADV throughout a 17 hour storm event. One time-averaged velocity measurement (5 min sample time, 1 Hz) and stream stage were recorded continuously throughout an 8 hour storm event using the ADCP. Physical stability was monitored by measuring channel geometry, grain roughness, and vegetation parameters (i.e. location, size, and density) before and after each storm event. Reynolds stresses, turbulent kinetic energy, and turbulence intensities were calculated for each velocity time series, resulting in a time distribution of shear stress and turbulence characteristics.

This research resulted in the development of methods for ADV and ADCP deployment throughout storm events, including the use of two custom fabricated mounts. The study also found that TKE increased with an increase in stage height, while Reynolds stresses indicated no linear trend. Applied shear stress estimated by average boundary shear stress was found to be roughly 18 to 43 times greater than applied shear stress estimated by turbulence statistics, which may alter the ability of models to predict erosion depending on the method used. Finally, a comparison of the ADV and ADCP indicated that the ADV shows higher potential for obtaining near-bank velocity measurements and estimating local applied shear stress. Ultimately, these results will provide information on current instrumentation and methods used in the field and will provide information on the distribution of streambank erosion potential throughout storm events.

Acknowledgments

It is a great pleasure to thank the many people who have helped me successfully complete my thesis. I am sincerely and heartily grateful to my advisor, Dr. Leslie Hopkinson, for the support and guidance she has given me throughout this process. I am sure it would not have been possible without her invaluable knowledge and continuous determination to help me succeed. With her everlasting encouragement, sound advice, and great ideas, Dr. Hopkinson has provided me with an exceptionally rewarding experience.

I would like to thank Dr. Donald D. Gray and Dr. Nicolas P. Zegre for being on my defense committee and for providing me with the very best education, wise advice, and kind assistance throughout my undergraduate and graduate studies. I owe sincere and earnest thankfulness to Will Ravenscroft and Karen Busby for kindly allowing me to borrow equipment and use their property for my research. I would like to show my gratitude to Dr. Darrell R. Dean, Jr for the valuable time that he spent teaching me how to use the survey equipment and for the kind advice and encouragement. I owe a deep gratitude to all of the educators who made learning fun and provided me with the right tools and knowledge to grow throughout my experience at West Virginia University.

I genuinely would like to thank all of my office buddies, especially Aaron Streets and Sean Abel, for their help with my research, their camaraderie and support throughout tough classes, and for all of the laughs that we shared. I wish to thank my loving girlfriend, Emily Kisner, for her positive encouragement through the difficult times and for always believing in me. I would also like to thank my entire family, especially my sisters, Shelby and Brooke, my grandparents, aunts, uncles, and cousins who provided me with caring support.

Lastly, and most importantly, I would like to dedicate this thesis to my parents, Charles M. Walburn and Susan R. Walburn for instilling in me the importance of a good education. They provided me with unconditional love, valuable knowledge, and limitless support my entire life. To them I owe my sincere and absolute gratitude.

Table of Contents

List of Figures

List of Tables

1.0 Introduction

1.1 Background

The U.S. has over 3.5 million miles of streams. The quality and unique properties of these systems are affected each year by natural sources, agricultural activities, hydromodifications (e.g., dams, channelization, and water diversions) and other various human activities. Sediment is a leading cause of water quality impairment for streams and rivers, polluting roughly 14% of declared impaired stream miles (USEPA, 2009). The movement of sediment causes damage to irrigation systems, navigation lanes, aquatic ecosystems, water treatment processes, and reduces the aesthetic and recreational value of rivers and streams. It is estimated that damages resulting from sediment in North America cost more than $16 billion annually (Osterkamp et al., 1998). In certain watersheds, streambank erosion has been found to contribute greater than 90% of the total sediment yield (Simon and Rinaldi, 2000; Fraley et al., 2009; Willett et al., 2012). Willett et al. (2012) note that streambank erosion is a dominant source contributing to sediment pollution and expresses the importance of adopting management practices to reduce streambank erosion.

Bank retreat occurs from a combination of fluvial erosion, subaerial processes, and mass failure (Thorne, 1982; 1990). Hydrology, geomorphology, and hydraulic characteristics can provide a better understanding of the dominant processes (Lawler et al., 1997). Because bank retreat is attributed to a combination of processes, bank protection plans and measures are vital and must identify the causes and effects of bank retreat (Thorne, 1982; Julien, 2002). This study focuses on the fluvial entrainment component of bank retreat. This process is often quantified by

the excess shear stress equation which states that the erosion rate is proportional to the difference between the applied and critical shear stress (Partheniades, 1965). The applied shear stress is often estimated based on the flow depth and bed slope, but research shows that local scour is likely due to turbulence fluctuations greater than the mean (Sumer et al., 2003; Diplas et al., 2008, Celik et al., 2010); therefore, near boundary turbulence statistics (e.g. Reynolds stress and turbulent kinetic energy) are also used to estimate turbulent shear stress.

1.2 Goals and Objectives

This research characterizes the turbulence structure of flow near the toe of a streambank throughout a storm event, during times of high shear stress. The specific objectives include the following:

1. Design and build a field mount to support in-stream velocimeters during high flow events.
2. Quantify the distribution of Reynolds stresses and turbulent kinetic energy (TKE) throughout a storm hydrograph.
3. Identify the relationship between hydraulic radius and turbulent stresses.

The results from this study provide information about the distribution of streambank erosion potential throughout storm events.

1.3 Study Design

Velocity and stream stage were measured at baseflow and throughout a storm event at an experimental cross-section (West Run in Morgantown, WV) using a Sontek 16-MHz ADV and a

Sontek SL3000. Physical stability of the cross-section was monitored by measuring channel geometry, grain roughness, and vegetation parameters (i.e. location, size, and density) before and after each storm event deployment. Turbulent kinetic energy, turbulence intensities, and Reynolds stresses were calculated to estimate the average boundary shear stress near the toe of a stream channel.

2.0 Literature Review

2.1 Streambank Retreat

Bank retreat occurs from a combination of fluvial erosion, subaerial processes, and mass failure (Thorne, 1982; 1990). Fluvial erosion results in the detachment of streambank particles, which leads to geotechnical instability. This instability can lead to a more rapid and sizeable retreat (Thorne, 1990). Hydrology, geomorphology, and hydraulic characteristics can provide a better understanding of the dominant processes involved in streambank retreat (Lawler et al., 1997). Because bank retreat is attributed to a combination of processes, there is a vital need to further understand these processes in order to develop and implement bank protection plans (Thorne, 1982; Julien, 2002). While the main focus of this study is fluvial erosion, the three processes contributing to streambank retreat are discussed in the following sections.

2.1.1 Subaerial Processes

Climate-driven processes known as subaerial processes contribute to bank retreat. Subaerial processes (e.g. shrink-swell and freeze-thaw processes) are usually recognized as "preparatory processes" that reduce the strength of the soil and allow fluvial erosion to more easily occur at the stream bank (Wynn and Mostaghimi, 2006a). These processes are independent of stream flow and are influenced by bank composition (Thorne, 1982). In certain events subaerial processes can directly deliver soil to a stream through soil desiccation or freeze-thaw cycling (Wynn and Mostaghimi, 2006b). The removal of fines through the movement of soil-water reduces soil cohesion and weakens the bank (Thorne, 1982). Inner bank strength can be reduced by soil moisture conditions (Thorne, 1982; Lawler et al., 1997). After extended

precipitation or snowmelt, soil strength is weakened by the resulting positive pore water pressure in poorly drained banks (Thorne, 1982). Vegetation helps to regulate stream bank soil moisture and temperature regimes by reducing solar exposure that can lead to an increase in surface evapotranspiration. Dense herbaceous vegetation can act as insulation for the streambank which, in turn, reduces diurnal fluctuations in soil temperature (Wynn and Mostaghimi, 2006b). Couper (2003) found that river banks with a high silt–clay content are the most susceptible to erosion by subaerial processes. Results from Wynn et al. (2008) also indicate that subaerial processes have a direct link to significant changes in the resistance of streambank soils to fluvial erosion.

Streambank soils are weakened by swelling and shrinking which result from becoming saturated and dried. This wet-dry cycling can cause fissures and cracks in the bank, making the bank more susceptible to erosion. The increased weight of the saturated soil resulting can also weaken bank strength (Thorne, 1982). Wynn et al. (2008) supported these finding by noting that soil erodibility (k_d) and critical shear stress (τ_c) of a streambank may vary seasonally due to rainfall fluctuations. Prosser et al. (2000) found that the desiccation of clays during the summer months and freeze-thaw cycling throughout the winter months were the primary subaerial processes that lead to soil erosion.

Water that freezes in the pores of streambank material also causes cracks that lead to a weakening of the bank material (Thorne, 1982). Recent studies have indicated that freeze-thaw cycling may contribute more to bank erosion than wetting-drying cycles (Couper and Maddock, 2001; Couper 2003). Additionally, Wynn et al. (2008) found a strong correlation between the variation of soil erodibility and the number of freeze-thaw cycles. The impact of vegetation on stream bank erosion due to subaerial processes is generally governed by the susceptibility of the soil to damage generated from freeze-thaw or wet-dry cycling. Recent studies have indicated that

subaerial processes mainly act on the upper portion of the stream bank due to thermal and moisture regulation by the stream, while hydraulic shear stresses and fluvial entrainment are greatest at the toe of the bank (Wynn and Mostaghimi, 2006b). Couper (2003) refers to this "vertical zoning".

2.1.2 Fluvial Entrainment

Flowing water in an alluvial channel exerts shear stresses (drag and lift forces on the boundaries) resulting in the detachment and entrainment surface particles (Thorne, 1982; 1998). For the boundary sediment to remain in place, the sediment must supply an internally derived resisting force that can counter-act the erosive forces applied by the flow (Thorne, 1998). When the bank material does not exert an equal and opposite force, fluvial scour occurs, and the material is transported downstream (Thorne, 1982; Lawler et al., 1997). Subaerial processes increase the rate of erosion caused by fluvial entrainment by weakening the soil (Lawler et. al., 1997). Fluvial entrainment occurs with both cohesive and non-cohesive banks in nature. With cohesive banks, aggregates are entrained in the flow. In the case of non-cohesive banks, individual soil particles are entrained in the flow (Lawler et. al, 1997).

Due to the variation in particle shapes and sizes, gravel-bed material can become packed and interlocked into intricate structures (Lawler et al., 1997). The infiltration of fine particles into the gravel-bed matrix can create as strong cementation effect. Field studies (Reid and Frostick, 1984; Reid et al., 1985) have shown that little sediment transport may occur during the rising limb of a storm hydrograph for the case of a stream that has had an extended period of storm inactivity. Conversely, the research notes that when flooding events occur consecutively,

the bed-material may remain loose and be more susceptible to fluvial entrainment on the rising limb of the storm hydrograph.

Factors that affect streambank failure include hydraulic parameters such as the magnitude of discharge, velocity, duration of the discharge, and the applied shear-stress magnitude and orientation. Bank erosion processes share a direct link to the lateral migration of alluvial channels. Flowing water directly affects bank erosion by applying active degrading forces which are resisted by passive forces of the bank material. This process results in a decrease in stability of sediment particles which can cause degradation of the streambank. Scouring at the toe of the streambank alters the thalweg location which can result in an increased steepness of the streambank (Julien, 2002).

The excess shear stress equation, initially proposed by Partheniades (1965), relates streambank erosion rate to the difference between the applied shear stress (τ_a) and the soil critical shear stress (τ_c). The equation predicts the erosion rate of fine grain soils due to scour and is expressed as follows (Partheniades, 1965; Hanson and Simon, 2001):

$$\varepsilon = k_d(\tau_a - \tau_c)^a \quad (1)$$

where ε is the erosion rate (m/s), k_d is the erodibility coefficient ($m^3/N{\cdot}s$), a is an exponent assumed to be 1, τ_a is the applied shear stress on the soil boundary (Pa), and τ_c is the critical shear stress (Pa). To initiate erosion, the applied shear stress must be greater than the critical shear stress (Equation 1; Hanson and Simon, 2001). The excess shear stress equation is used to predict fluvial erosion in the Bank Stability and Toe Erosion Model (BSTEM) (Midgley et al., 2012).

The parameters k_d and τ_c are functions of soil properties and must be estimated or measured. The critical shear stress is defined as the stress at which soil particles are entrained (Osman and Thorne, 1988). There are several methods used to determine τ_c. The median particle diameter of the soil is typically used to estimate τ_c for non-cohesive soils (Midgley et al., 2012). Analytical procedures based on the diffusion principles of a submerged circular jet were developed by Hanson and Cook (1997) to determine k_d and τ_c *in situ*. Critical shear stress can also be calculated in flume studies (Smerdon and Beasley, 1961; Hanson et al., 1999; Papanicolaou et al., 2007), estimated based on soil characteristics (Smerdon and Beasley, 1961), or assumed to be zero (Hanson et al., 1999).

The erosion of fine grained sediments can be attributed to many factors such as soil structure, clay content and type, and soil moisture content, which makes k_d and τ_c difficult to quantify (Grissinger, 1982; Rinaldi et al., 2008). Hanson (1990) developed an *in situ* method to measure k_d and τ_c using a submerged jet test device. Clark and Wynn (2007) recommended τ_c be measured *in situ* based on a comparison of empirical and field methods to estimate the parameter.

The soil erodibility coefficient, k_d, is used to describe the rate that soil particles are detached, once erosion is initiated (Hanson et al., 2002). Hanson and Simon (2001) determined that k_d can be estimated as a function of τ_c using the following equation:

$$k_d = 0.2\tau_c^{-0.5} \quad (2)$$

Osman and Thorne (1988) developed an empirical method for estimating the initial rate of soil erosion, if τ_c could be determined, using the following relationship:

$$R = 223 \times 10^{-4} \tau_c e^{-0.13\tau_c} \quad (3)$$

where R is the initial rate of soil erosion (gm/cm^{2}·min). Clark and Wynn (2007) analyzed the empirical methods used to estimate soil erodibility (Hanson and Simon, 2001; Osman and Thorne, 1988) and found that the empirical methods yielded similar k_d values. However, the k_d values from the empirical methods were generally two orders of magnitude smaller than k_d values from jet test measurements. Clark and Wynn (2007) recommend field validation of the empirical methods over a range of soil types to develop methods of estimating k_d.

Applied shear stress is calculated using both direct and indirect methods. Direct measurements of shear stress are generally only applicable in laboratory flumes (Bhowmik, 1982; Hopkinson and Wynn-Thompson, 2012). The parameter τ_a is commonly calculated based on channel slope and flow depth with the average boundary shear stress equation (Chang, 2002):

$$\tau_a = \gamma_w R_h S \quad (4)$$

where γ_w is the specific weight of water (N/m^{3}), R_h is the hydraulic radius of the channel (m), and S is the water surface slope, equal to channel bed slope in assumed uniform flow (Bhowmik, 1982; Chang, 2002). Research shows that erosion is potentially attributed to turbulence fluctuations greater than the mean (Sumer et al., 2003; Diplas et al., 2008, Celik et al., 2010); therefore, near boundary turbulence statistics (Reynolds stress and turbulent kinetic energy) are used to estimate turbulent shear stress. Turbulent kinetic energy (TKE) has been used to

represent turbulent shear stress using the following relationship that was developed in tidal systems (Soulsby, 1983):

$$\tau = 0.19 * TKE \tag{5}$$

where τ is the local applied shear stress (N/m^2) and turbulent kinetic energy (TKE) is defined by the following equation (Biron et al., 2004):

$$TKE = \rho 0.5(\overline{u'^2} + \overline{v'^2} + \overline{w'^2}) \tag{6}$$

where, ρ is the water density (kg/m^3), and u', v', and w' represent the instantaneous velocity fluctuations away from the time averaged velocity for each component in the downstream (u), lateral (v), and vertical (w) directions (m/s). Daniels and Rhoads (2004) used the TKE method to estimate near-bed shear stresses in a meander bend of a stream. However, Hopkinson and Wynn-Thompson, (2012) suggest that this method might not be the best for stream systems with large roughness.

Near-boundary Reynolds stresses are also used to estimate the applied shear stress (Nepf, 2012). The lateral (τ_{uv}) and vertical (τ_{uw}) Reynolds stress components (Pa) are defined by the following equations (Schlichting and Gersten, 2000):

$$\tau_{uv} = -\rho\overline{u'v'} \tag{7}$$

$$\tau_{uw} = -\rho\overline{u'w'} \tag{8}$$

The lateral Reynolds stress (τ_{uv}) quantifies the lateral momentum exchange and is calculated using of the downstream and lateral velocity fluctuations (Equation 7). The vertical Reynolds stress (τ_{uw}) quantifies the vertical momentum exchange and is calculated with the downstream and vertical velocity fluctuations (Equation 8).

2.1.3 Streambank Failure:

Streambank failure occurs when the mechanical strength of the bank material is overcome by gravitational forces in response to geotechnical instability (Lawler et al., 1997). The type of failure depends on the geotechnical properties of the bank material, bank geometry, and the bank stratigraphy (Thorne, 1990). Streambank failure occurs differently for non-cohesive, cohesive, and stratified banks (Thorne, 1990; Lawler et al., 1997; Julien, 2002). Flood events are identified as one of the major causes of channel geometry changes through bank erosion (Julien, 2002).

There are three failure modes that are typical for alluvial rivers. In the case of non-cohesive granular material, grain removal at the toe of the outer bank prompts the downward movement of the bank material when the angle of the bank exceeds the angle of repose of the material. With cohesive bank materials, rotational failure is common and the occurrence of tension cracks may help to increase the bank erosion process. The third failure mode occurs in alluvial streams flowing in stratified deposits. There is a mobilization of the underlying non-cohesive material which leaves the overlying cohesive material unsupported and more susceptible to tension cracks and mass failure.

Julian and Torres (2006), examining the hydraulic erosion of cohesive riverbanks, found that all of the bank failures occurring in the river channel were directly attributed to hydraulic undercutting. The results from the study also suggest that peak flow intensities have a direct link

to hydraulic erosion of cohesive riverbanks. Wynn and Mostaghimi (2006a) note that riparian vegetation can have an important stabilizing effect on a streambank by reducing soil erosion through root reinforcement. Wynn et al. (2004) suggested that riparian forests may provide better streambank erosion protection than herbaceous riparian buffers due to a better distribution and a greater amount of long, large diameter roots.

2.2 Measuring near-boundary turbulence

2.2.1 Instrumentation: ADV and ADCP

Acoustic Doppler velocimeters (ADV) measure high frequency, three-dimensional velocity with high accuracy over a range of flows. Voulgaris and Trowbridge (1998) evaluated the ability of using an ADV for turbulence measurements in a flume study. The study concluded that the ADV can measure mean velocity and Reynolds stress within 1% of the estimated true value. The analysis also showed that turbulence intensity of the vertical component of velocity can be determined accurately by the ADV, while the downstream component of velocity may suffer from a large noise term due to the geometry of the probe (Voulgaris and Trowbridge, 1998).

Acoustic Doppler Current Profilers (ADCP) have the ability to measure three-dimensional or two- dimensional velocity profiles with high accuracy over a range of flows and applications using transducers and electronics. ADCPs are often used in river and streamflow applications, current monitoring in channels and estuaries, and discharge measurements. Shields and Rigby (2005) noted that the use of ADCPs have great potential for studying river characteristic at the reach scale. It is also noted that specific guidelines for ADCP settings and

configurations must be developed for a range of different riverine site conditions (Shields and Rigby, 2005).

A Sontek 16-MHz acoustic Doppler velocimeter (ADV) Field was used in this study to measure velocity and stage throughout a storm event in this study. The hardware for the Sontek 16-MHz ADV Field is composed of two main components: signal processing hardware and probe hardware. The signal processing hardware is contained in a submersible canister. The signal processing hardware performs the signal generation and processing required for the ADV to take velocity measurements. The probe hardware consists of a signal conditioning module and a cable mounted acoustic sensor. The acoustic sensor contains three acoustic receivers and one acoustic transmitter which take velocity measurements. Velocity is measured at a distance of 5 cm from the acoustic transmitter with a control volume of 0.09 cm^3 (Sontek/ YSI, 2000)

A Sontek SL3000 was used in this study to measure velocity and stream stage throughout storm events. The SL3000 is an acoustic Doppler current profiler that measures water velocity, stage, and total water volumetric flowrate in a horizontal facing orientation. The SL3000 has three acoustic beams including one beam that points in the positive vertical direction, and the other two that are directed upstream and downstream at a 25° angle. The upward-looking beam measures stream stage, while the two slanted horizontal beams measure the two-dimensional water velocity profile (Sontek/ YSI, 2009).

2.2.2 Field studies of near-boundary turbulence

Rominger (2010) performed a study at the Outdoor StreamLab in Minneapolis on the effects of added vegetation on sand bar stability and stream hydrodynamics. The study utilized a concrete headbox that supplied water to the Outdoor StreamLab stream from the Mississippi

River. The Outdoor StreamLab contains three meander bends with riffles that were constructed in the straight sections to imitate a natural stream. A Nortek Vectrino ADV was used in this study to measure three-dimensional velocity of the stream in the (*u*, *v*, and *w*) directions. Velocity was measured at 10 points along the horizontal y-axis and at multiple locations in the z-axis at each of the cross-sections. Bank-full flood events were created and controlled on a weekly basis throughout the study and lasted approximately 9 hours with a constant flow rate of 208 ± 5 L/s. The Nortek ADV recorded velocity measurements in an interval of 120-240 s at 25 Hz at each point. Rominger (2010) also noted that the velocity data were filtered to remove any data points containing a low correlation or low signal-to-noise ratio. Channel geometry surveys were performed throughout the study to monitor changes in the stream geometry. The experiment examined the implications for erosion by using the Shields parameter (Rominger, 2010).

The results from this study show that the stream bed geometry and the flow field were drastically changed after the addition of the vegetation. The addition of the vegetation changed the secondary circulation of flow significantly enough to cut off a source of water and sediment to the point bar. Sediment deposition occurred throughout the vegetation located near the inner stream bank which verifies previous research that notes the positive feedback that vegetation has in the stabilization of land forms (Rominger, 2010).

Daniels and Rhoads (2004) performed a study to explore the effect of a partial large woody debris (LWD) dam on the spatial pattern of turbulent kinetic energy and shear stress in a meander bend of a stream in East Central Illinois, USA. Three-dimensional velocity components were measured in the field using an ADV. The velocity components were measured at a rate of 25 Hz over a 60 second interval. Daniels and Rhoads (2004) note that the alignment of the probe sensor is critical when three-dimensional velocity data is obtained in the field. A mounting

system was utilized to secure the ADV in position to ensure proper data collection and reduce the possibility of operator-induced errors. The velocity data was filtered to remove high-magnitude errors from the recorded time series (Daniels and Rhoads, 2004). TKE was calculated using the downstream, vertical, and lateral velocity fluctuations. Values of near-bed shear stress were calculated using the TKE method found in Kim et al. (2000) (Equation 5). Daniels and Rhoads (2004) concluded that TKE method resulted in unbiased estimate of bed shear stress when near-bed flow is highly three dimensional. The method is not affected by extreme deviations between the flow path and the orientation of sampling cross sections (Daniels and Rhoads, 2004). The results from this study indicate that the net effect of the LWD obstruction locally increases maximum TKE values and creates a zone of stagnant fluid along the outer bank, which shifts the zone of maximum TKE away from the toe of the outer bank downstream.

Strom and Papanicolaou (2007) conducted a field study to examine the turbulent structure of flow around a naturally formed cluster bedform in a mountain stream using an ADV. An examination of the ability of the ADV to make measurements in shallow flow over a cobble bed was also assessed in the study. It can be noted that problems with ADV measurements can be generally attributed to interference of the sample volume with the boundary, acoustic signal interference due to boundary reflection, large mean shear gradients, and high levels of turbulence. Cross-sectional geometry of the stream was measured throughout the study using a total station. A SonTek 10-Mhz ADV (lab version) with a cable mounted probe was used in the study by Strom and Papanicolaou (2007) to measure velocity at a rate of 25 Hz with a sampling interval of 120 seconds. Also, a rigid mounting apparatus with movable legs was fabricated for the ADV used in the study.

The data were filtered to remove low quality measurements within the time series based on correlation values below 70 and a signal-to-noise ratio below 15 (Strom and Papanicolaou, 2007). The study found that cluster microforms act to locally modify the turbulent structure of flow by shifting a location of the roughness layer and the zone of primary production and dissipation of turbulent energy up towards the center of the water column. Strom and Papanicolaou (2007) also conclude that ADV measurements in natural clear-water shallow flows around obstacles are difficult to obtain due to regions of high turbulent intensity, signal interference from boundary reflections, and low concentrations of suspended particles in the flow.

2.2.3 Laboratory studies of near-boundary turbulence

Hopkinson and Wynn (2009) performed a flume study to analyze vegetation impacts on near bank flow using a SonTek 16-Mhz side-looking MicroADV. The goal of the research was to evaluate variations in three-dimensional velocity structure and turbulence characteristics with three different vegetation treatments: tree, shrub, and grass. Velocity was sampled at a rate of 25 Hz over an interval of 60 seconds. The resulting data were filtered to remove erroneous data from the series. Hopkinson and Wynn (2009) characterized flow turbulence by evaluating turbulence intensities, average TKE estimates, and Reynolds stresses. The turbulent intensities were calculated in the streamwise (u), lateral (v), and vertical (w) directions. TKE was evaluated using Equation 6. Hopkinson and Wynn (2009) note that the turbulence generated from the upright shrub treatment in the study increased the Reynolds stresses and TKE near the toe of the streambank, which is the area most susceptible to fluvial erosion.

Dey et al. (2011) performed an experimental flume study to quantify near-bed turbulence characteristics at an entrainment threshold of non-cohesive sediments. A four-beam Nortek Vectrino ADV probe (downward facing orientation) was used to capture instantaneous three-dimensional velocity components at a sampling rate of 100 Hz over a duration of 300 s. The results from the study indicate a streamwise acceleration as well as an increase in streamwise and vertical turbulence intensities during sediment entrainment. For sediment entrainment to occur, the pressure energy diffusion changes to a negative magnitude, indicating a gain in turbulence production. The results from the study may provide useful information on how to analyze sediment entrainment in models.

3.0 Methods

Fluvial entrainment, initiated by near-boundary turbulence, is the main driver of streambank retreat as it leads to unstable streambank geometries (Hopkinson and Wynn, 2009). This research characterized the turbulence structure of flow near the streambank toe throughout a storm event. Three-dimensional velocity was measured at baseflow and through a storm hydrograph at an experimental cross-section (West Run in Morgantown, WV) using a Sontek 16-MHz ADV. Near-bank velocity and stream stage were also measured throughout baseflow and storm events using a Sontek SL3000. Precipitation data corresponding to each of the storm events analyzed throughout the study can be found in tables 3 and 4.

3.1 Site Description

A reach of West Run located in Monongalia County, West Virginia, USA was selected for this study (Figure 1). The site was chosen based on the following characteristics: 1) wadeable at baseflow; 2) at least four bankfull widths in length; 3) relatively straight to minimize secondary currents; and, 4) ease of access.

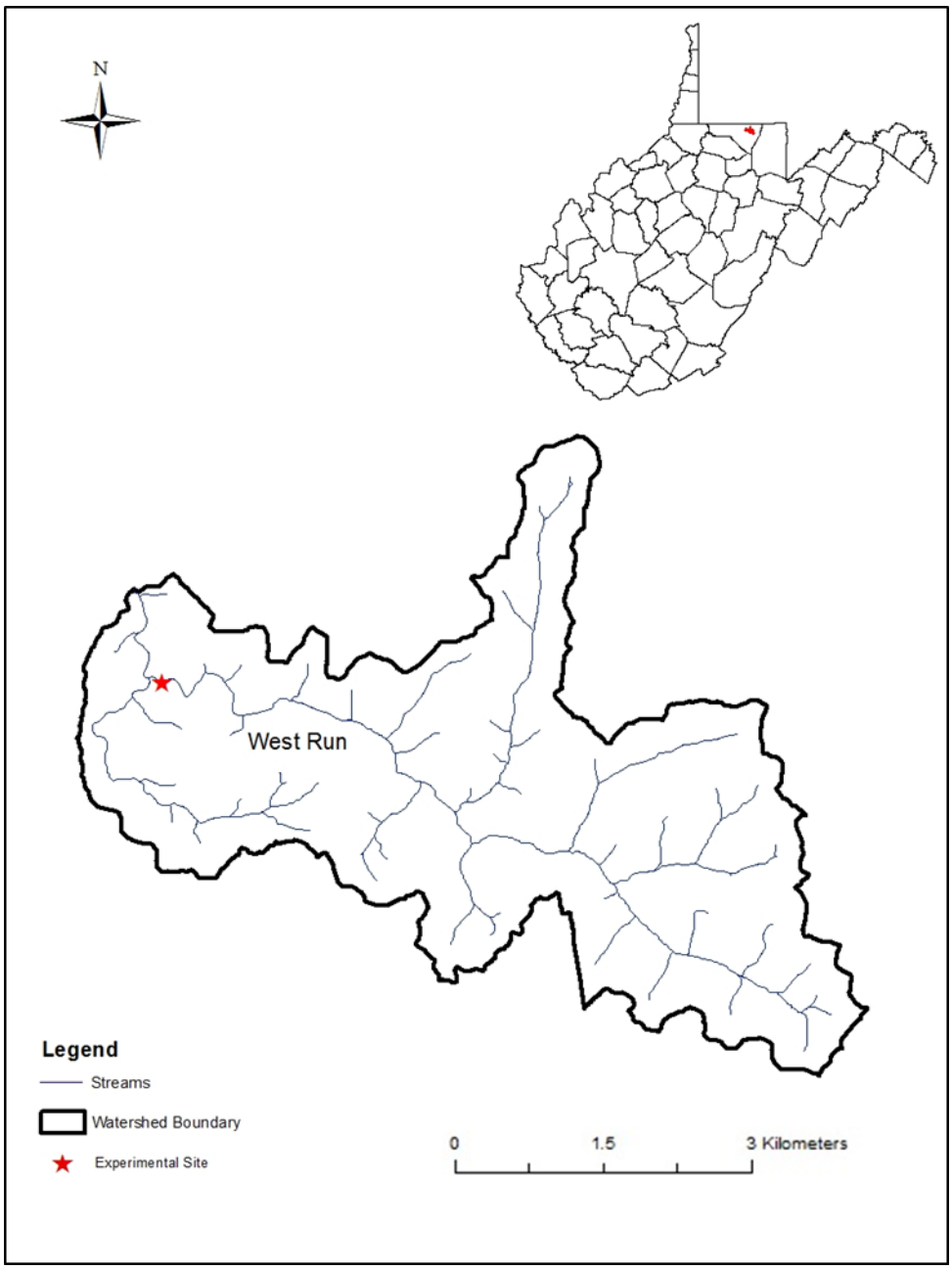

Figure 1. West Run watershed containing experimental field site

The West Run watershed drains directly into the Monongahela River on the northern edge of Morgantown, WV. The West Run watershed is approximately 22 km^2 and located completely in Monongalia County. Flooding has become more common recently due to the increased

development in the watershed. The flooding may be attributed to increased runoff generated from impervious surfaces within the watershed. The primary vegetation type in the West Run watershed is oak dominated deciduous forest. The watershed also contains a substantial amount of shrub/grassland (West Virginia Water Research Institute, 2008).

Figures 2a and 2b show the density and location of the vegetation on the field streambank and the left streambank at the selected experimental cross section. The experimental field streambank, where the Sontek devices were deployed, consisted primarily of grasses, small herbaceous plants, and limited woody debris. The left streambank had a significantly larger amount of woody debris contained within the primary flow channel in comparison to the field streambank (right bank). The left streambank also contained grasses outside of the primary channel with herbaceous plants and small trees.

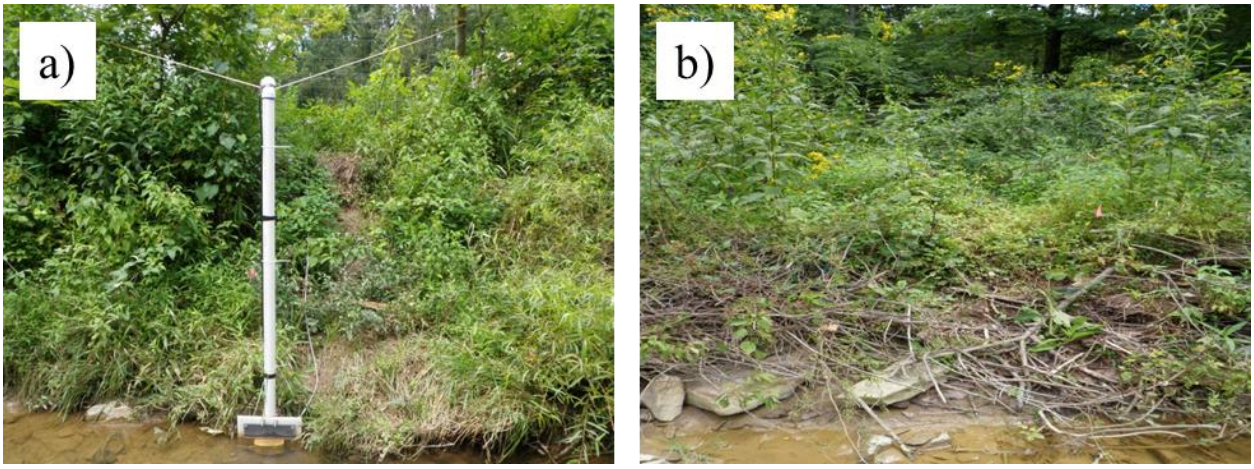

Figure 2. a) Field streambank where measurements were completed (right bank); and, b) Left streambank, opposite of the experimental streambank.

The selected cross-section has an average bankfull width of approximately 8 m and a bankfull depth of 1.2 m. The thalweg, or zone of maximum depth, is generally located near the base of the right bank for the selected reach of the stream. The bed material at the study site consists of coarse sands, fine to coarse gravels, and small to medium cobbles with a few small boulders. The average slope of the reach was 0.0079.

3.2 Physical Measurements

Physical stability of the stream bank was monitored by measuring channel geometry, grain roughness, and vegetation parameters (i.e. location, size, and density) before and after each storm event.

3.2.1 Site Survey

A preliminary site survey was performed at the beginning of the study to document the location and cross-sectional geometry of the stream at the field site. The preliminary site survey was completed in three days during June, 2011. The survey equipment included a Leica TC600 Total Station, a Carlson PDA, and a rod and prism. Field surveys were performed to obtain the cross-sectional geometry of five different locations along the length of the stream at the study site. One of the five cross-sections was selected as the experimental site at which the velocity and stage measurements would be recorded throughout the study. A longitudinal stream survey was also completed to obtain the average slope of the streambed at the experimental site. An azimuth was determined at the beginning of the survey near the baseline located approximately parallel to the stream. The purpose of a baseline is to have documented points along the same bearing that the survey instrument can be placed upon. A hand compass was used to determine the azimuth that was used to place the baseline of the survey. Once the azimuth was recorded, a

nail was driven into the ground at the first designated point along the baseline. A number of different steps were completed to set up the survey equipment and perform a site survey. A detailed survey procedure (Appendix B) was developed with the assistance of Dr. Darrell Dean and used to perform the preliminary site survey and each of the deployment surveys.

The survey data were downloaded and analyzed to determine a suitable location to mount the Sontek SL3000 and the Sontek 16-MHz ADV (YSI; San Diego, CA) for data collection. The cross-section survey data were also used in a log file to calculate flow parameters for the Sontek SL3000. A survey was completed at the experimental cross-section before and after each data collection deployment to track any changes in the streambed or streambank geometry. Each pre- and post-deployment survey consisted of a detailed cross-sectional survey where the top of the bank, bottom edge of the bank, edge of the water, edge of the bed, and the thalweg were recorded (Harrelson et al., 1994). An example of a cross-section created from a field survey completed on 10/11/2011 at West Run is shown in the following figure; all cross-section data can be found in Appendix C.

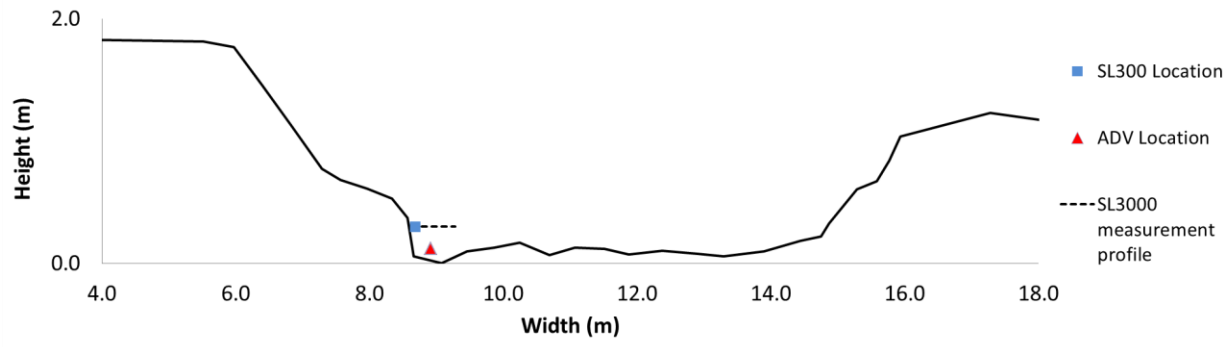

Figure 3. Experimental cross-section at West Run, WV indicating the measurement locations of the velocimeters used in the study (vertical exaggeration)

3.2.2 Vegetation

Vegetation placement, size, and density were measured at the beginning of the study. Vegetation was monitored throughout the study with photo documentation. There was no noticeable change in vegetation density throughout the study period. Table 1 was compiled from the initial vegetation data collection on 8/12/11. Four sample locations were selected along the streambank at the experimental study site to perform the vegetation analysis. A metal square (0.03 m^2) was placed over each sample area allowing the blades of grass inside the measurement area to be counted. Ten stems from each of the four sample areas were chosen at random and cut at their base. A pair of calipers was used to measure the diameter of each of these stems at three equally spaced locations along their length (Table 1).

Table 1. Vegetation density (stems/cm^2) and diameter (cm)

Sample	Stem Count	Density	Stem 1	Stem 2	Stem 3	Stem 4	Stem 5	Stem 6	Stem 7	Stem 8	Stem 9	Stem 10
1	86	0.27	0.18	0.16	0.12	0.36	0.21	0.19	0.15	0.17	0.21	0.12
			0.17	0.17	0.11	0.37	0.20	0.19	0.14	0.17	0.19	0.12
			0.17	0.15	0.10	0.36	0.19	0.18	0.13	0.16	0.18	0.11
2	93	0.29	0.11	0.34	0.16	0.14	0.18	0.25	0.42	0.13	0.11	0.19
			0.10	0.27	0.15	0.13	0.15	0.23	0.46	0.14	0.10	0.18
			0.09	0.30	0.13	0.12	0.15	0.21	0.37	0.15	0.10	0.15
3	126	0.40	0.16	0.14	0.19	0.12	0.16	0.21	0.19	0.15	0.29	0.18
			0.16	0.14	0.20	0.13	0.15	0.20	0.18	0.14	0.27	0.19
			0.15	0.13	0.19	0.12	0.15	0.19	0.18	0.14	0.26	0.18
4	112	0.35	0.30	0.11	0.17	0.12	0.17	0.30	0.14	0.15	0.16	0.13
			0.31	0.11	0.18	0.12	0.16	0.29	0.13	0.14	0.16	0.13
			0.30	0.10	0.17	0.10	0.15	0.29	0.13	0.13	0.16	0.12

3.2.3 Channel Roughness

Throughout the study a series of pebble counts were completed before and directly after a storm event where velocity and stage data were collected using the Sontek equipment. A modified Wolman Pebble Count (Wolman, 1954) was used to quantify grain roughness in the stream channel. The Wolman Pebble Count requires the observer to randomly select 100

particles along a desired path and measure them with a gravelometer. This process was completed only at the experimental cross-section. The distributions collected in each sample are presented in Appendix C. The 84th percentile (D_{84}) and the median particle size (D_{50}) were recorded to characterize the bed roughness (Table 2). The median particle size ranged from 22 mm to 41 mm throughout the study period. D_{50} and D_{84} values were calculated to track any significant changes in bed material.

Table 2. D_{50} and D_{84} from the grain size distributions. Before deployment (B); After deployment (A)

	SL3000 Deployment 1		SL3000 Deployment 2		SL3000 Deployment 3		ADV Deployment 1		ADV Deployment 2	
	B	**A**	**B**	**A**	**B**	**A**	**B**	**A**	**B**	**A**
D_{50} (mm)	32	35	29	32	32	22	30	39	41	31
D_{84} (mm)	94	110	87	120	120	80	150	120	130	120

3.3 Velocity Measurements

Velocity was measured near the streambank with both a Sontek SL3000 and a Sontek 16-MHz ADV. The measurement location of the ADV probe was 0.27 m off of the streambank at a height of 0.17 m from the stream bed at the experimental cross-section. The measurement control volume of the ADV was 0.12 m above the stream bed. The SL3000 was secured as close to the stream bank as possible with the aid of a fabricated mount and a bed-driven steel pin as discussed in the following sections, and the measurement location of the SL3000 was located 0.30 m above the stream bed.

3.3.1 Sontek SL3000

The SL 3000 is an acoustic Doppler current meter that measures water velocity, stage, and total water volumetric flowrate in a horizontal facing orientation. The SL3000 has three acoustic beams including one beam that points in the positive vertical direction, and the other two that are directed upstream and downstream at a 25° angle. The upward-looking beam measures stream stage, while the two slanted beams measure the two-dimensional water velocity.

3.3.1.1 SL3000 Mount

A mount was constructed to support the Sontek SL3000 for data collection in the stream. The mounting device was designed to meet the requirements of the SL3000 as well as the geometric limitations of the streambank. Figures 4a and 4b show the mounting arm that was fabricated for the SL3000. The mount arm was designed and built to a total length of 7.5 m to span the required length of the streambank. It was constructed out of schedule 40 PVC pipe. The mounting arm was designed to be adjustable with a series of holes drilled through the side of the PVC pipe end towards the mount base. Bolts and nuts were used to secure the end of the mount arm to the mount base with the help of four metal brackets. Figure 5b depicts how the mount arm and the base are connected using the bolts. The mount arm also incorporates a 90° downward bend that allows the SL3000 to be mounted vertically in the stream.

A metal pin was forced into the stream bed directly under the vertical end of the mounting arm where the SL3000 was secured. The open end of the mount arm was placed over the metal pin which allowed the mount arm to be stationary in the stream and also returned to the exact same location in the event that the mount was removed. Extra support was added to the mount arm in the form of ropes. Holes were drilled through the PVC pipe towards the 90° bend and a rope was run through the holes and attached to fence posts located on the top of the stream

bank. The rope allowed the arm to be adjusted to a precise height and also added additional stability to the mounting apparatus.

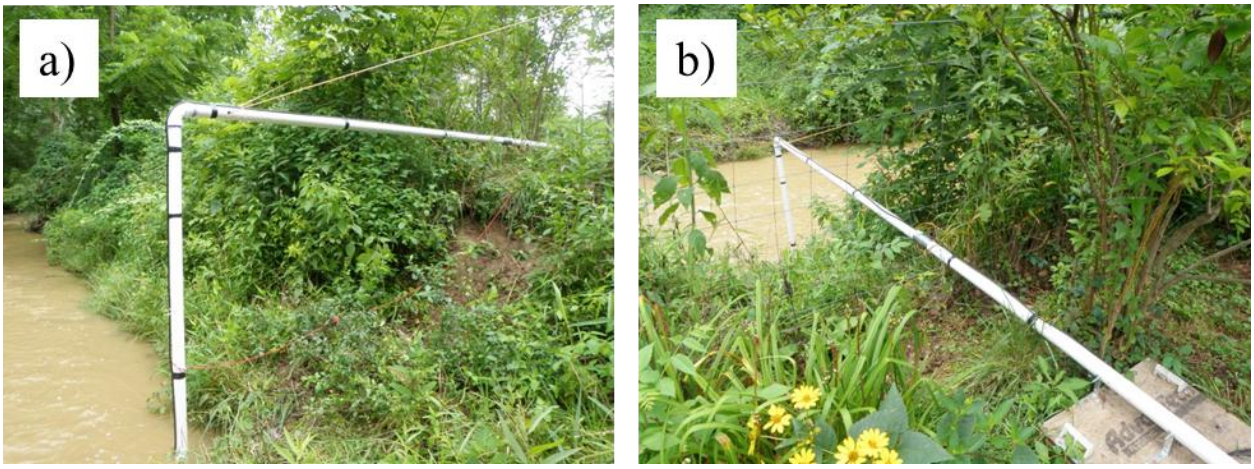

Figure 4. a) Front view of the SL3000 mount arm and b) rear view of the SL3000 mount arm

Figures 5a and 5b show the base that was constructed to support the mount arm and the battery that was used to supply power to the SL3000 during deployments. The mount base was constructed with Advantech subflooring and pressure treated 2 x 4 studs. Two hinges were added to join the sections of the mount base together in order to be able to lift the mount arm out of the water for maintenance on the SL3000. Four metal brackets were attached to the smaller section of the mount base in order to secure the mount arm. The design allowed the PVC mount arm to fit between each set of brackets and be secured with long bolts and nuts. A deep cycle marine battery used to power the SL3000 was placed on the larger section of the mount base.

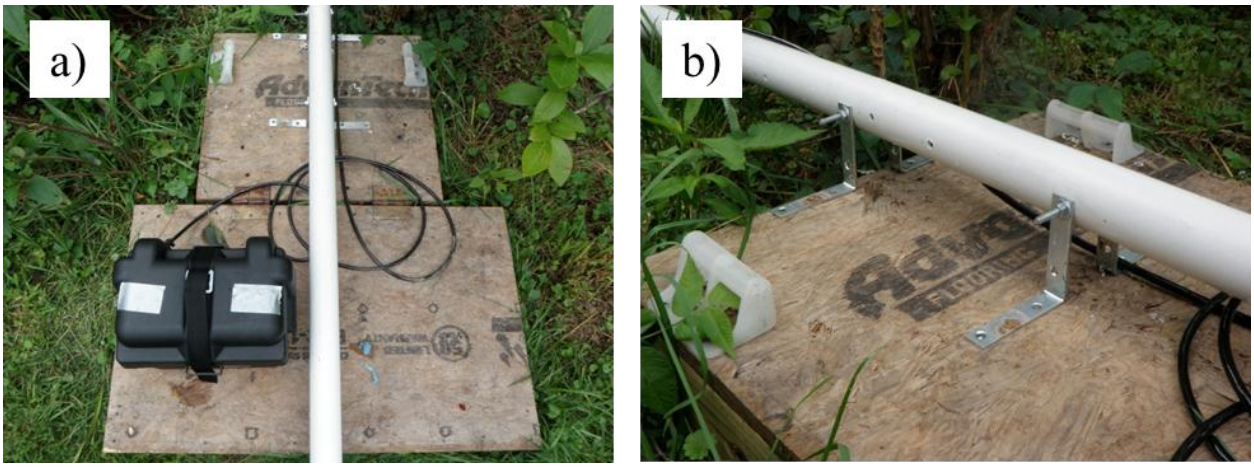

Figure 5. a) SL3000 mount base containing battery and b) SL 3000 mounting brackets

Figure 6 shows the mounting plate that was fabricated to secure the SL3000 to the mount arm. The entire mounting plate consisted of a factory Sontek mounting plate that was joined to a larger section of a plastic cutting board with bolts. The factory Sontek mounting plate was designed to be attached to flat surfaces so a new design was created that allowed the SL3000 to be mounted on a pipe. Holes were drilled at the top and bottom of the plastic cutting board where two U-bolts with hardware were added in order to secure the plate to the mount arm.

Figure 6. SL3000 mounting plate

3.3.1.2 SL3000 velocity measurement procedure

Sontek ViewArgonaut was used to develop template files containing deployment specific operating parameters for the SL3000. Three deployments were completed with the SL3000 throughout the study period. The template file created for the SL3000 deployment 1 utilized a muilti-cell profiling mode to record velocity data. A continuous sampling technique was selected for each of the SL3000 deployments due to the fact that there were no power supply or data limitations. The PowerPing option was activated in each of the SL3000 deployments for optimal system performance. Velocity was measured at 1 Hz for each of the SL3000 deployments. The template file for SL3000 deployment 1 was configured to measure the velocity profile using 5 cells with an averaging interval of 300 s and a sampling interval of 300 s. A minimum blanking distance (distance to the start of the first cell) of 0.1 m was selected for the template based on the suggested parameters listed in the Sontek Argonaut-SL system manual. The cell size for the

deployment was 0.2 m with the integrated velocity cell beginning at 0.2 m and ending at 1.0 m. Figure 7 shows a detailed schematic of the multi-cell velocity profiling setup used in SL3000 deployment 1.

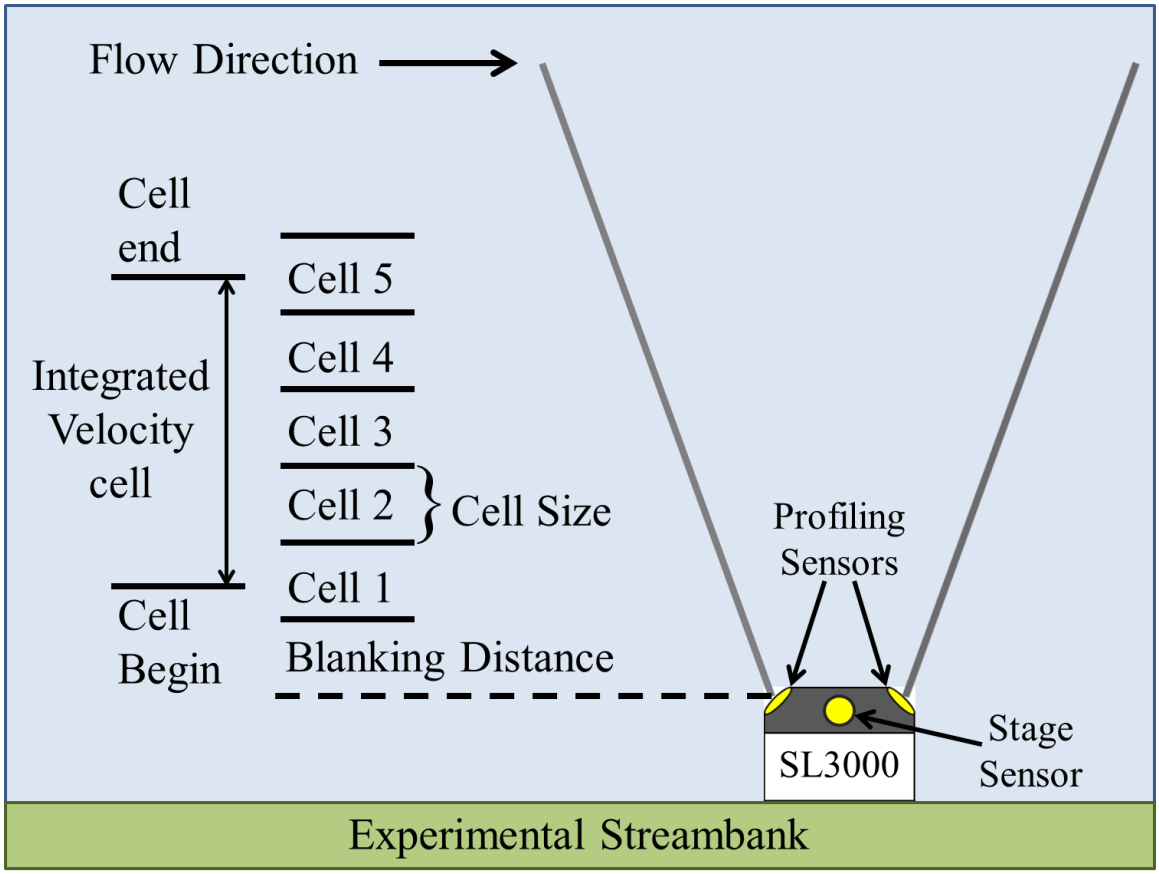

Figure 7. SL3000 multi-cell velocity profiling setup (plan view adapted from Sontek/YSI, 2009)

Based on the objective to quantify near-bank turbulence, a different template file was created and implemented in SL3000 deployment 2 and 3. This template file was configured to measure the velocity profile using a single cell with an averaging interval of 300 s and a sampling interval of 300 s. The cell size used in the template file was 0.5 m with a blanking distance of 0.1 m.

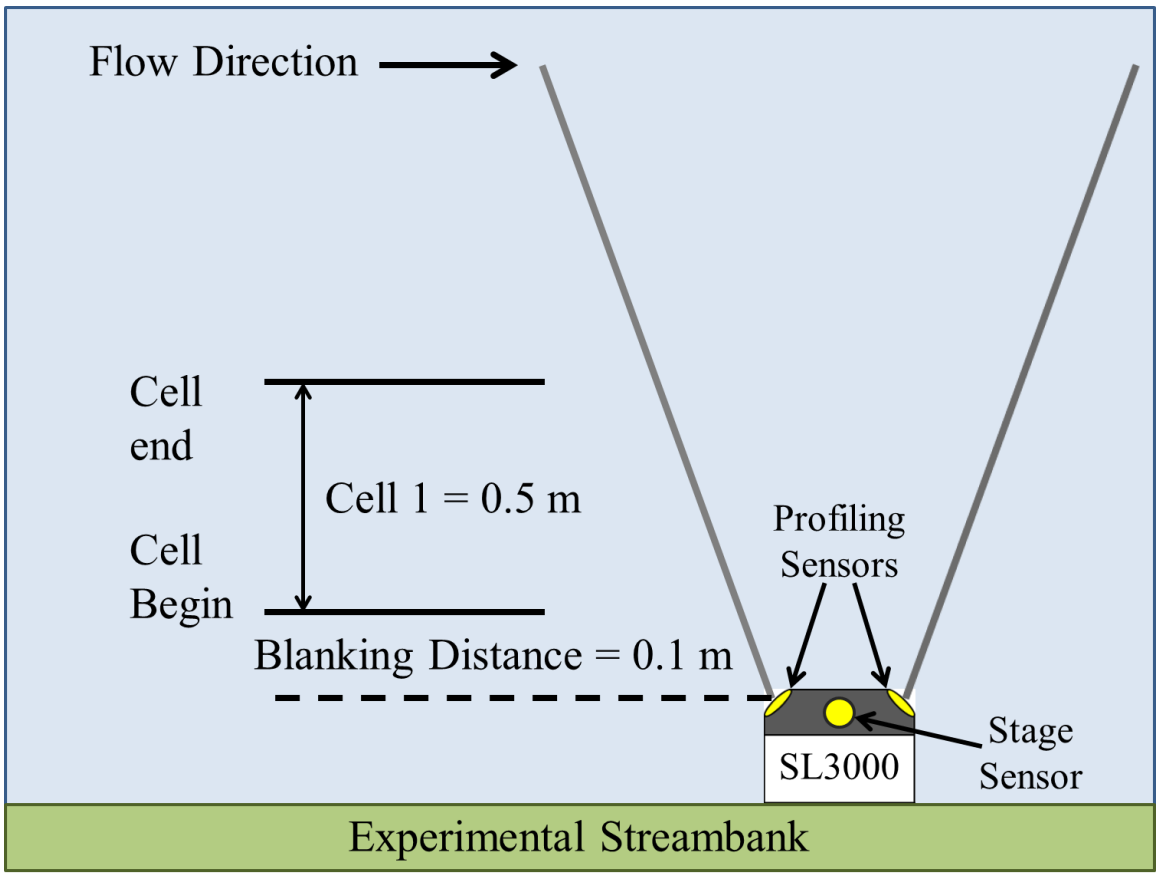

Figure 8. SL3000 single cell velocity profiling setup (plan view adapted from Sontek/YSI, 2009)

Table 3. SL3000 deployment information

	SL3000 Deployment 1		SL3000 Deployment 2		SL3000 Deployment 3	
	Start	**End**	**Start**	**End**	**Start**	**End**
Date	7/18/2011	7/19/2011	8/12/2011	8/16/2011	8/17/2011	8/22/2011
Time	16:10:00	15:25:00	18:00:00	10:25:00	20:00:00	13:10:00
Precip. (cm)	*		4.1		0.9	

*Data not available

3.3.2 Sontek 16-MHz ADV Field

The hardware for the Sontek 16-MHz ADV Field is composed of two main components: signal processing hardware and probe hardware. The signal processing hardware is contained in a submersible canister. The signal processing hardware performs the signal generation and processing required for the ADV to take velocity measurements. The probe hardware consists of a signal conditioning module and a cable mounted acoustic sensor. The acoustic sensor contains three acoustic receivers and one acoustic transmitter which take velocity measurements. Velocity is measured at a distance of 5 cm from the acoustic transmitter and has a measurement control volume of 0.09 cm^3 (Sontek/ YSI, 2000).

3.3.2.1 ADV Mount Description

An in-stream mount was designed for the ADV to record velocity and stage measurements throughout storm events. The mount consisted of two main components including a mounting arm and a submergible frame. The mounting arm was constructed out of a long steel footer pin, electrical conduit, electrical pull elbow, and stainless steel nuts, washers, and bolts. Figure 9a shows the assembled materials that were used to create the mounting arm and Figure 9b shows the ADV probe mounted in-stream on the mounting arm.

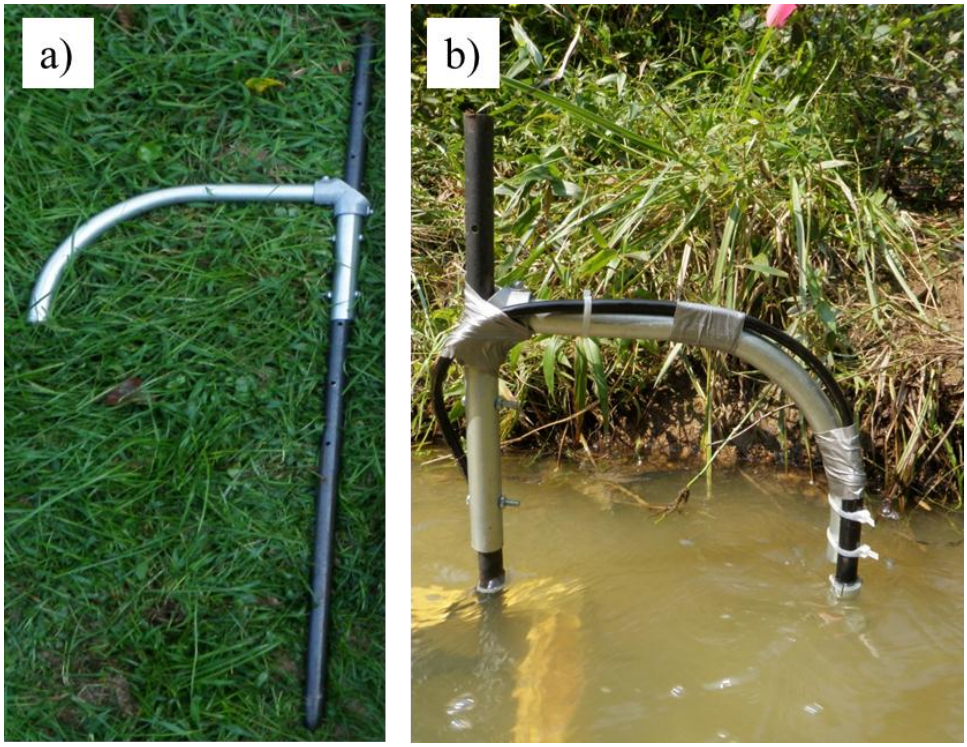

Figure 9. a) and b) ADV mount arm

A piece of the electrical conduit was cut to length and connected to the bottom end of the electrical pull elbow. A small flat metal plate attached to the electrical pull elbow was removed in order to allow the footer pin to slide through the opening. A second section of electrical conduit was cut to length and bent using a conduit bender forming a 90° angle. The bent section of the electrical conduit was then connected to the remaining opening of the pull elbow forming an arm. The electrical conduit arm was drilled through its diameter at two specific locations that coincided with the holes in the steel footer pin. The steel footer pin was then inserted through the pull elbow and electrical conduit and attached using the stainless steel hardware.

The second component of the ADV mount consisted of a basic submergible frame that was constructed out of pressure treated 2x4 studs. The studs were cut to length and then screwed

together to form a rectangular frame. The purpose of the frame was to securely contain the underwater canister and the signal conditioning module along with the underwater cables. These components of the ADV were attached to the frame using utility straps. The frame was placed over the steel footer pins that were driven into the stream bed. The footer pins acted as a stabilizing unit to help secure the frame under water. Figure 10a shows the submergible ADV frame with the attached conditioning module and underwater canister. Figure 10b shows the submergible ADV frame mounted in-stream on the steel footer pins at the experimental field site.

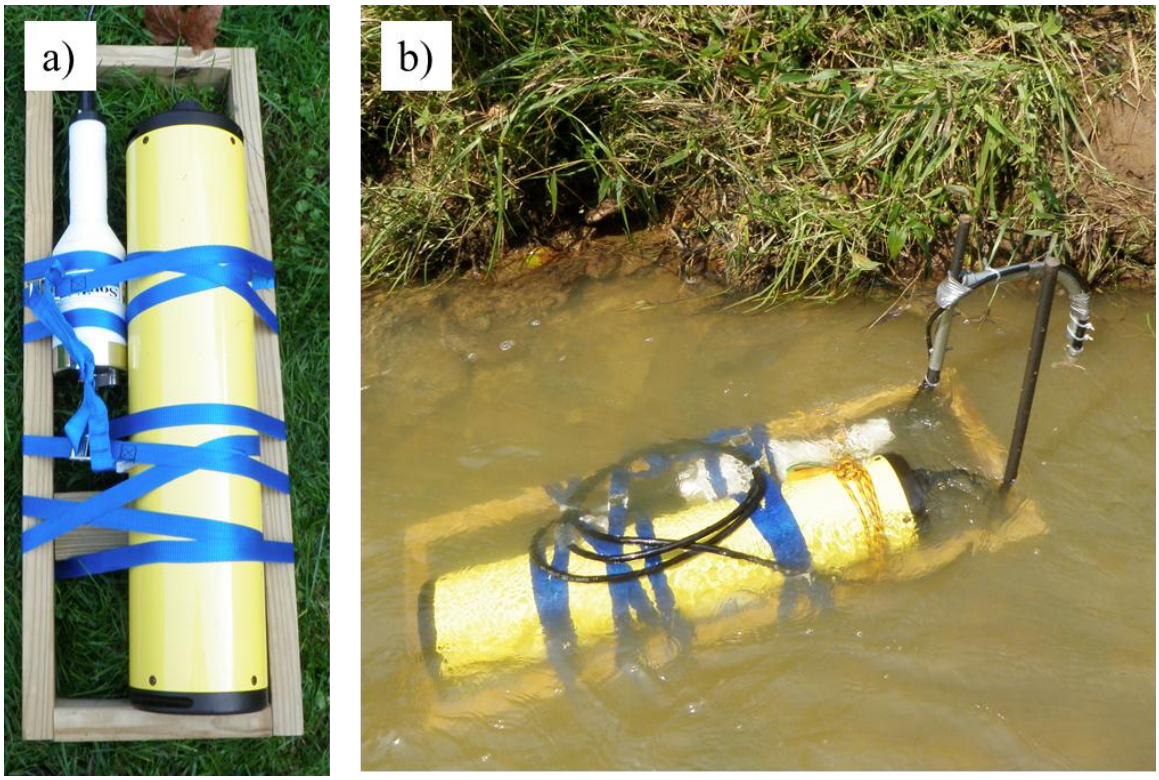

Figure 10. a) and b) Submergible ADV frame

3.3.2.2 Velocity Measurement Procedure

A single burst sampling method was used to measure the velocity and stage throughout the deployment. The ADV was configured at a burst interval of 7 min and a sample time of 2

min. This means that the ADV recorded data for 2 min and then rested for 5 min. This cycle of sampling data for a period of 2 min every 7 min continued throughout the entire deployment. Velocity was measured at 25 Hz and each burst contained 2750 samples. Deployment 2 was selected for data analysis as it had a full set of data. Sontek ViewHydra was used to filter the ADV velocity data. Measured points with correlation values below 70% or a signal-to-noise ratio value below 15 were removed from the data set using the ViewHydra program.

Table 4. ADV deployment information

	ADV Deployment 1		ADV Deployment 2	
	Start	**End**	**Start**	**End**
Date	9/14/2011	9/15/2011	10/11/2011	10/13/2011
Time	15:00:00	17:08:00	23:00:00	11:24:00
Precip. (cm)	1.80		1.50	

3.4 ADV Data Analysis

Time-averaged velocity components and turbulence statistics were examined throughout a storm event. A resulting data set containing 151 filtered samples were used to perform the data analysis.

3.4.1 ADV Statistics

Reynolds stresses, turbulent kinetic energy, and turbulence intensities were calculated from the velocity data for each velocity time series. Reynolds stresses provided information about momentum exchange. The lateral Reynolds stress quantifies the lateral momentum exchange and is calculated using the downstream and lateral velocity fluctuations (Equation 7). The vertical Reynolds stress quantifies the vertical momentum exchange and is calculated with the downstream and vertical velocity fluctuations (Equation 8). This analysis required separating

the instantaneous velocity fluctuations (u', v', w') from the time-averaged velocity ($\overline{u}, \overline{v}, \overline{w}$) for each velocity component.

Turbulent kinetic energy (TKE), which is a measure of overall turbulence, was calculated for each velocity time series (Equation 6). The turbulence intensities for each velocity component, which are a measure of the violence of turbulence in the downstream (u), lateral (v), and vertical (w) directions, (RMS_u, RMS_v, and RMS_w) were also calculated (Equations 9-11).

$$RMS_u = \sqrt{\overline{u'^2}} \tag{9}$$

$$RMS_v = \sqrt{\overline{v'^2}} \tag{10}$$

$$RMS_w = \sqrt{\overline{w'^2}} \tag{11}$$

4.0 Results and Discussion

4.1 ADV Results

4.1.1 Storm Event

The results discussed in the following sections correspond to the October 11-13, 2011 deployment. This deployment was one of two that resulted in the most complete data set. Throughout this time span, an approximately 17 hour storm event occurred in which the ADV recorded three-dimensional velocity and stream stage. The data set used for the analysis consisted of 151 samples each containing 2750 individual data measurements. Figure 11 shows the stage height of the stream throughout the storm event.

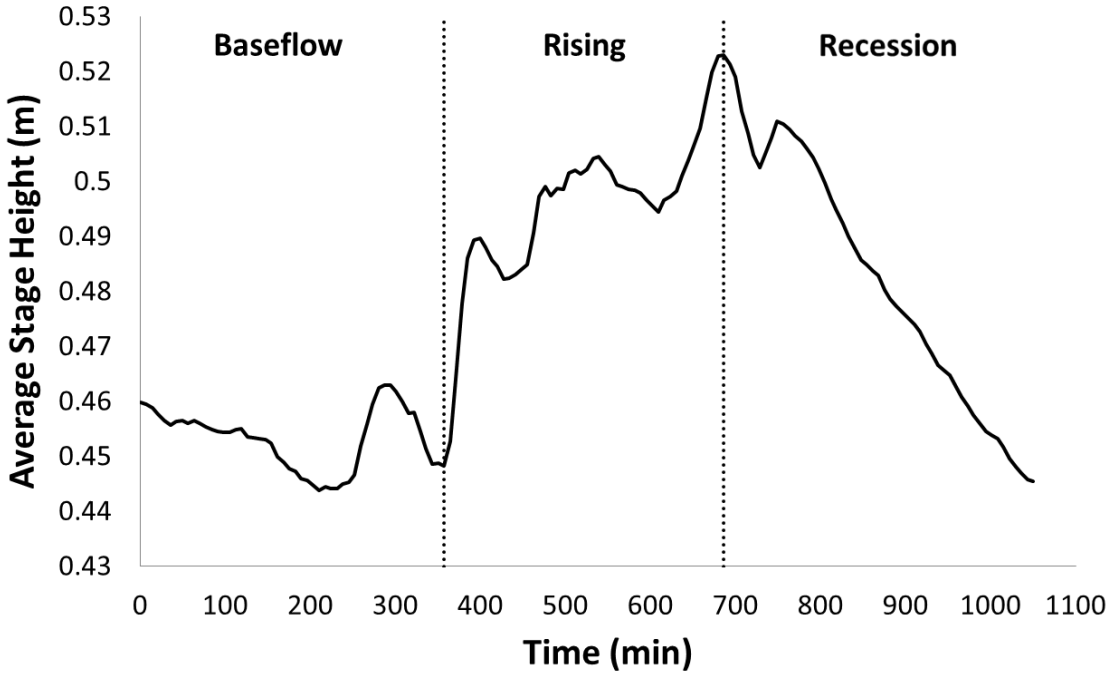

Figure 11. Stream stage height vs. time through a storm event starting on 10/11/2011

The data were analyzed and divided into three categories: baseflow, rising limb, and recession limb (Figure 11). The peak value of stage height was selected as the separation point between the rising and recession limbs; the division was also influenced by the velocity measurements (Figure 14). The intervals contain approximately equal amounts of velocity measurements with baseflow containing 52 samples, rising limb containing 47 samples, and the recession limb containing 52 samples. The minimum stage height throughout baseflow was 0.44 m. The stage height of the stream at peak flow was 0.52 m. This difference results in a stage height fluctuation of 0.08 m throughout the storm event. Figure 12 depicts the stream stage fluctuation at the experimental cross-section throughout the storm event. While the difference in water depth seems minor, the system is actively widening as there is bedrock control on the streambed. The maximum depth observed for this study represents the depth just before the flow extends over a bench, which would have resulted in energy dissipation.

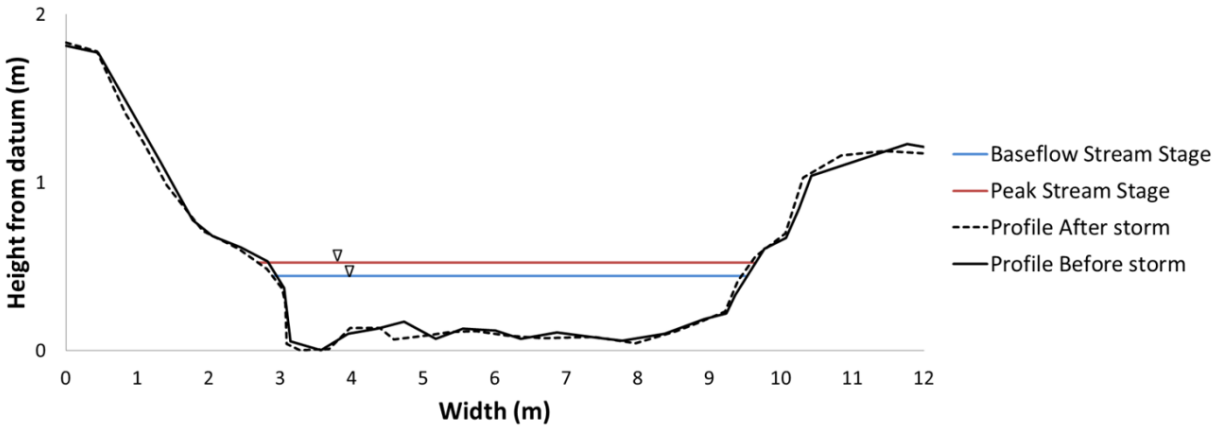

Figure 12. Experimental stream cross-section (vertical exaggeration) showing baseflow and peak stream stage height through a storm event starting on 10/11/2011

The stream flow remained in the primary channel throughout the storm event. The stream site is flashy due to the urban environment in which the watershed is encompassed. Minimal changes in stream geometry were detected from the plots of the cross-sectional stream profiles before and after the single storm. The area of the experimental cross-section increased by less than 1% from the pre-storm survey to the post-storm survey. The survey data reflects a minimal change in cross-sectional area which may be attributed to fluvial scour and bank erosion that may have occurred throughout the storm event. It should also be noted that the change in cross-sectional area is highly dependent on the field technician's ability to perform the on-site survey. Therefore, human error in the measurement of the cross section may also account for the change that is seen in the pre and post-storm areas. Each of the pre- and post-storm cross-section plots can be found in Appendix C.

Vegetation size and density was monitored before and after this storm event with picture documentation (Figure 13). No significant changes in vegetation were observed (stem density = 0.33 stems/cm^2).

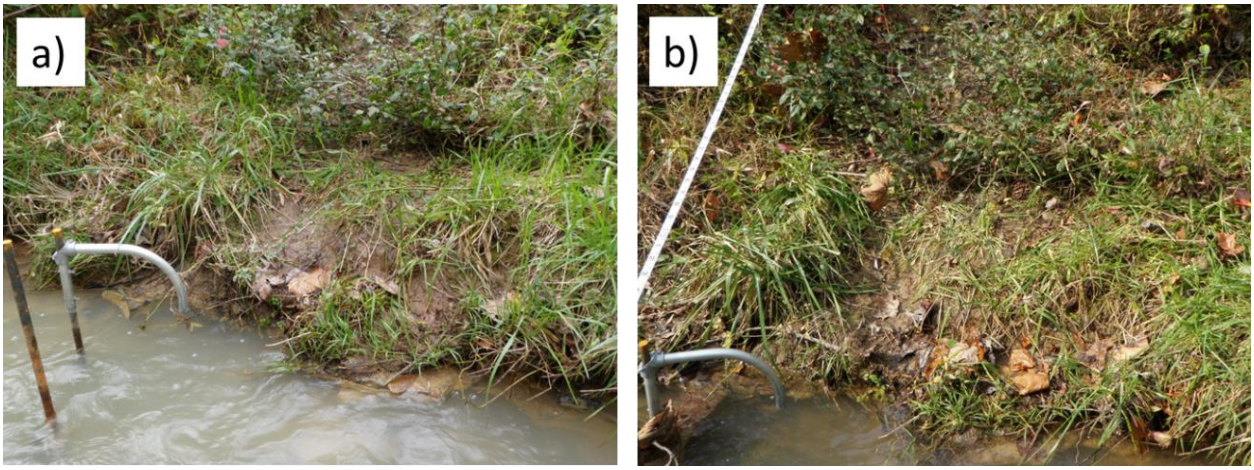

Figure 13. a) Pre-storm vegetation documentation on 10/10/2011; b) Post-storm vegetation documentation on 10/13/2011

Channel roughness was also monitored before and after the deployment using a modified Wolman Pebble Count. The D50 and D84 of the channel prior to the deployment were 41 mm and 130 mm, respectively. The D50 and D84 of the channel after the deployment were 31 mm and 120 mm respectively, resulting in no substantial change in bed roughness throughout the deployment.

The Sontek 16 MHz ADV measured three-dimensional velocity throughout the storm event. The overall magnitudes of velocity increased with an increase in stream stage throughout the storm event (Figure 14). The downstream and lateral velocity components showed a larger increase in absolute magnitude than the vertical component of the velocity. The lateral component of velocity shows a larger change in magnitude due to vortex shedding and resistance from the vertical boundary which may be attributed to the measurement location of the ADV probe. The near-bank measurement location is unique and differs from recent studies that focus mainly on near-bed measurements (Daniels and Rhoads, 2004; Dey et al., 2011).

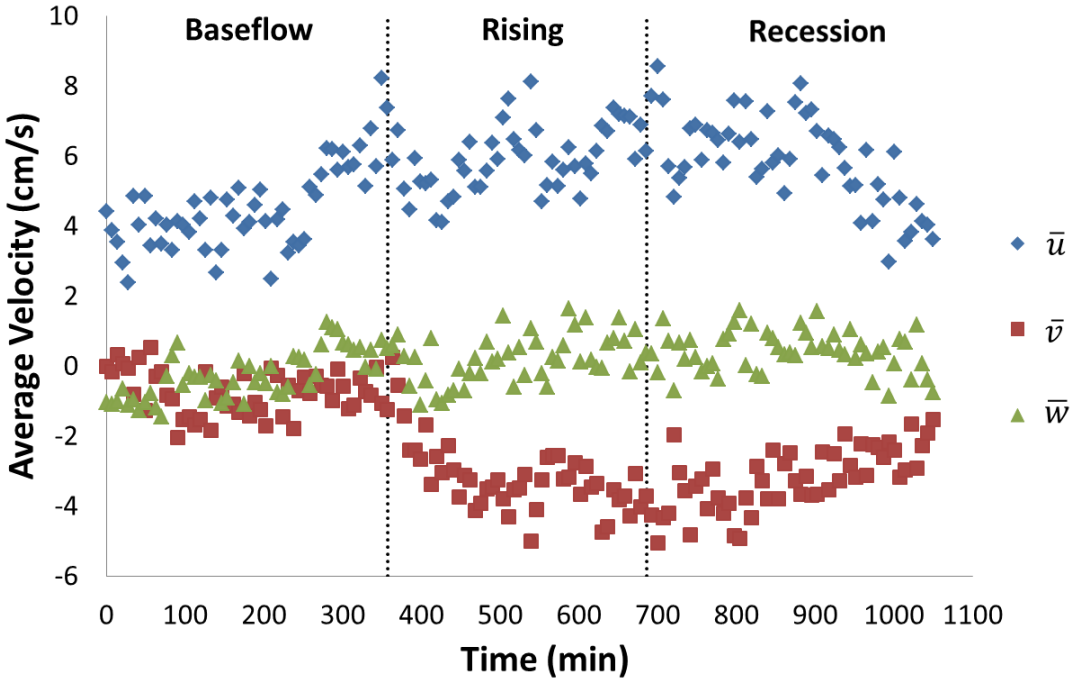

Figure 14. Time–averaged velocity for each velocity component ($\bar{u}, \bar{v}, \bar{w}$) through a storm event starting on 10/11/2011

The overall mean magnitude of the time-average downstream component of velocity increased by 30% from baseflow to the rising limb. The data also indicated that the overall magnitude of the time-average lateral component of velocity increased by 316% from baseflow to the rising limb and the overall magnitude of the time-average vertical component of velocity increased by 184% from baseflow to the rising limb (Table 5).

Table 5. Velocity statistics for the mean, median (in italics), and range (in parentheses) values.

	Baseflow	Rising	Recession
$\bar{u}$ **(cm/s)**	4.53	5.91	5.88
	4.25	*5.88*	*5.90*
	(5.83)	(4.03)	(5.58)
$\bar{v}$ **(cm/s)**	-0.77	-3.19	-3.21
	-0.78	*-3.26*	*-3.17*
	(2.57)	(5.25)	(3.54)
$\bar{w}$ **(cm/s)**	-0.25	0.21	0.41
	-0.30	*0.20*	*0.42*
	(2.7)	(2.76)	(2.46)

4.1.2 Reynolds Stresses

The Reynolds stress component, $\tau_{uv,}$ ranged from 0.27 Pa to 1.41 Pa throughout baseflow, 0.22 Pa to 1.82 Pa throughout the rising limb and 0.11 Pa to 1.88 Pa throughout the recession limb. τ_{uw} ranged from -1.05 Pa to 0.65 Pa throughout baseflow, -0.80 Pa to 0.39 Pa throughout the rising limb, and -0.93 Pa to 0.30 Pa throughout the recession limb (Figure 15). The greater magnitude of τ_{uv} as compared to τ_{uw} indicates that the lateral momentum exchange is dominant which supports previous observations by Hopkinson and Wynn (2009) in a study of constructed streambanks with dense bank vegetation.

The Reynolds stress tensor, τ_{uw}, represents the magnitude of vertical momentum exchange. This Reynolds stress component more than doubles in magnitude from baseflow to the rising limb of the hydrograph (Table 6). The mean and median values of τ_{uv} remained approximately constant throughout the storm hydrograph.

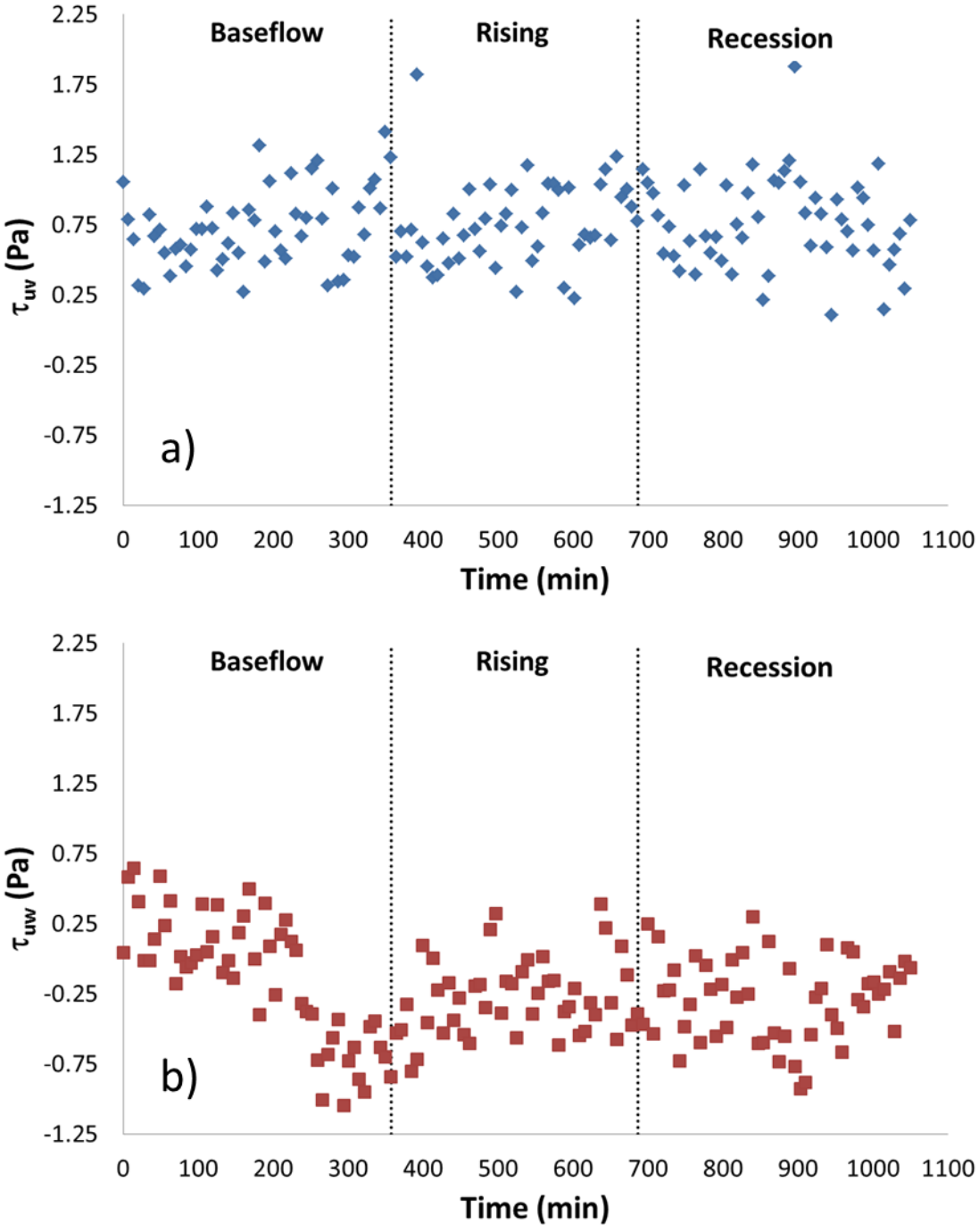

Figure 15. a) Reynolds stress component τ_{uv} vs. time; b) Reynolds stress component τ_{uw} vs. time through a storm event starting on 10/11/2011

Table 6. Reynolds stress components statistics for the mean, median (in italics), and range (in parentheses).

	Baseflow	Rising	Recession
τ_{uv} (Pa)	0.73	0.75	0.77
	0.71	*0.71*	*0.75*
	(1.14)	(1.59)	(1.77)
τ_{uw} (Pa)	-0.13	-0.28	-0.29
	-0.02	*-0.31*	*-0.25*
	(1.70)	(1.19)	(1.12)

4.1.3 Turbulence Intensities and TKE

Turbulence intensities are a measure of the violence of turbulence fluctuations. An overall increase in magnitude was apparent for the mean turbulence intensities of each velocity component from baseflow to the rising limb. The overall magnitude of the mean turbulence intensity component RMS_u increased by 12% from baseflow to the rising limb. The overall magnitude of the mean turbulence intensity component RMS_v increased by 18% from baseflow to the rising limb. The overall magnitude of the mean turbulence intensity component RMS_w increased by 25% from baseflow to the rising limb (Table 7).

Turbulent kinetic energy (TKE), which is a measure of overall turbulence, is comprised of the three turbulence intensity components. RMS_u accounted for 40% of the total TKE, while RMS_v accounted for 28% of the total TKE; RMS_w accounted for 32% of the total TKE. The results obtained from this study differ from the results obtained by Daniels and Rhoads (2004) where the mean percentage contributions to TKE were 49% from RMS_u, 32% from RMS_v, and 19% from RMS_w. The data suggests that the larger contribution of RMS_w to TKE, in comparison to the study by Daniels and Rhoads (2004), may be attributed to the measurement location of the ADV probe, influence of a nearly vertical bank, or submerged vegetation. The distribution of RMS_w is different than the distributions of RMS_u and RMS_v (Figure 16). The plot of RMS_w with

time shows a significantly larger jump in the distribution from baseflow to the rising limb, which indicates that this component may have important implications for erosion prediction near the toe of a streambank (Figure 16). The distribution of RMS_u and RMS_v with time are similar but RMS_v is less in magnitude. This result is expected as ($\bar{u}$) is the greatest velocity component. The range is the greatest on the rising limb of the RMS_w component, which indicates that the largest vertical exchange is occurring on the rising limb (Table 7).

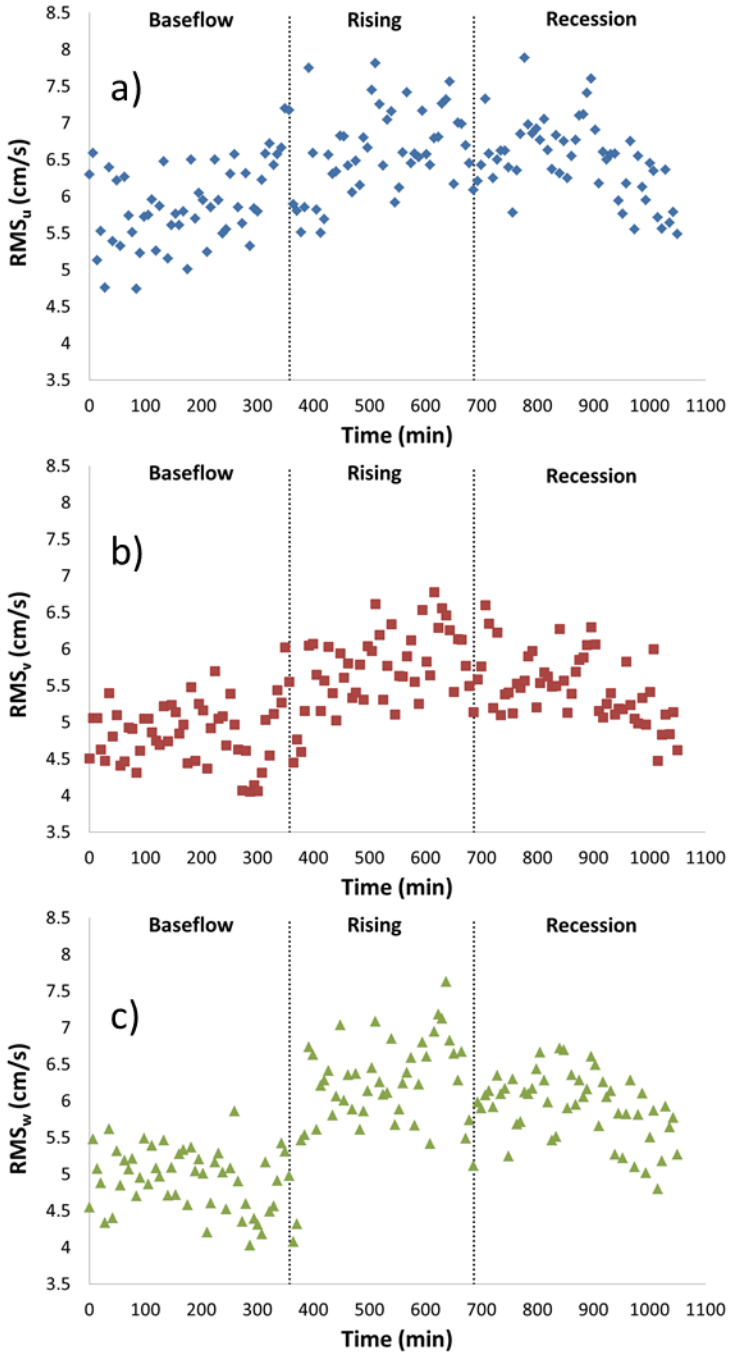

Figure 16. a) Turbulence intensity component RMS_u vs. time; b) turbulence intensity component RMS_v vs. time; c) turbulence intensity component RMS_w vs. time through a storm event starting on 10/11/2011

Table 7. Turbulence intensity statistics (RMS_u, RMS_v, and RMS_w) for the mean, median (in italics), and range (in parentheses) values.

	Baseflow	Rising	Recession
RMS_u (cm/s)	5.90	6.59	6.49
	5.84	*6.58*	*6.52*
	(2.45)	(2.31)	(2.41)
RMS_v (cm/s)	4.86	5.72	5.47
	4.92	*5.77*	*5.41*
	(1.97)	(2.33)	(2.12)
RMS_w (cm/s)	4.93	6.18	5.92
	4.99	*6.24*	*5.98*
	(1.83)	(3.55)	(1.92)

TKE as the flow approached the peak was 38% greater than the average TKE at baseflow. The distribution also reflects the change in stage throughout the storm hydrograph. The plot of TKE with time (Figure 17) follows the general trend of the velocity distributions (Figure 14). The TKE plot also resembles the RMS_w plot which indicates that the vertical turbulence fluctuations likely have a substantial impact on erosion potential throughout the rising limb of a storm hydrograph. The previous statement is also supported by the large value of the range of TKE on the rising limb (Table 8), indicating that significant fluvial erosion may occur throughout this period assuming elevated TKE values represent potential for erosion (Sumer et al., 2003; Diplas et al., 2008, Celik et al., 2010). These results need further verification with field measurements of erosion.

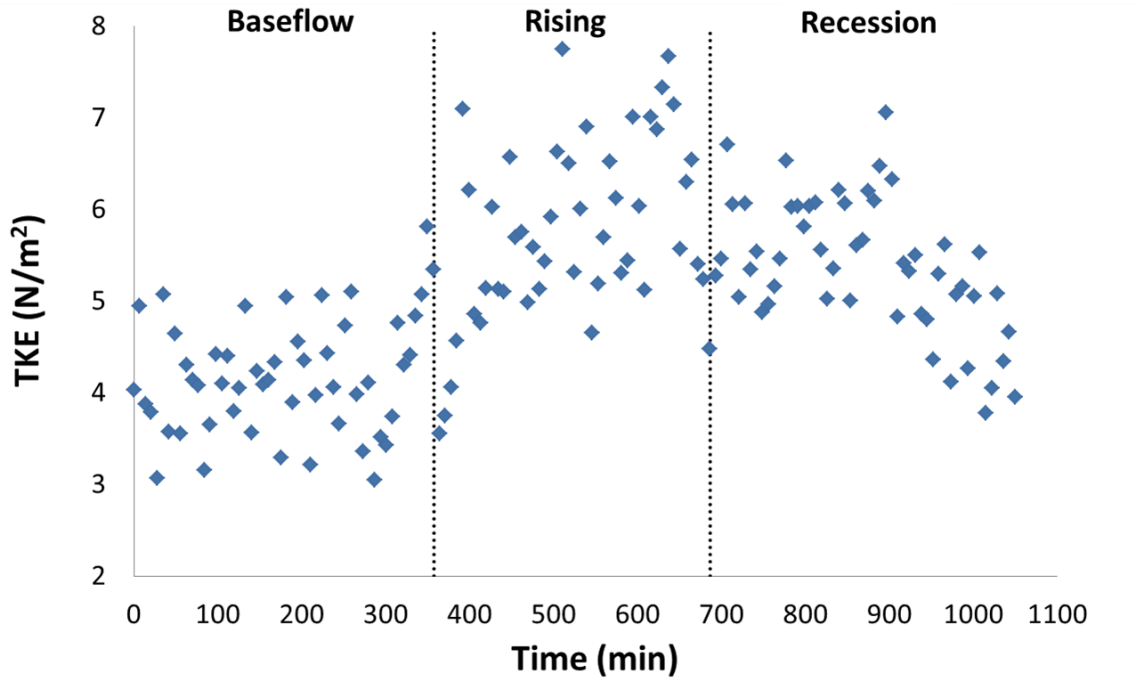

Figure 17. Distribution of turbulent kinetic energy with time for the 10/11/2011 storm event

Table 8. TKE statistics for the mean, median (in italics), and range (in parentheses) values.

	Baseflow	Rising	Recession
TKE (N/m^2)	4.18	5.77	5.39
	4.11	*5.70*	*5.39*
	(2.76)	(4.19)	(3.27)

4.1.4 Influence of stage height

The excess shear stress equation states that erosion rates are proportional to the difference in applied shear stress and critical shear stress (Hanson and Simon, 2001). Streambank applied shear stress is often estimated using the average boundary shear stress equation (Equation 4). Because it is likely that erosion occurs due to increased turbulence (Daniels and Rhoads, 2004), turbulence statistics (e.g. TKE, Reynolds stress) can estimate τ_a. This section evaluates τ_a predictions using Equation 4 and by turbulence statistics (Equations 5, 7, and 8).

While Equation 4 uses easily obtainable field data to approximate local applied shear stress, the equation over-estimated the local applied shear stress as estimated with turbulence characteristics by roughly 18 to 43 times (Figure 21). Trends associated with hydraulic radius were sought out for possible prediction of erosion potential throughout a storm event.

For the given range of hydraulic radii, the overall mean values of τ_{uv} and τ_{uw} are 0.75 Pa and -0.23 Pa respectively. Reynolds stresses did not significantly increase with an increase in water depth (Figure 18). This may be due to the measurement location of the ADV. The results suggest that Reynolds stresses are roughly the same value at every time throughout a storm hydrograph. Further validation from field measurements over a wide range of discharges is needed.

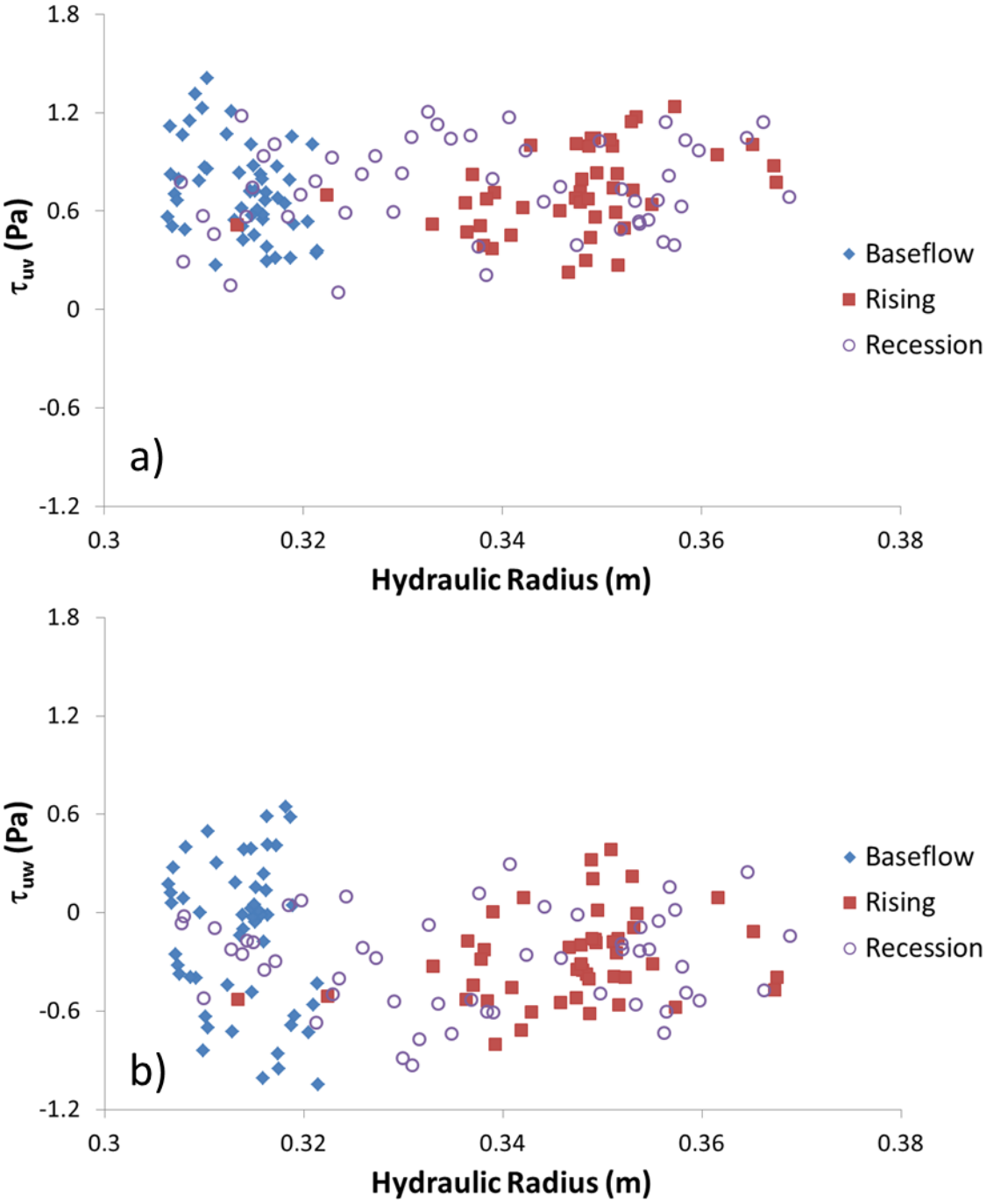

Figure 18. a) Reynolds stress component τ_{uv} vs. hydraulic radius; b) Reynolds stress component τ_{uw} vs. hydraulic radius through a storm event starting on 10/11/2011

For the given range of hydraulic radii, the overall mean magnitude of TKE was 5.09 N/m^2. The magnitude of the mean TKE throughout the rising limb was larger than the mean TKE value throughout baseflow and the recession limb. A linear regression (R^2 = 0.41, P-value = $1.3E^{-18}$) indicates that TKE increases linearly with an increase in hydraulic radius (Figure 19).

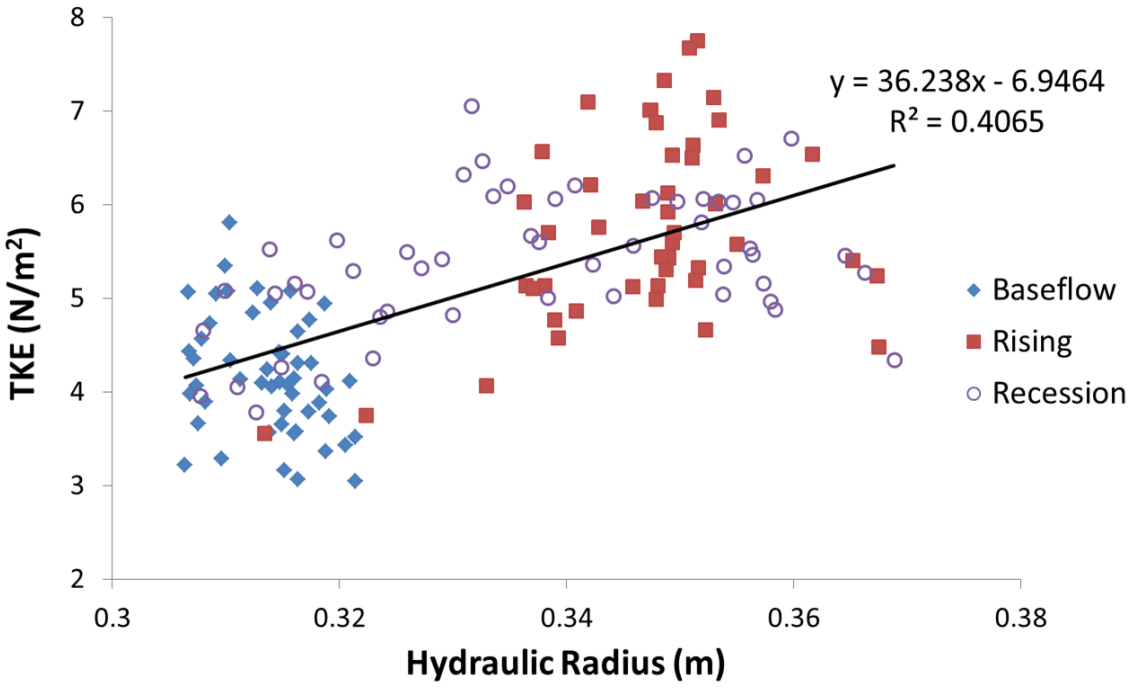

Figure 19. Turbulent kinetic energy vs. hydraulic radius through a storm event starting on 10/11/2011

Median applied shear stresses estimated by TKE were an order of magnitude greater than the Reynolds stresses during the storm event. A linear regression (R^2 = 0.41, P-value = $1.3E^{-18}$) indicates that applied shear stresses estimated by TKE increase linearly with an increase in hydraulic radius (Figure 20).

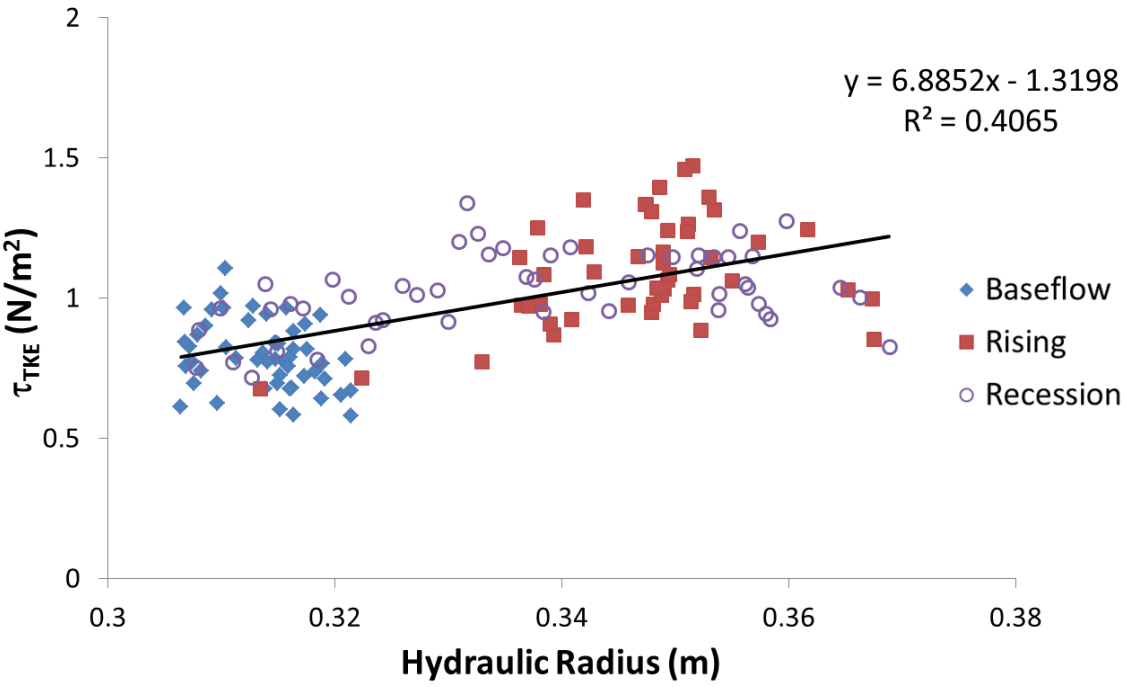

Figure 20. τ_{TKE} vs. hydraulic radius through a storm event starting on 10/11/2011

A comparison of the magnitudes and slopes of τ_{TKE} and τ_{avg} indicates significant differences (Figure 21). Applied shear stress estimated by average boundary shear stress was roughly 18 to 43 times greater than applied shear stress estimated by TKE. This comparison indicates that calculating the estimated applied shear stress using these two methods would produce significantly different results. Erosion prediction would be greatly influenced by the use of the different methods which incorporates a large range of possible error. The slopes of the distributions also differ, which indicates that erosion prediction using each of the methods would result in dissimilar rates throughout a storm event.

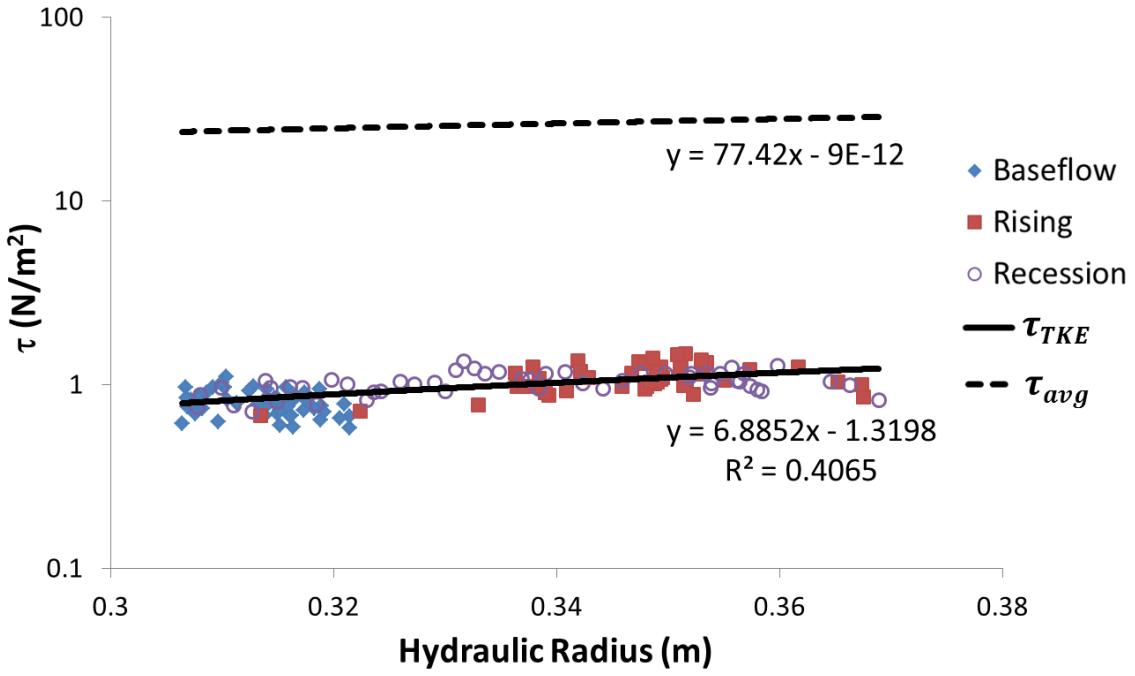

Figure 21. Average boundary shear stress and applied shear stress estimated by TKE vs. hydraulic radius through a storm event starting on 10/11/2011 (y-axis in log scale)

4.2 ADCP Results

Two-dimensional velocity and stage were measured using a Sontek SL3000 at the experimental cross-section at baseflow and throughout a storm event (5 min sample time at 1 Hz). Velocity samples were analyzed by calculating turbulence parameters: Reynolds stresses, turbulent kinetic energy (TKE), and turbulence intensity.

4.2.1 Storm Event

The results discussed in the following sections correspond to the August 12-16, 2011 SL3000 deployment. This deployment was one of three that resulted in the most complete data set. Throughout this time span, an approximately eight hour storm event occurred in which the SL3000 recorded two-dimensional velocity and stream stage. The data set used for the analysis consisted of 101 time-averaged samples. Figure 22 shows the velocity components and stage

height of the stream throughout the storm event. The overall magnitudes of the downstream and lateral velocity components increased from baseflow through the rising limb of the storm hydrograph.

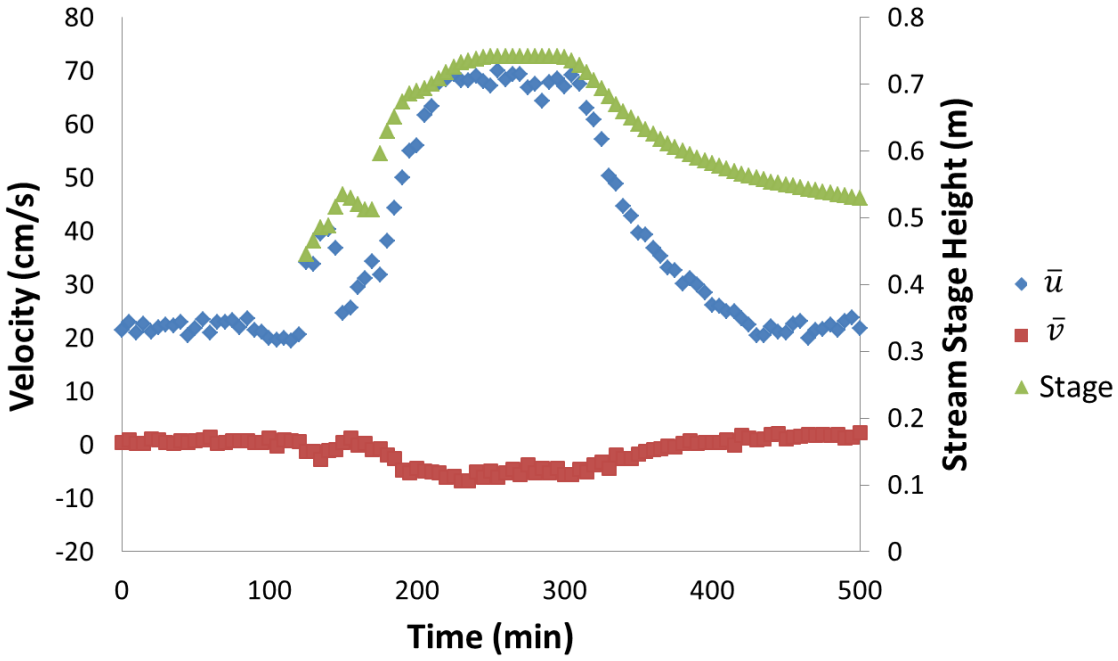

Figure 22. Time-averaged velocity ($\bar{u}$ and $\bar{v}$) and stream stage height vs. time through a storm event starting on 8/14/2011

The minimum stage height throughout baseflow was 0.45 m. The stage height of the stream at peak flow was 0.74 m. This difference results in a stage height fluctuation of 0.29 m throughout the storm event. Figure 23 depicts the stream stage fluctuation from baseflow to peak flow at the experimental cross-section throughout the storm event.

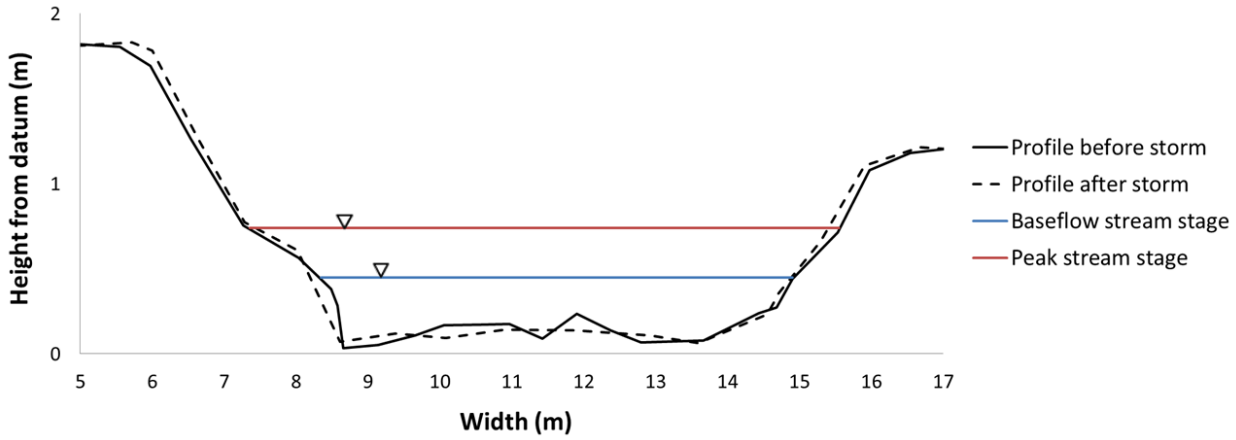

Figure 23. Experimental stream cross-section (vertical exaggeration) showing baseflow and peak stream stage height through a storm event starting on 8/14/2011

The stream flow remained in the primary channel throughout the baseflow portion of the storm event. Throughout the rising limb of the storm hydrograph the flow extended over a bench resulting in increased energy dissipation. Minimal changes in stream geometry were detected from the plots of the cross-sectional stream profiles before and after the single storm. The total area of the experimental cross-section increased by less than 2% from the pre-storm survey to the post-storm survey. The survey data reflects a minimal change in cross-sectional area which may be attributed to fluvial scour and bank erosion upstream or human error in data collection.

Vegetation size and density was monitored before and after this storm event with picture documentation (Figure 24). No major changes in vegetation were observed (stem density = 0.33 stems/cm^2). Channel roughness was also monitored before and after the deployment using a modified Wolman Pebble Count. The D50 and D84 of the channel prior to the deployment were 29 mm and 87 mm, respectively. The D50 and D84 of the channel after the deployment were 32 mm and 120 mm, respectively.

Figure 24. a) Pre-storm vegetation documentation on 8/12/2011; b) Post-storm vegetation documentation on 8/16/2011

4.2.2 Turbulence Statistics

Due to limitations of the instrument, only the stream-wise and lateral velocity components of flow were used to calculate turbulence statistics for the data set. A modified version of equation 6 is used in this section to provide an understanding of the overall turbulence of the flow recorded by the SL3000 (Equation 12). Generally, the downstream (u), lateral (v), and vertical (w) components of flow are used to calculate TKE. However, the SL3000 contains two profiling sensors and only has the capability to measure two-dimensional flow. Since the SL3000 was deployed in a horizontal orientation for this study, the downstream and lateral components of flow were the only available data that could be incorporated into the calculation of the turbulence statistics. Another significant drawback of the SL3000 is the fact that the individual velocity time series cannot be analyzed. The output files for the SL3000 only contain the time-averaged data for the deployment.

$$TKE_{ADCP} = \rho 0.5(\overline{u'^2} + \overline{v'^2}) \quad (12)$$

Figure 25 depicts the distribution of the downstream and lateral turbulence intensity throughout time. The average value of RMS_u was 17.1 cm/s with a maximum observed value of 26.0 cm/s. The average value of RMS_v was 6.05 cm/s with a maximum observed value of 10.4 cm/s.

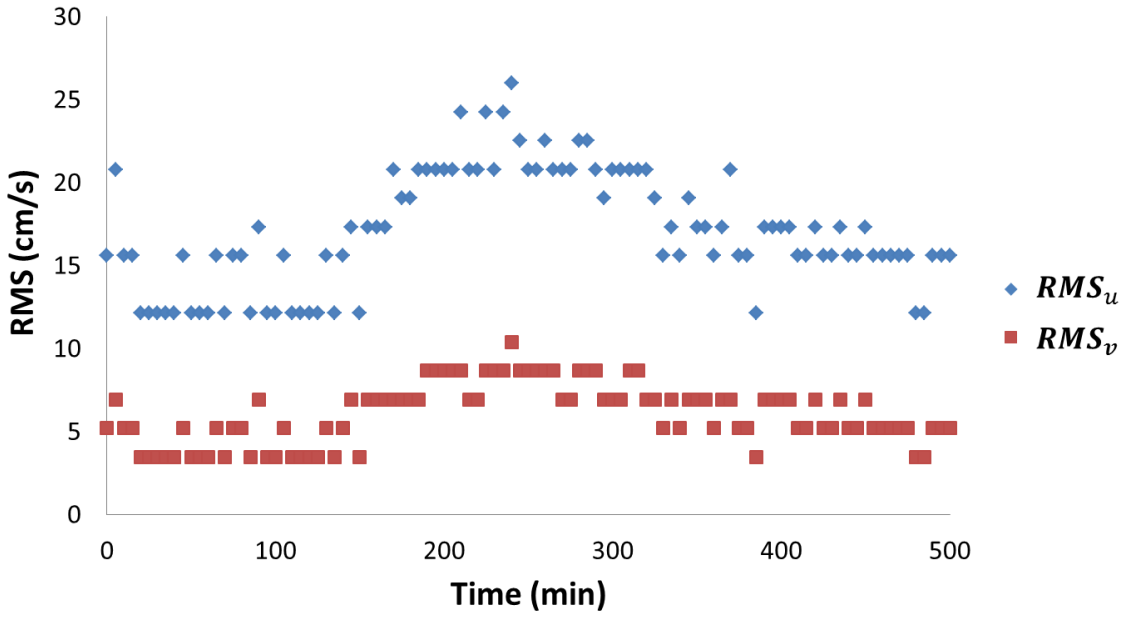

Figure 25. Turbulence intensity components RMS_u and RMS_v vs. time through a storm event starting on 8/14/2011

Figure 26 depicts the distribution of turbulent kinetic energy throughout time. The distribution of TKE_{ADCP} increased with the rising limb and decreased with the recession limb of the hydrograph. The average value of TKE_{ADCP} is 17.2 N/m^2 with a maximum observed value of 39.2 N/m^2.

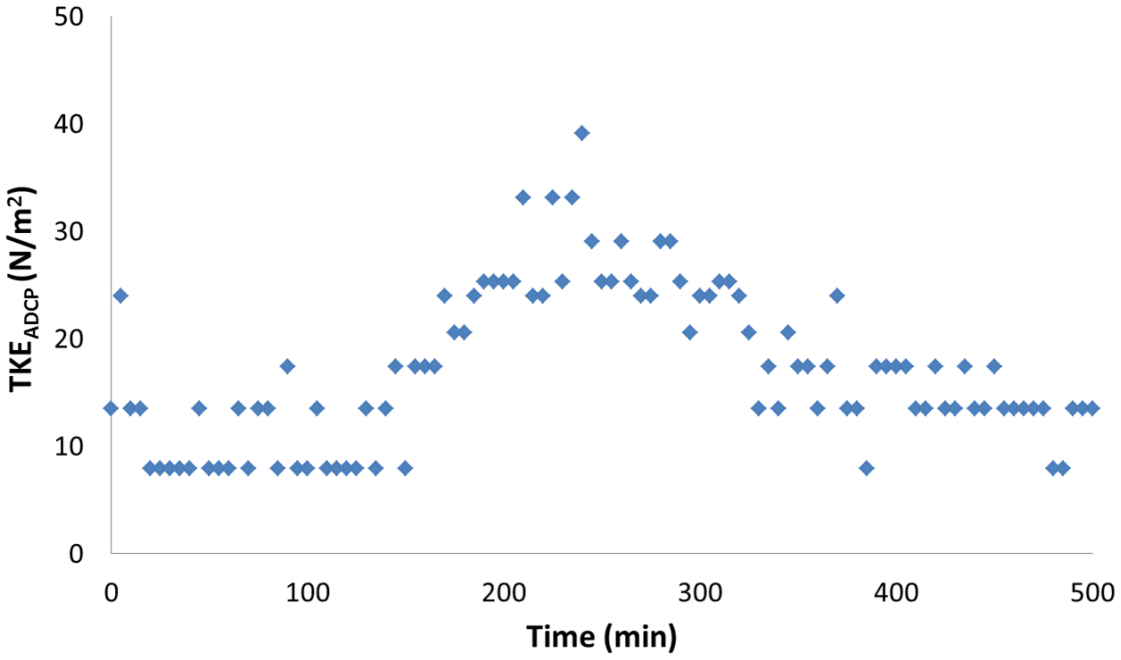

Figure 26. Distribution of turbulent kinetic energy with time for the 10/11/2011 storm event

4.2.3 Influence of stage height

Like the analysis completed with the ADV, the influence of stage height was considered. Comparison of the magnitudes of $\tau_{TKE_{ADCP}}$ and τ_{avg} show considerable differences (Figure 27). Applied shear stress estimated by average boundary shear stress was roughly 5 to 20 times greater than applied shear stress estimated by TKE_{ADCP} ($\tau_{TKE_{ADCP}} = 0.19 \times TKE_{ADCP}$). The slopes of the distributions of TKE_{ADCP} and applied shear stress estimated by TKE_{ADCP} are

negative, while the slope of applied shear stress estimated by average boundary shear stress is positive, which indicates that erosion prediction using each of the methods would result in dissimilar results. This comparison indicates that calculating the estimated applied shear stress using these methods would produce significantly different results. Erosion prediction would be greatly influenced by the use of the different methods, which incorporates a large range of possible error.

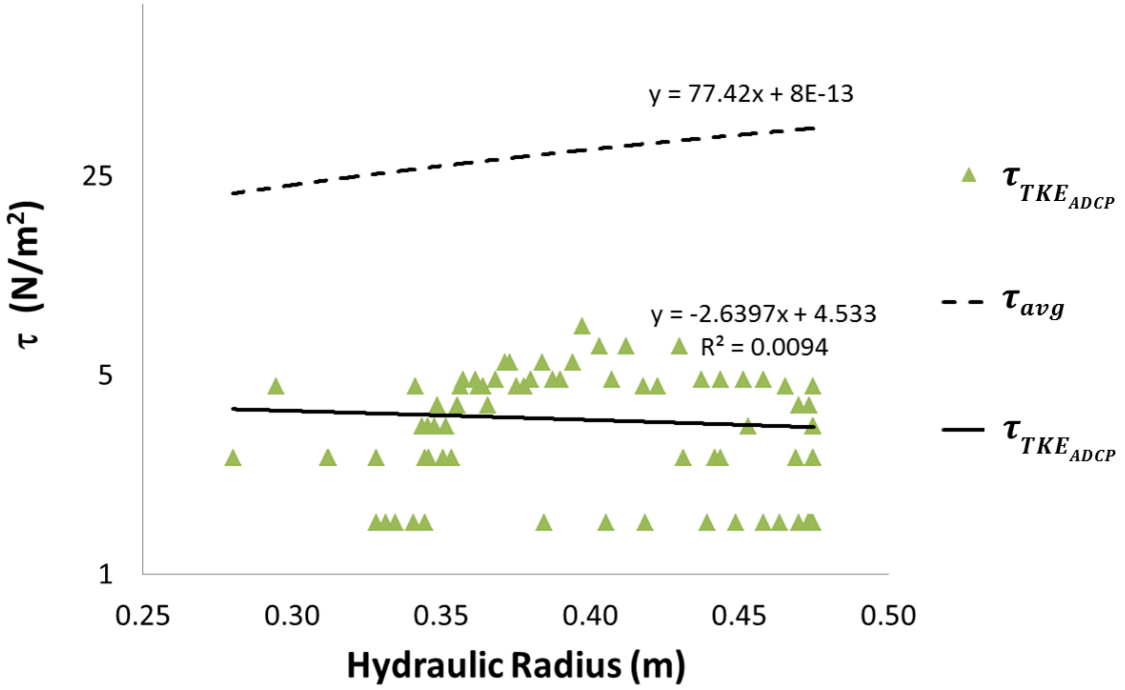

Figure 27. Average boundary shear stress and applied shear stress estimated by TKE_{ADCP} vs. hydraulic radius through a storm event starting on 8/14/2011(y-axis in log scale)

4.3 Comparison of ADV and ADCP

Only the lateral and stream-wise components of velocity are compared in this section due to limitations in the measurement capability of the SL3000 (See section 4.2.2). The data suggest that measured values of velocity using an ADV and an ADCP may result in substantially different results (Figures 21 and 27). These differences may be attributed to a number of

variables. The difference in the size of the measurement control volume varied between the ADV and ADCP. The ADV has the capability to measure a very small control volume (0.09 cm^3) with respect to the large profiling length of the ADCP (0.5 m). The ADCP averages the two-dimensional velocity over this length, while the ADV has the capability to record instantaneous three-dimensional values of velocity in a small control volume. The ADCP also incorporates a minimum 10 cm blanking distance from the face of the instrument to the start of the sample interval. This blanking distance, along with a much larger sampling area with respect to the ADV, may limit the ability of the ADCP to obtain near-bank velocity data in future studies. The frequency of measurement of the ADV (25 Hz) and SL3000 (1 Hz) may also have contributed to the noticeable differences in the obtained field data.

It is notable that the downstream ($\bar{u}$) and lateral ($\bar{v}$) components of velocity measured by the SL3000 were greater than the downstream and lateral components of velocity measured by the ADV for the larger values of hydraulic radii (Figure 28). However, the lateral velocity component measured by the ADV was greater than the lateral velocity component measured by the SL3000 for smaller values of hydraulic radii (Figure 28 b). This difference in the results may be influenced by the large sampling volume over which the velocity is averaged using the SL3000 or the different measurement frequency of the two instruments.

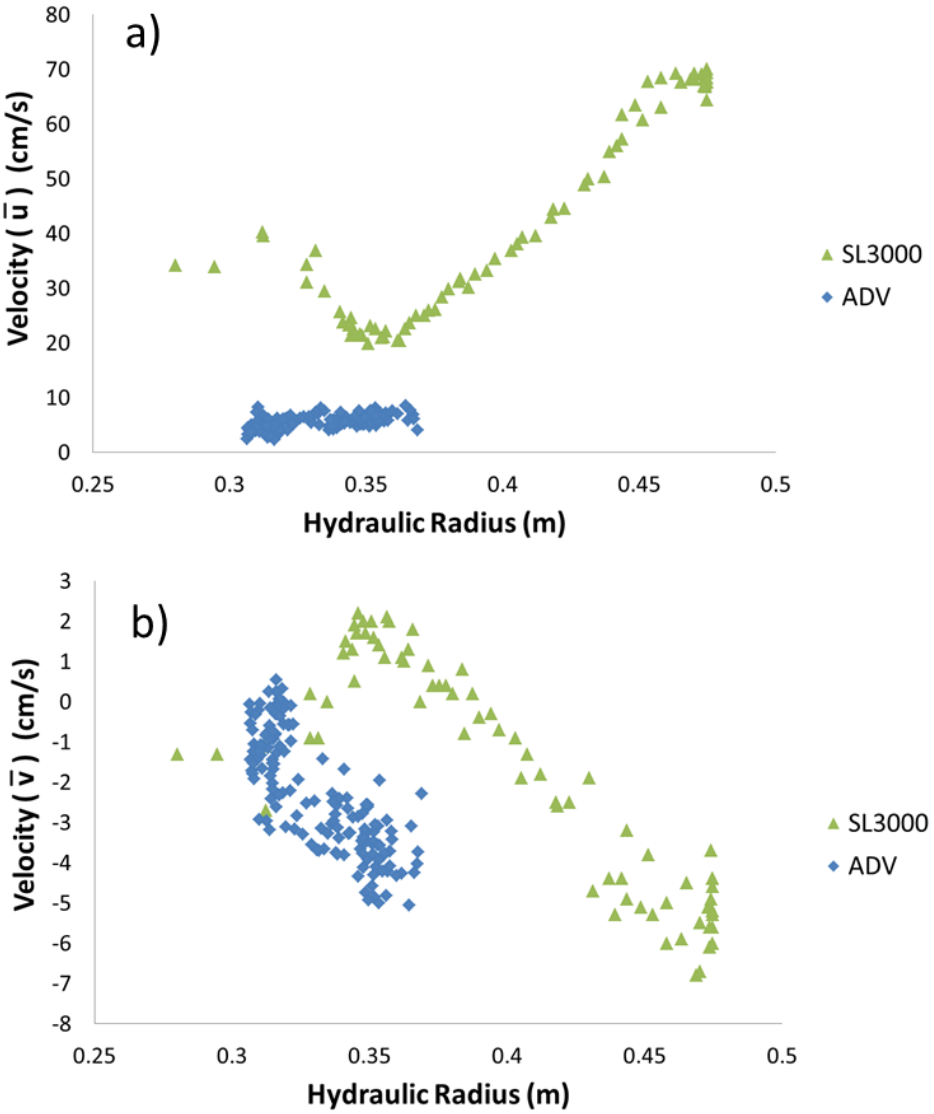

Figure 28. a) Time-averaged velocity ($\bar{u}$) vs. hydraulic radius for the ADV and SL3000; b) Time-averaged velocity ($\bar{v}$) vs. hydraulic radius for the ADV and SL3000

This study provided a useful comparison of the measurement capabilities between an ADV and an ADCP. It was found that the ADCP had many favorable attributes including ease of use and the ability to be deployed for an extended period of time without incurring problems with memory or power limitations. The ADCP also has the capability to calculate stream discharge in the user-specified log file developed initially for the instrument deployment. The ADV has memory and power limitations which dictate the sampling frequency, sample time, and duration of testing. The replacement cost of the power source for the ADV would be much higher with respect to replacing the power source for the ADCP used in this study. A drawback to the ADCP in measuring near-bank velocity is the blanking distance required for deployment and the large sample area over which the measurements are recorded. The ADV was able to obtain velocity data in a small control volume near the stream bank.

The mounting apparatus for the ADV appeared to be more favorable for near-bank measurements. The mounting apparatus for the ADCP required significant material and space, which may have interfered in the data collection and streambank characteristics (roughness, shape, shielding). The ADV shows the higher potential for estimating local applied shear stress due to its ability to obtain measurements close to the streambank at high frequencies with no initial calibration. The ADV also does not interfere with bank vegetation. Although the ADCP was easy to set up and use over extended periods of time, it lacked the ability to obtain three-dimensional velocity, which is important in analyzing the turbulent structure of flow.

5.0 Conclusions and Future Work

5.1 Conclusions

The goal of this research was to characterize the turbulence structure of flow near the toe of a streambank throughout a storm event, at times of high shear stress. The specific objectives included the following:

1. Design and build a field mount to support in-stream velocimeters during high flow events.
2. Quantify the distribution of Reynolds stresses and turbulent kinetic energy (TKE) throughout a storm hydrograph.
3. Identify the relationship between hydraulic radius and turbulent stresses.

Near-bank velocity was measured with an ADV and a SL3000 (ADCP) through two individual storm events. This research resulted in the following:

1. Methods were developed for ADV and ADCP deployment throughout storm events, including the use of two custom fabricated mounts.
2. While Reynolds stress was expected to follow trends with increasing stage height, the results obtained indicated no linear trend. TKE, on the other hand, increased with increasing stage height which may shed useful insight into erosion potential throughout storm events.

3. A comparison of the ADV and ADCP used in this study indicate that the ADV shows the higher potential for estimating local applied shear stress due to its ability to obtain three-dimensional velocity measurements close to the streambank at high frequencies with no initial calibration.
4. Applied shear stress estimated by average boundary shear stress was 18 to 43 times greater than those estimated by turbulence statistics. The result may alter the ability of models to predict erosion depending on the method that is used.
5. Significant ADCP limitations were found in the ability to estimate near-bank turbulence. The most notable limitations include the control volume size, location of measurement, measurement frequency, and the inability to analyze velocity time series data.

5.2 Future work

This research resulted in methods to measure near-bank turbulence; however there were limitations and opportunities for future work. Adding in secondary circulation parameters would help to provide insight into the turbulent characteristics of the flow. There is also a need to relate near-bank turbulence to actual erosion rates. The results from this study need to be confirmed at multiple locations with a range of systems, varying bank geometries, multiple stages of instability, a range of bank vegetation types and densities, and temporal effects.

6.0 References

Bhowmik, N. G, (1982). Shear stress distribution and secondary currents in straight open channels. In *Gravel-Bed Rivers*, 31-62. Hey, R. D., J.C. Bathurst, and C. R. Thorne, ed. New York, NY: John Wiley and Sons.

Biron PM, Robson C, Lapointe MF, Gaskin SJ. (2004). Comparing different methods of bed shear stress estimates in simple and complex flow fields. Earth Surface Processes Landforms 29: 1403–1415. DOI:10D1002/esp.1111.

Celik, A. O., Diplas, P., Dancey, C. L., & Valyrakis, M. (2010). Impulse and particle dislodgement under turbulent flow conditions. *Physics of Fluids, 22*(4), 046601. doi:10.1063/1.3385433

Chang, H. H. (2002). *Fluvial Processes in River Engineering.* Malabar, FL.: Krieger Publishing.

Clark, L. A., & Wynn, T. M. (2007). Methods for determining streambank critical shear stress and soil erodibility: Implications for erosion rate predictions. *Transactions of the Asabe, 50*(1), 95-106.

Couper, P. (2003). Effects of silt-clay content on the susceptibility of river banks to subaerial erosion. *Geomorphology, 56*(1-2), 95-108. doi:10.1016/S0169-555X(03)00048-5

Couper, P., & Maddock, I. (2001). Subaerial river bank erosion processes and their interaction with other bank erosion mechanisms on the river arrow, Warwickshire, UK. *Earth Surface Processes and Landforms, 26*(6), 631-646. doi:10.1002/esp.212

Daniels, M., Rhoads, B.L. (2004). Spatial pattern of turbulence kinetic energy and shear stress in a meander bend with large woody debris. Paper presented at the *Riparian Vegetation and Fluvial Geomorphology,* pp. 87-97.

Dey, S., Sarkar, S., & Solari, L. (2011). Near-bed turbulence characteristics at the entrainment threshold of sediment beds. *Journal of Hydraulic Engineering, 137*(9), 945-958. doi:10.1061/(ASCE)HY.1943-7900.0000396

Diplas, P., Dancey, C. L., Celik, A. O., Valyrakis, M., Greer, K., & Akar, T. (2008). The role of impulse on the initiation of particle movement under turbulent flow conditions. *Science, 322*(5902), 717-720. doi:10.1126/science.1158954

Fraley LM, Miller AJ, Welty C. (2009). Contribution of in-channel processes to sediment yield of an urbanizing watershed. J. AWRA 45: 748-766.

Grissinger, E. H, (1982). Bank erosion of cohesive materials. In *Gravel-Bed Rivers*, 273-287. Hey, R. D., J.C. Bathurst, and C. R. Thorne, ed. New York, NY: John Wiley and Sons.

Hanson, G. (1990). Surface erodibility of earthen channels at high stresses .2. developing an insitu testing device. *Transactions of the ASAE, 33*(1), 132-137.

Hanson, G. J., and K. R. Cook. (1997). Development of Excess shear stress parameters for circular jet testing. ASAE Paper No. 972227. Minneapolis, Minn.: ASAE.

Hanson, G. J., K. R. Cook, and A. Simon. (1999). Determining erosion resistance of cohesive materials. In *Proceedings of the ASCE International Water Resources Engineering Conference.* CD-ROM. Seattle, WA: ASCE.

Hanson, G., & Simon, A. (2001). Erodibility of cohesive streambeds in the loess area of the midwestern USA. *Hydrological Processes, 15*(1), 23-38. doi:10.1002/hyp.149

Harrelson, C. C., Rawlins, C. L., Potyondy, J. P., & Rocky Mountain Forest and Range Experiment Station (Fort Collins,Colo.). (1994). *Stream channel reference sites: An illustrated guide to field technique* No. 245). Fort Collins, Colo. (240 W. Prospect Rd., Ft. Collins 80526): U.S. Dept. of Agriculture, Forest Service, Rocky Mountain Forest and Range Experiment Station.

Hopkinson, L., & Wynn, T. (2009). Vegetation impacts on near bank flow. *Ecohydrology, 2*(4), 404-418. doi:10.1002/eco.87

Hopkinson, L., & Wynn-Thompson, T. (2012). Streambank shear stress estimates using turbulent kinetic energy. *Journal of Hydraulic Research, 50*(3), 320-323. doi:10.1080/00221686.2012.684771

Julian, J., & Torres, R. (2006). Hydraulic erosion of cohesive riverbanks. *Geomorphology, 76*(1-2), 193-206. doi:10.1016/j.geomorph.2005.11.003

Julien, P. Y. (2002). Ch. 8: River stabilization. *River mechanics* (pp. 234). Cambridge, U.K. ;New York: Cambridge University Press.

Kim, S. C., C.T. Friedrichs, J.P.Y. Maa, and L.D. Wright. (2000). Estimating bottom stress in a tidal boundary layer from acoustic Doppler velocimeter data. *Journal of Hydraulic Engineering*, 126 (6), 399-406.

Lawler, D. M., C. R. Thorne, and J. M. Hooke. (1997). Bank erosion and instability. In *Applied Fluvial Geomorphology for River Engineering and Management*. C. R. Thorne, R. D. Hey, and M. D. Newson, eds. New York, N.Y.: John Wiley and Sons.

Luppi, L., Rinaldi, M., Teruggi, L. B., Darby, S. E., & Nardi, L. (2009). Monitoring and numerical modelling of riverbank erosion processes: A case study along the cecina river (central italy). *Earth Surface Processes and Landforms, 34*(4), 530-546. doi:10.1002/esp.1754

Midgley, T. L., Fox, G. A., & Heeren, D. M. (2012). Evaluation of the bank stability and toe erosion model (BSTEM) for predicting lateral retreat on composite streambanks. *Geomorphology, 145–146*(0), 107-114. doi:10.1016/j.geomorph.2011.12.044

Nepf, H. M. (2012). Hydrodynamics of vegetated channels. *Journal of Hydraulic Research, 50*(3), 262-279. doi:10.1080/00221686.2012.696559

Osman, A. M., and C. R. Thorne. (1988). Riverbank stability analysis I: theory. *J. Hydraulic Eng.* 114(2): 134-150.

Ostercamp W.R., Heilman P., and Lane L.J. Internation Journal of Sediment Research. Vol. 13, No.4, Dec. (1998). Economic Considerations of a Continental Sediment Monitoring Program.

Papanicolaou, A. N., Elhakeem, M., & Hilldale, R. (2007). Secondary current effects on cohesive river bank erosion. *Water Resources Research, 43*(12), W12418. doi:10.1029/2006WR005763

Partheniades, E. (1965). Erosion and deposition of cohesive soils. *J. Hydraulics Division Proceedings of the American Society of Civil Engineers* 91(HY1): 105-139.

Prosser, I., Hughes, A., & Rutherfurd, I. (2000). Bank erosion of an incised upland channel by subaerial processes: Tasmania, Australia. *Earth Surface Processes and Landforms, 25*(10), 1085-1101. doi:10.1002/1096-9837(200009)25:10<1085::AID-ESP118>3.0.CO;2-K

Reid, I., Frostick, L. E., & Layman, J. T. (1985). The incidence and nature of bedload transport during flood flows in coarse-grained alluvial channels. *Earth Surface Processes and Landforms, 10*(1), 33-44. doi:10.1002/esp.3290100107

Reid, L. & Frostick, L.E. (1984) Particle interactions and its effect on the thresholds of initial and final bed load motion in coarse alluvial channels. In: Sedimentology of Gravels and Conglomerates (ed. by F.H. Koster & R.L. Steel). Can. Soc. of Petrol. Geol. Mem. 10, 61-68 .

Rinaldi, M., Mengoni, B., Luppi, L., Darby, S. E., & Mosselman, E. (2008). Numerical simulation of hydrodynamics and bank erosion in a river bend. *Water Resources Research, 44*(9), W09428. doi:10.1029/2008WR007008

Rominger, J. T., Lightbody, A. F., & Nepf, H. M. (2010). Effects of added vegetation on sand bar stability and stream hydrodynamics. *Journal of Hydraulic Engineering, 136*(12), 994-1002. doi:10.1061/(ASCE)HY.1943-7900.0000215

Schlichting H, Gersten K. 2000. Boundary-Layer Theory, 8th ed. Springer-Verlag: Berlin, Germany.

Shields, F., & Rigby, J. (2005). River habitat quality from river velocities measured using acoustic doppler current profiler. *Environmental Management, 36*(4), 565-575. doi:10.1007/s00267-004-0292-6

Simon A, Rinaldi M. (2000). Channel instability in the loess area of the Midwestern United States. J. AWRA 36: 133-150.

Simon, A., & Collison, A. (2002). Quantifying the mechanical and hydrologic effects of riparian vegetation on streambank stability. *Earth Surface Processes and Landforms, 27*(5), 527-546. doi:10.1002/esp.325

Smerdon, E. T., and R. P. Beasley. (1961). Critical tractive forces in cohesive soils. *Agric. Eng.* 26-29.

Sontek/YSI. (2001). ADV field/ Hydra acoustic Doppler velocimeter (field) operation manual.

Sontek/YSI. (2009). Argonaut-SL system manual. Firmware version 12.0.

Soulsby, R.L. (1983). The bottom boundary layer of shelf seas. Physical oceanography of coastal and shelf seas, 189–266, B. Johns, ed. Elsevier, Amsterdam.

Strom Kyle B., & Papanicolaou Athanasios N. (2007). ADV measurements around a cluster microform in a shallow mountain stream. *Journal of Hydraulic Engineering, 133*(12), 1379-1389.

Sumer, B., Chua, L., Cheng, N., & Fredsoe, J. (2003). Influence of turbulence on bed load sediment transport. *Journal of Hydraulic Engineering-Asce, 129*(8), 585-596. doi:10.1061/(ASCE)0733-9429(2003)129:8(585)

The West Virginia Water Research Institute, & The West Run Watershed Association. (2008). *Watershed based plan for west run of the monongahela river* (Watershed Plan West Virginia Department of Environmental Protection.

Thorne, C. R. (1990). Effects of vegetation on riverbank erosion and stability, chapter 10. In Thornes JB (Ed.), *Vegetation and erosion* (pp. 125-144). West Sussex, England: John Wiley and Sons.

Thorne, C. R. (1982). Processes and mechanisms of river bank erosion. In *Gravel-bed Rivers, 227-259.* Hey, R. D., J. C. Bathurst, and C. R. Thorne, ed. New York, NY: .John Wiley and Sons.

Thorne, C. R. (1998). River width adjustment. I: Processes and mechanisms. *Journal of Hydraulic Engineering, 124*(9), 881.

USEPA. (2009), National Water Quality Inventory: 2004 Report to Congress. EPA 841-R-08-001. USEPA: Washington, DC.

Voulgaris, G., & Trowbridge, J. (1998). Evaluation of the acoustic doppler velocimeter (ADV) for turbulence measurements. *Journal of Atmospheric and Oceanic Technology, 15*(1), 272-289. doi:10.1175/1520-0426(1998)015<0272:EOTADV>2.0.CO;2

Willett C.D., Lerch R.N., Schultz R.C., Berges S.A., Peacher R.D., Isenhart T.M. (2012). Streambank erosion in two watersheds of the Central Claypan Region of Missouri, United States. J. Soil and Water Conservation 67(4): 249-263.

Wolman, M. G. (1954). A method of sampling coarse river-bed material. *Trans. Am. Geophys. Union, 35*, 951 – 956.

Wood, A. L., Simon, A., Downs, P. W., & Thorne, C. R. (2001). Bank-toe processes in incised channels: The role of apparent cohesion in the entrainment of failed bank materials. *Hydrological Processes, 15*(1), 39-61. doi:10.1002/hyp.151

Wynn, T. M., Henderson, M. B., & Vaughan, D. H. (2008). Changes in streambank erodibility and critical shear stress due to subaerial processes along a headwater stream, southwestern virginia, USA. *Geomorphology, 97*(3-4), 260-273. doi:10.1016/j.geomorph.2007.08.010

Wynn, T., & Mostaghimi, S. (2006) a. The effects of vegetation and soil type on streambank erosion, southwestern virginia, USA. *Journal of the American Water Resources Association, 42*(1), 69-82. doi:10.1111/j.1752-1688.2006.tb03824.x

Wynn, T., & Mostaghimi, S. (2006) b. Effects of riparian vegetation on stream bank subaerial processes in southwestern virginia, USA. *Earth Surface Processes and Landforms, 31*(4), 399-413. doi:10.1002/esp.1252

Wynn, T., Mostaghimi, S., Burger, J., Harpold, A., Henderson, M., & Henry, L. (2004). Variation in root density along stream banks. *Journal of Environmental Quality, 33*(6), 2030-2039.

7.0 Appendices

Appendix A: ADV and SL3000 Field Procedure and Checklists

Field Procedure

Pre-storm:

- Survey the stream cross-section at the test site
- Document vegetation of the stream by taking pictures (US,DS,LB,RB)
- Perform a Modified Wolman pebble count on the stream cross-section
- Set up the instrument
- Document the height and location of the instrument.
- Input the height of the instrument into the ViewArgonaut or SonUtils program
- Run the Deployment
- Download the survey data

Post-Storm:

- Stop the Deployment
- Survey the stream cross-section at the test site
- Document vegetation of the stream by taking pictures (US,DS,LB,RB)
- Perform a Modified Wolman pebble count on the stream cross-section
- Download the survey data
- Download rain gauge data
- Download the recorded deployment data file off of the instrument
- Open the deployment data file in one of the post-processing programs and examine the data
- Export the data files
- Open the exported data files in excel and plot the output graphs

SL3000 Checklist:

Material List

½” wrench	
Ratchet and ½” socket	
Duct tape	
Electrical tape	
Zip ties	
Mounting Plate	
Camera	
U bolts and hardware	
Underwater cable	
RS232 cable	
SL 3000	
Battery and Box	
SL 3000 mounting bolts	
Torque wrench	
Laptop	
Measuring Tape	

Input data

File Name	Site_Test#_Date_Initials.ARG
Averaging Interval (s)	300
Sampling Interval (s)	300
Cell Begin (m)	0.1
Cell End (m)	0.6
Profiling Mode	no
Blanking Distance (m)	0.1
Cell Size (m)	0.5
Number of Cells	1
Temperature Mode	Measured
Enable Flow Display	no
PowerPing	yes
Burst Mode	no
Baud Rate	9600

Field Activities

Take Pictures of RB,LB,US,DS	
Note any change in vegetation	
Note any visible bank erosion	

Data Download

Location: Zack Walburn > My Documents > Sontek SL 3000 > SL3000 Raw Data

16-MHz ADV Checklist:

Material List

Tool kits	
Mount	
Duct tape	
Electrical tape	
Zip ties	
Underwater cables	
RS232 cable	
ADV and Box	
Laptop	
Measuring Tape	
Camera	

Input data

File Name	Site_Test#_Date_Initials.adr
VelRange	3
SampRate (hz)	25
CoordSystem	XYZ
TempMode	Measured
BurstInterval (s)	420
SamplesPerBurst	2750
SampleTime (s)	120
Overhead (s)	10
Baud Rate	19200

Field Activities

Take Pictures of RB,LB,US,DS	
Note any change in vegetation	
Note any visible bank erosion	

Data Download

Location: Zack Walburn > My Documents > Sontek 16-MHz MicroADV > ADV Raw Data

Appendix B: Survey Procedure

Procedure for Developing a Cross Section Survey using the Leica TC600 Total Station

Setup

1. Drive a nail or rebar into the ground at a desired location.
2. Center the tripod legs and attached tribrach over the nail using the optical plummet.
3. Step on each tripod shoe to secure the tripod to the ground.
4. Use the leveling screws to center the cross hairs of the optical plummet over the nail.
5. Level the tripod by adjusting the legs so that the bubble is in the center of the bull's eye level on the tribrach.
6. Loosen the bolt connecting the tribrach to the tripod and slide the tribrach while using the optical plummet to center the cross hairs over the nail. Tighten the bolt once the tribrach is in the desired position.
7. Use the leveling screws on the tribrach again to center the bubble in the bull's eye level.
8. Repeat steps 5 and 6 as necessary, until both centering and leveling are achieved.
9. Ensure that both the horizontal and vertical motion clamps are unclamped on the total station.
10. Carefully place the total station onto the tribrach ensuring that the arrow on the tribrach clamp is facing up. The instrument will be secured once the tribrach clamp is turned and the arrow is facing downward.
11. Perform the electronic leveling on the total station.
12. Attach the Carlson data collector to the total station by lining up the red dot on the connecting cable with the corresponding mark on the receiving port of the instrument.

Survey

1. Set rod height = instrument height. > Set up prism/target beyond last cross section station.
2. Determine azimuth (AZ) of baseline (Guess or use hand compass).
3. Open SurvCE on the Carlson data collector and create a new job.
4. Establish 1st point coordinate (ex. 101).
5. Equipment tab > Select total station > Select TC600 > Load > Green check
6. Orient baseline AZ – Get coordinates of back sight (BS).
    - Sight BS target (ex. 110) / telescope
    - Survey tab > Store points
    - Enter BS point no.
    - BS, AZ
    - BS button > Use Azimuth
    - Continue
    - Set angle and read
    - Green Check
    - Label BS etc.
7. Exit Store Points
8. Cogo tab > Manual traverse
9. Enter occupy & BS point numbers.
10. Enter target point ID > Rt = 0°, HD = 50.00 ft > Calculate > Store
11. Repeat for 3rd, 4th, & 5th base station for each cross-section.
12. Exit Cogo tab
13. Stake points tab > Enter point # on baseline > Green check
14. Ensure rod height = instrument height
15. Place rod along baseline at approximate desired point # > [R] button = read > note direction and distance to move rod > Find correct location (when in/out & left/right is zero) > Physically drive a nail into the ground at this point >Mark location with a flag or stake.
16. Set all points on baseline.

17. Occupy each baseline station

- BS – can be either BL(101) or BS(110)
- Equipment tab > Load TC600 > Green check
- Survey tab > Store points > Green check
- Tripod legs icon (upper right) > enter occupy & BS points.
- BS button (lower left)
- Set angle (or set angle and read- this will display any discrepancies)
- Turn (90° or 270°) depending on BS point.
- Take readings on cross section (set initial point # on section)

Pack up and Return Equipment

1. Turn off Carlson data collector, disconnect all cables, and return to case.
2. Turn the power off on the instrument.
3. Equalize the leveling screws. There is a ring on the leveling screws to use in equalizing.
4. Open the horizontal and vertical motion clamps
5. Equalize both the horizontal and vertical motion tangent screws (Line up with the white line).
6. Dismount the instrument from the tripod.
7. Return the instrument to its case. The objective lens should face the handle and the tribrach clamp should face up in the case.
8. After the telescope and tribrach are in the correct positions, lightly clamp the horizontal and vertical motions.
9. Lower all three tripod legs to the lowest position and lock them into place.
10. Clean the tripod shoes and prism pole points with water and paper towels to remove any dirt or mud.
11. Ensure all equipment is clean and dry and replace back into their respective equipment lockers.

Appendix C: Physical Measurements

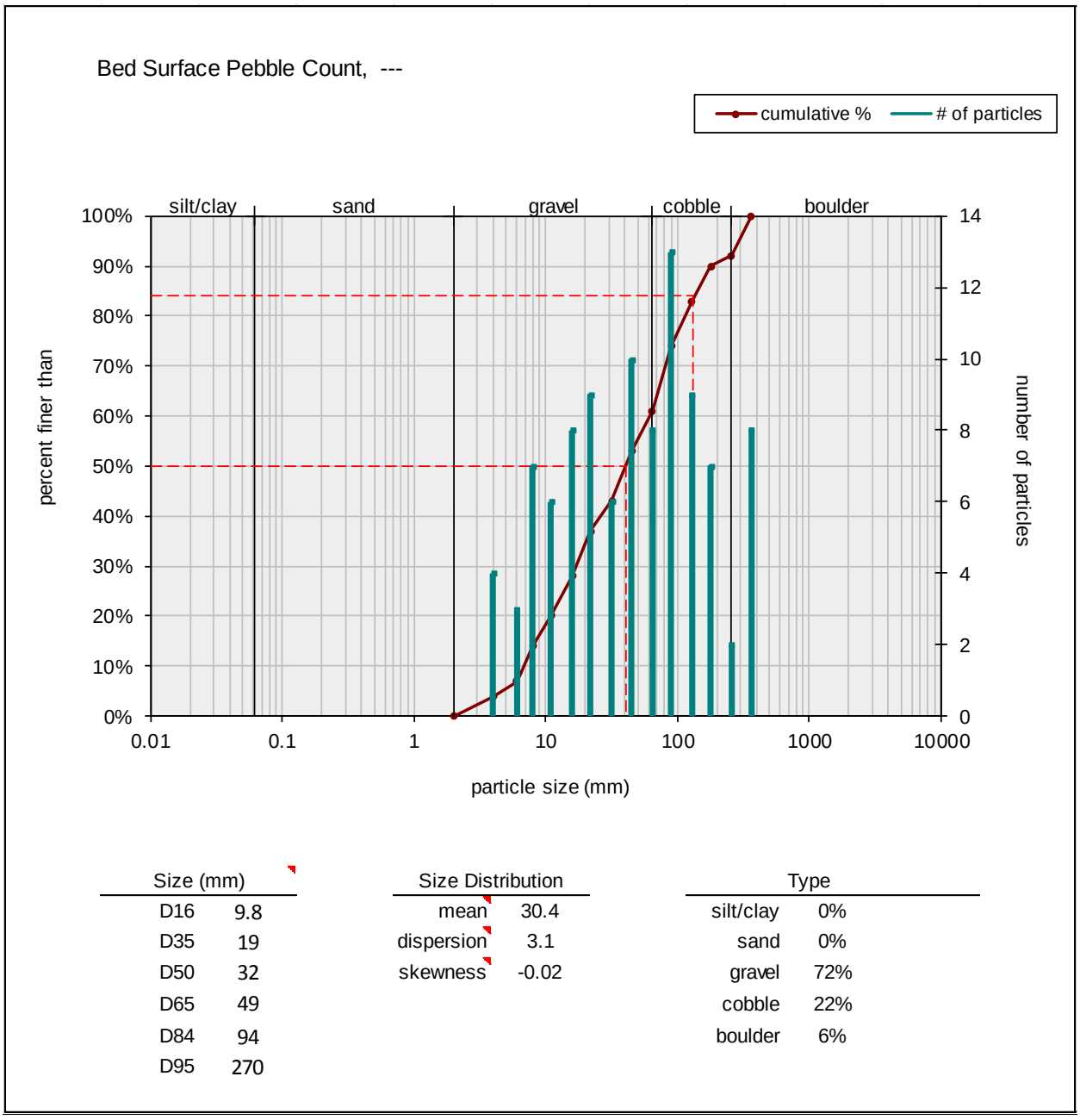

Figure 29. Grain size distribution plot for SL3000 deployment 1 pre-storm on 7/18/2011

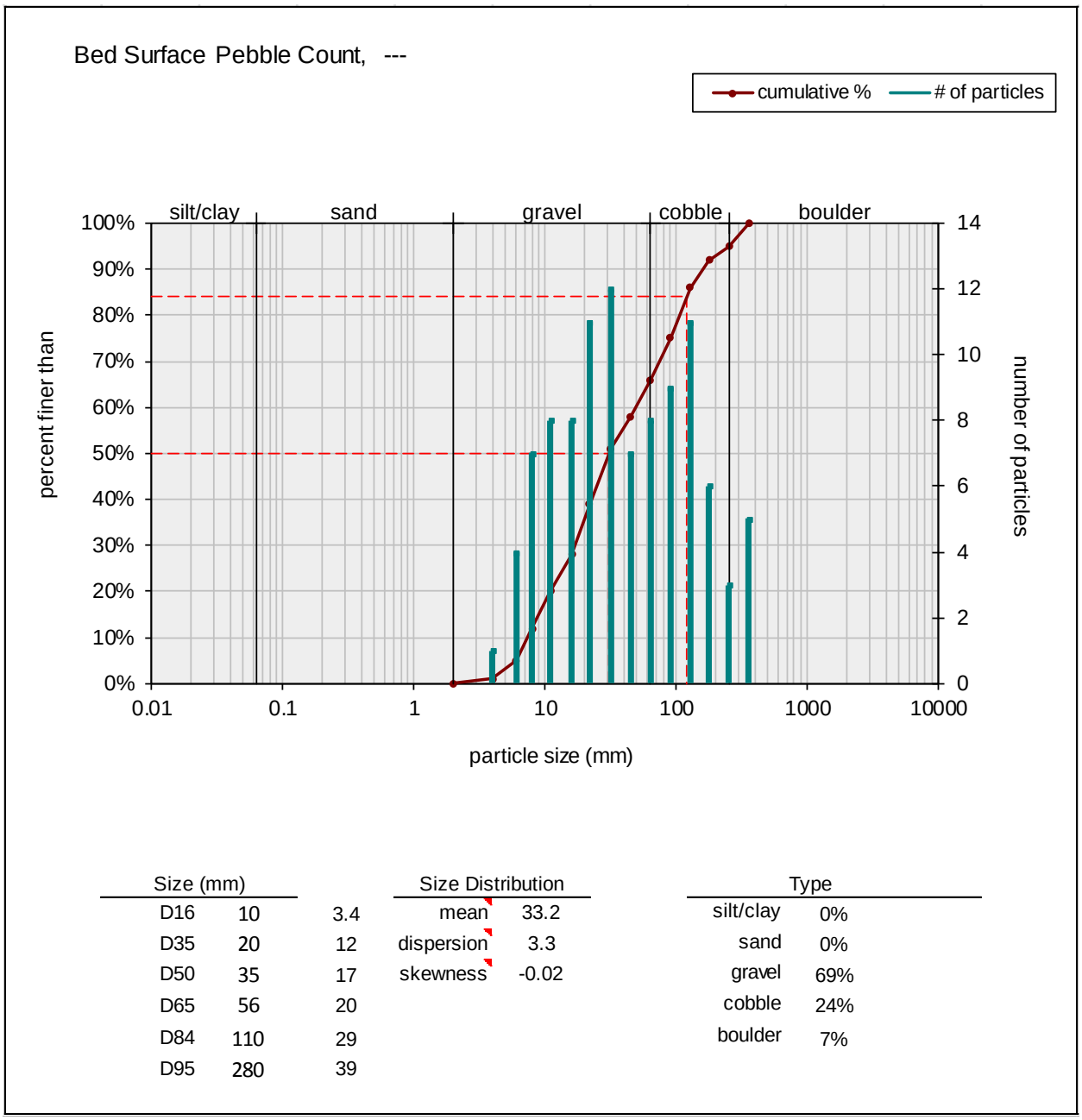

Figure 30. Grain size distribution plot for SL3000 deployment 1 post-storm on 7/19/2011

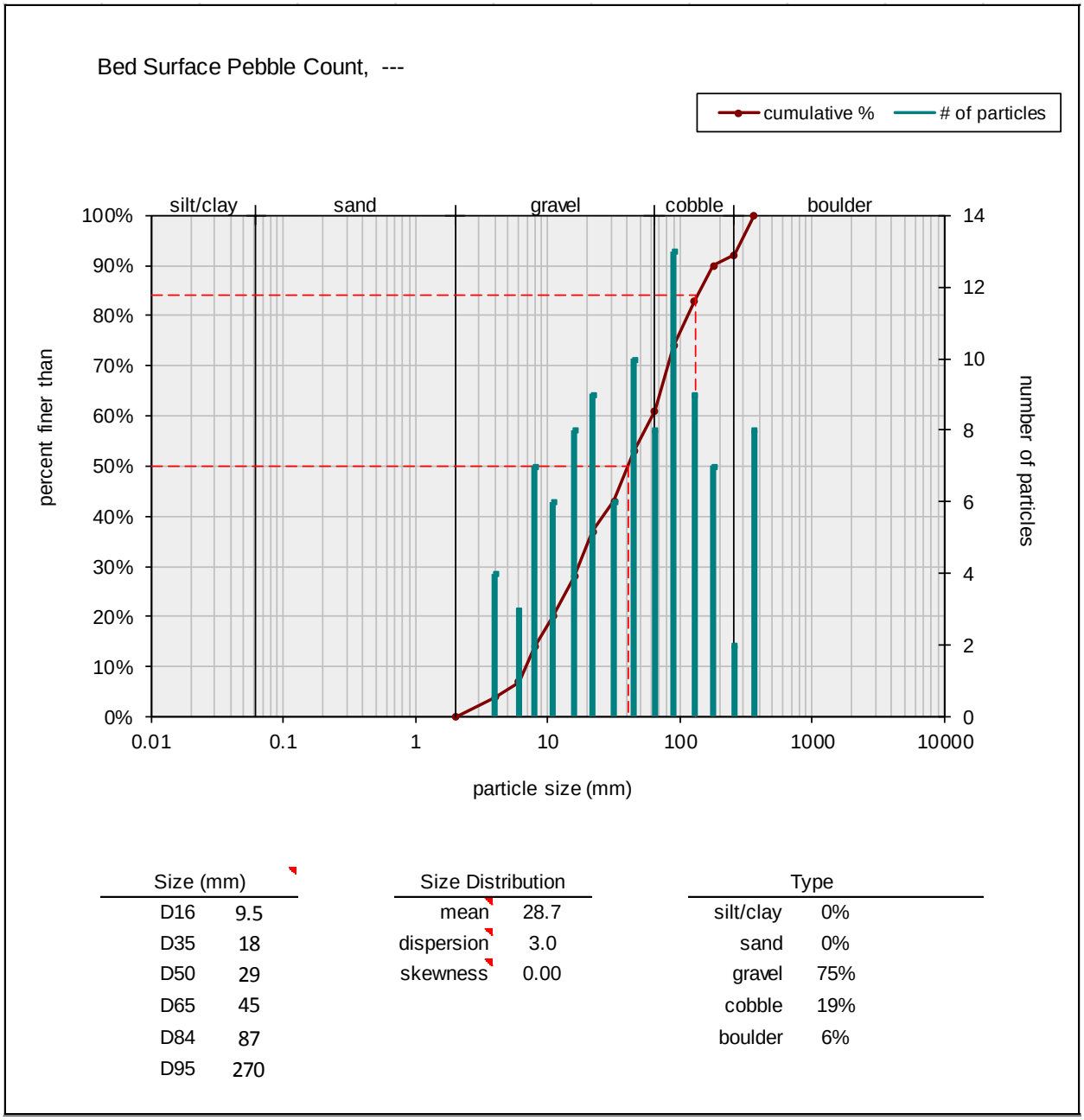

Figure 31. Grain size distribution plot for SL3000 deployment 2 pre-storm on 8/12/2011

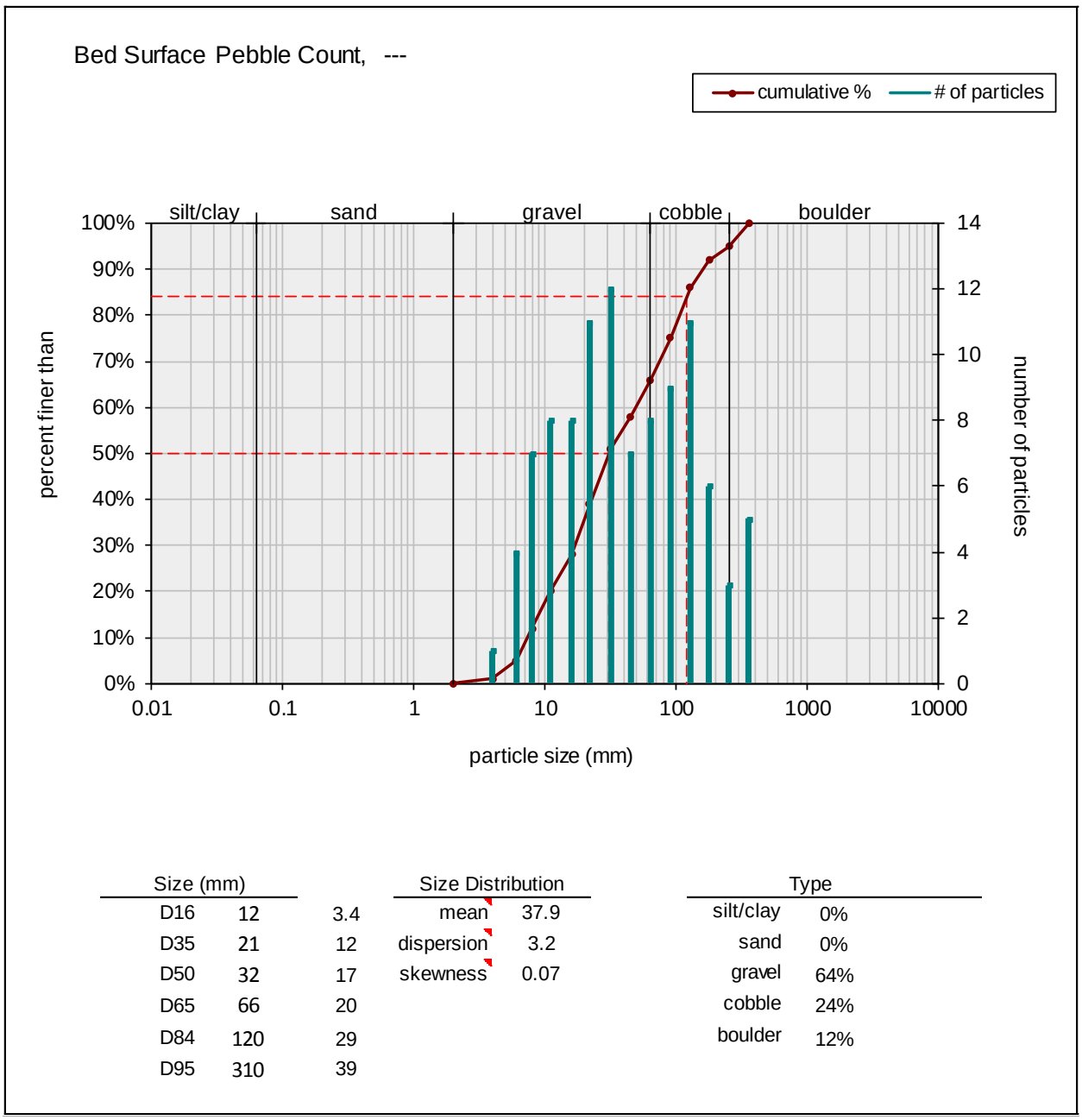

Figure 32. Grain size distribution plot for SL3000 deployment 2 post-storm on 8/16/2011

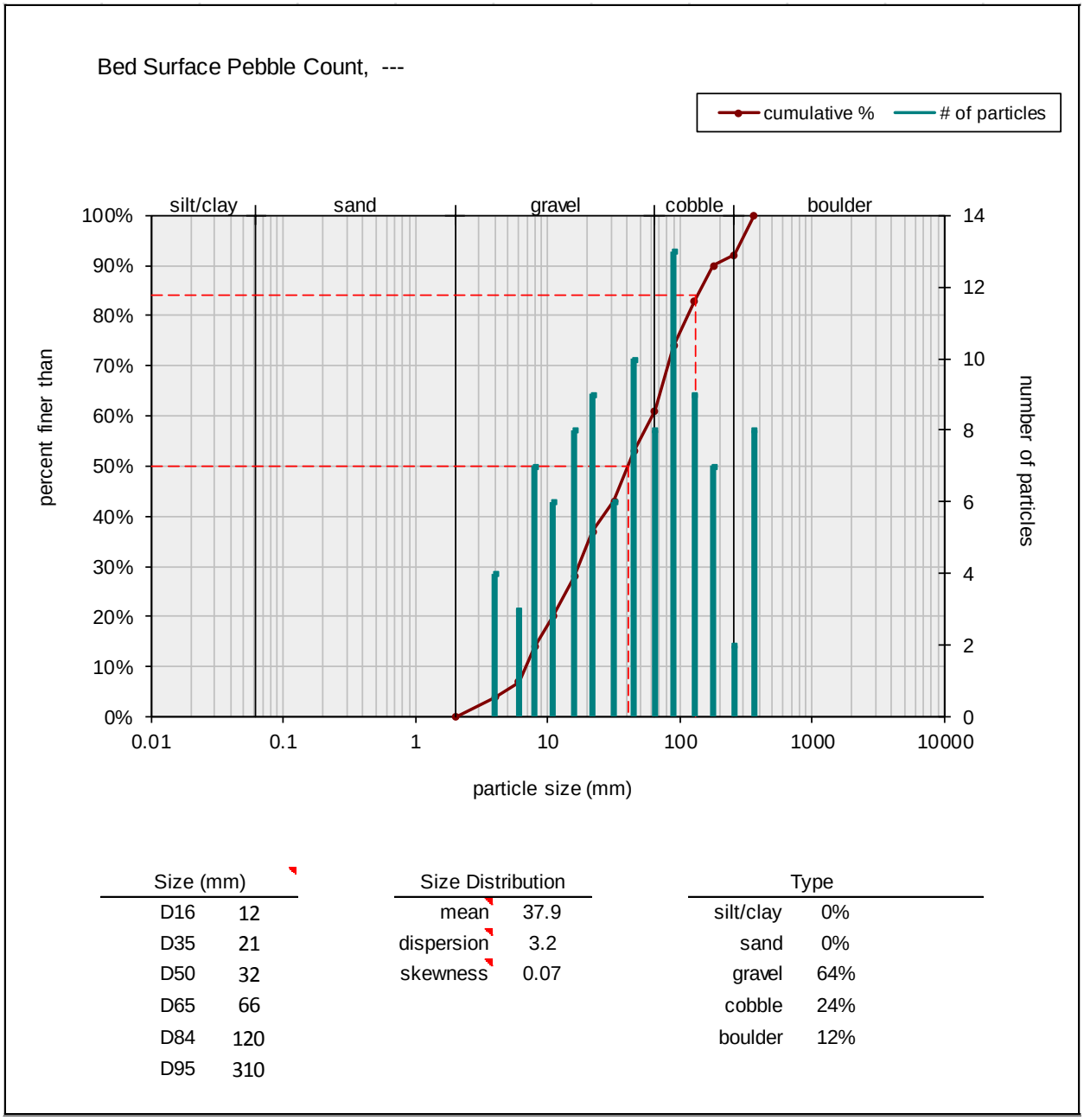

Figure 33. Grain size distribution plot for SL3000 deployment 3 pre-storm on 8/17/2011

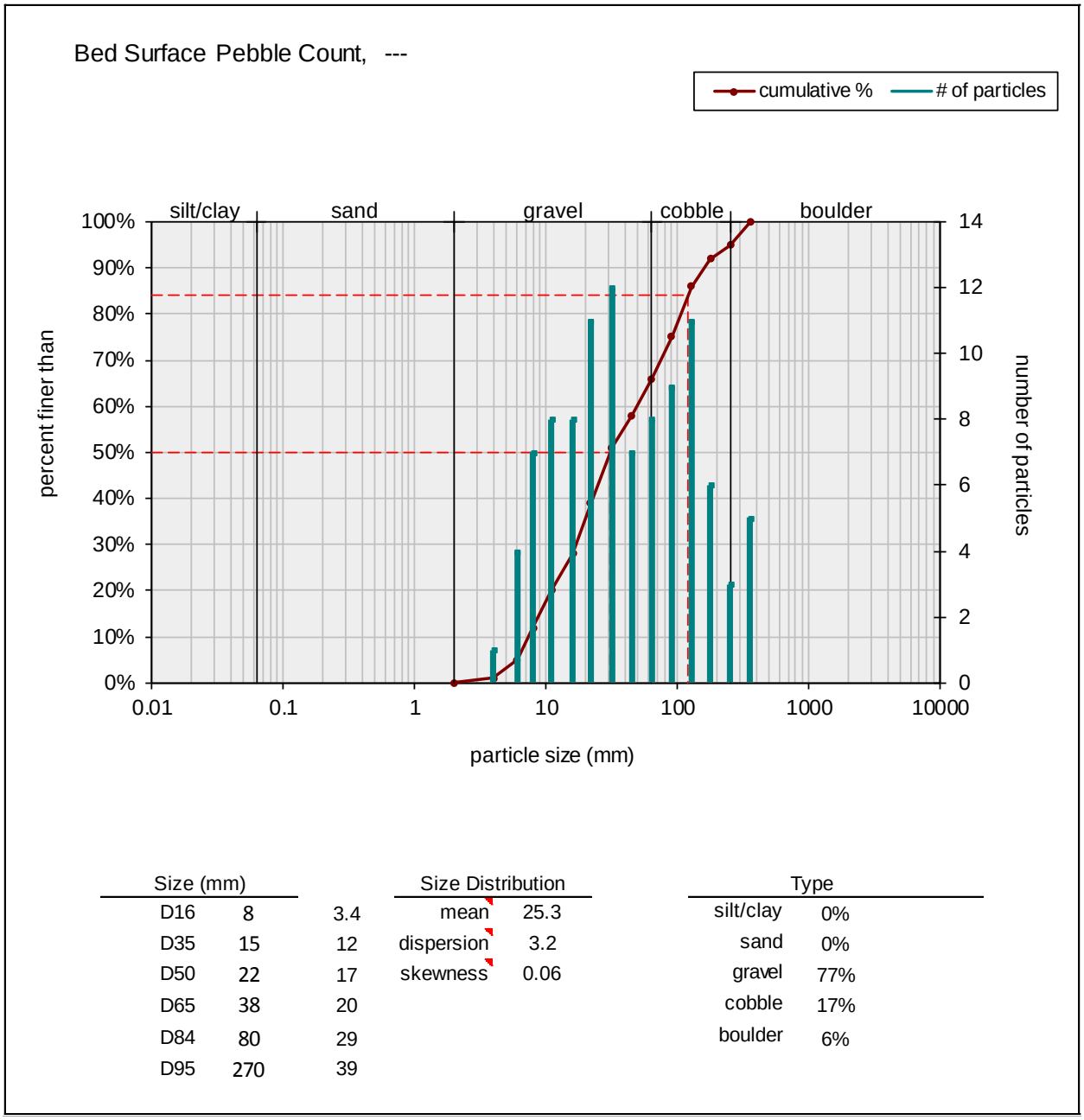

Figure 34. Grain size distribution plot for SL3000 deployment 3 post-storm on 8/22/2011

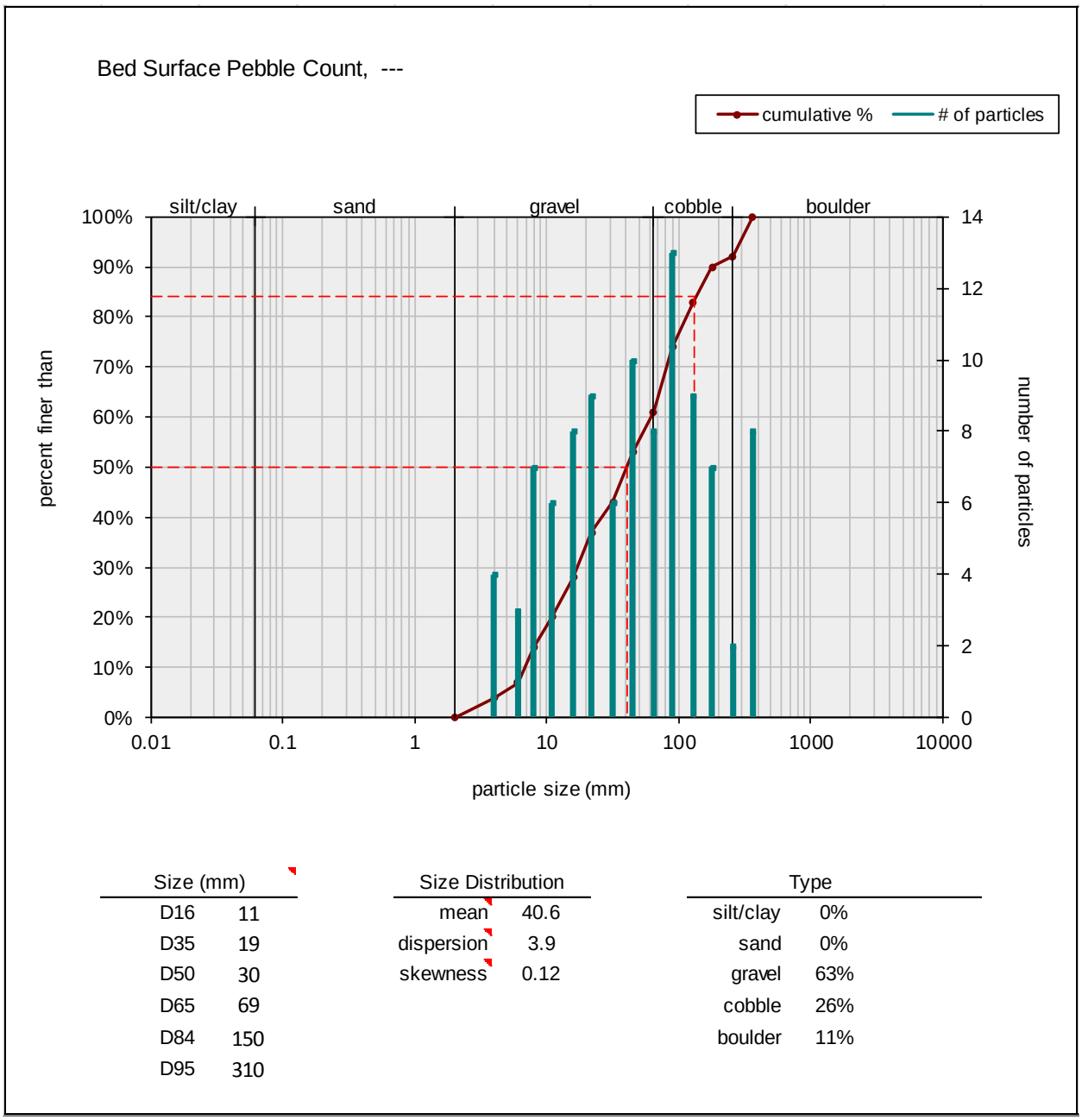

Figure 35. Grain size distribution plot for ADV deployment 1 pre-storm on 9/14/2011

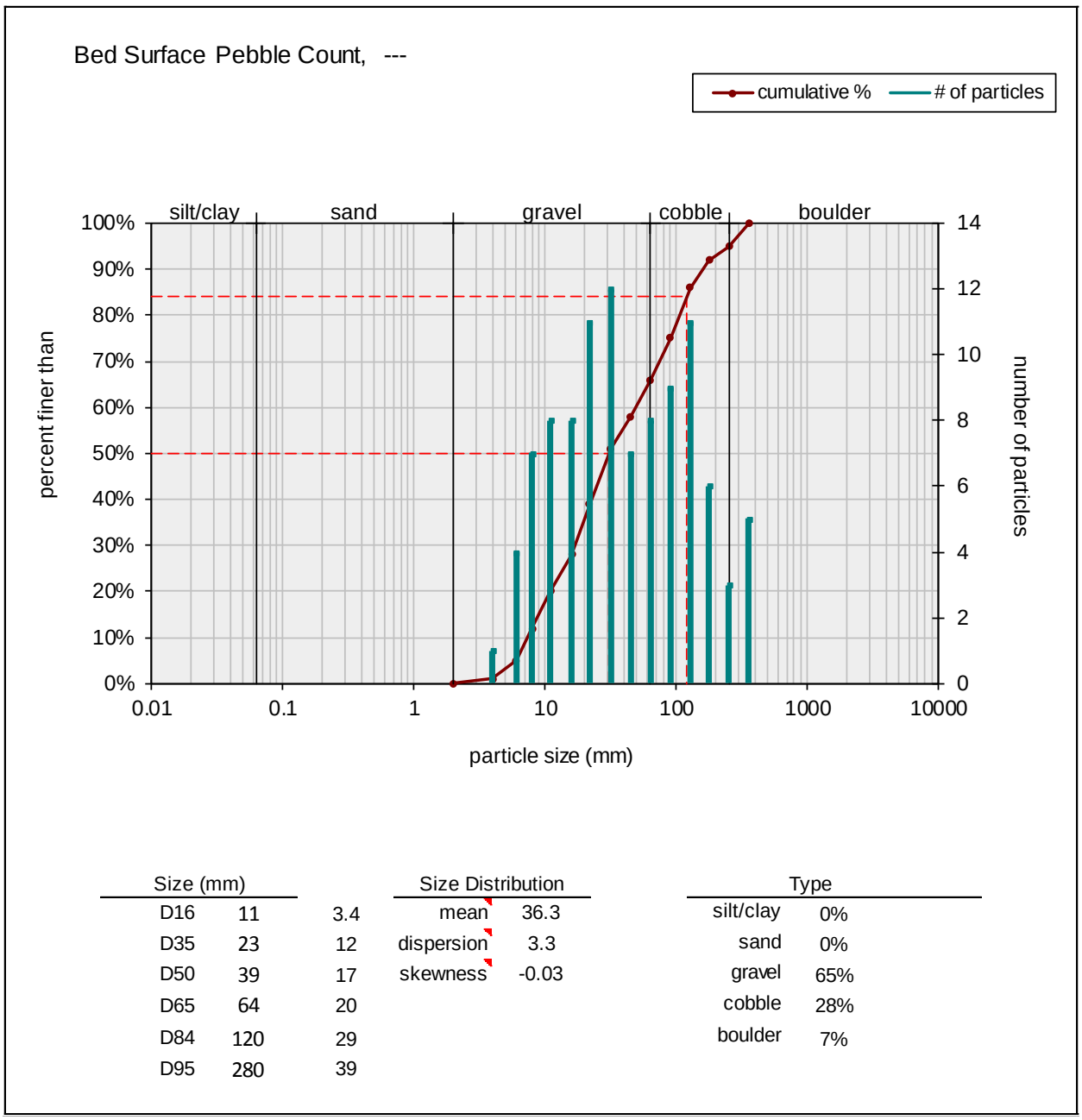

Figure 36. Grain size distribution plot for ADV deployment 1 post-storm on 9/15/2011

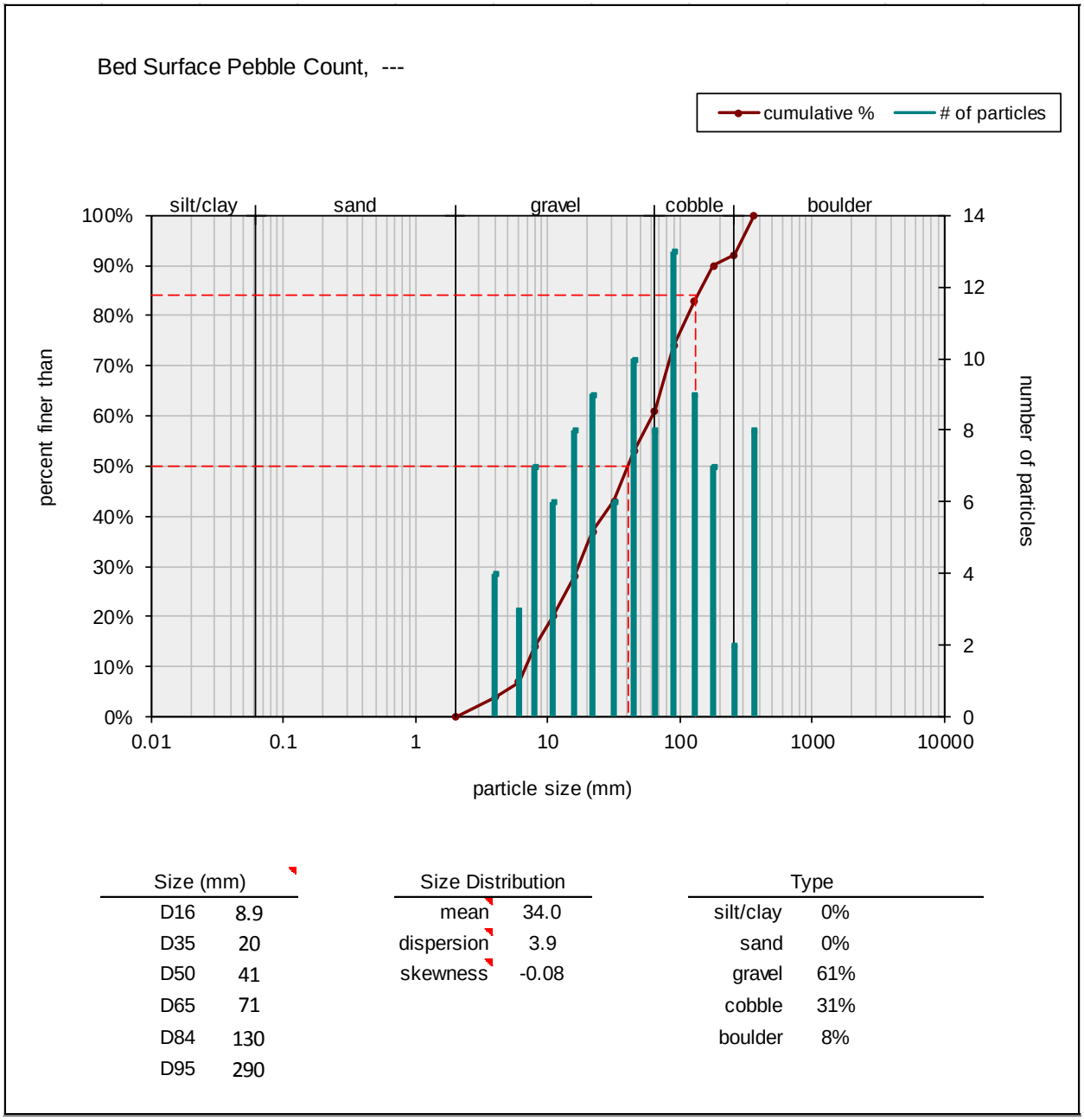

Figure 37. Grain size distribution plot for ADV deployment 2 pre-storm on 10/11/2011

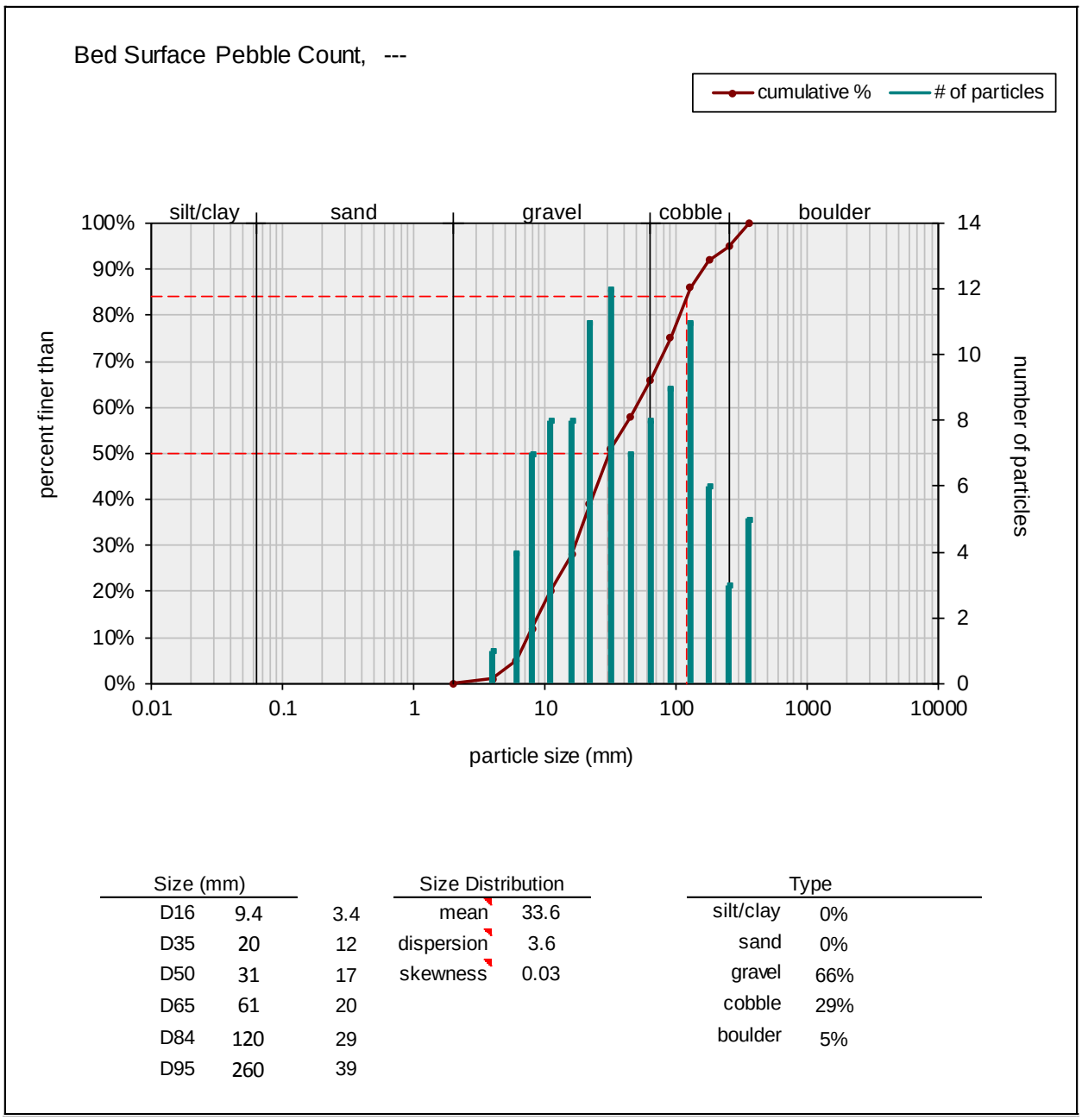

Figure 38. Grain size distribution plot for ADV deployment 2 post-storm on 10/13/2011

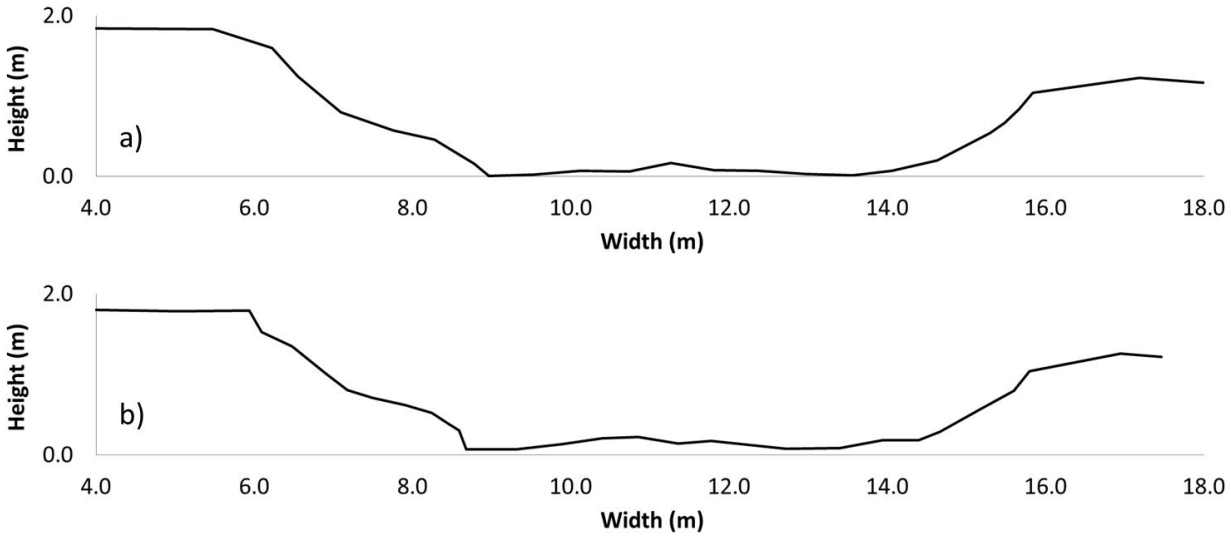

Figure 39. a) West Run experimental cross-section profile SL3000 deployment 1 pre-storm; b) West Run experimental cross-section profile SL3000 deployment 1 post-storm

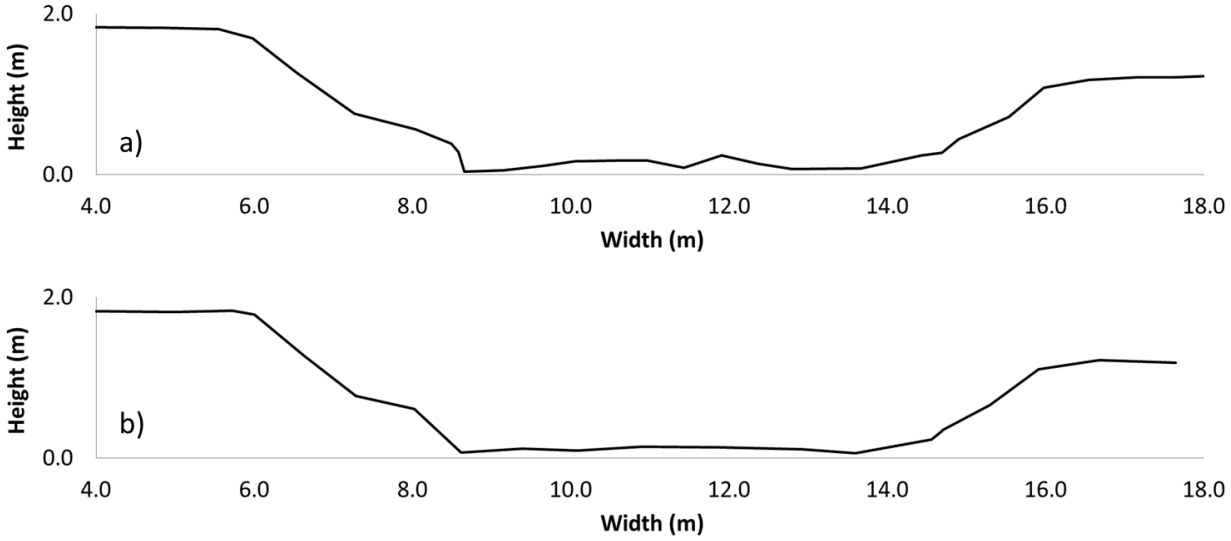

Figure 40. a) West Run experimental cross-section profile SL3000 deployment 2 pre-storm; b) West Run experimental cross-section profile SL3000 deployment 2 post-storm

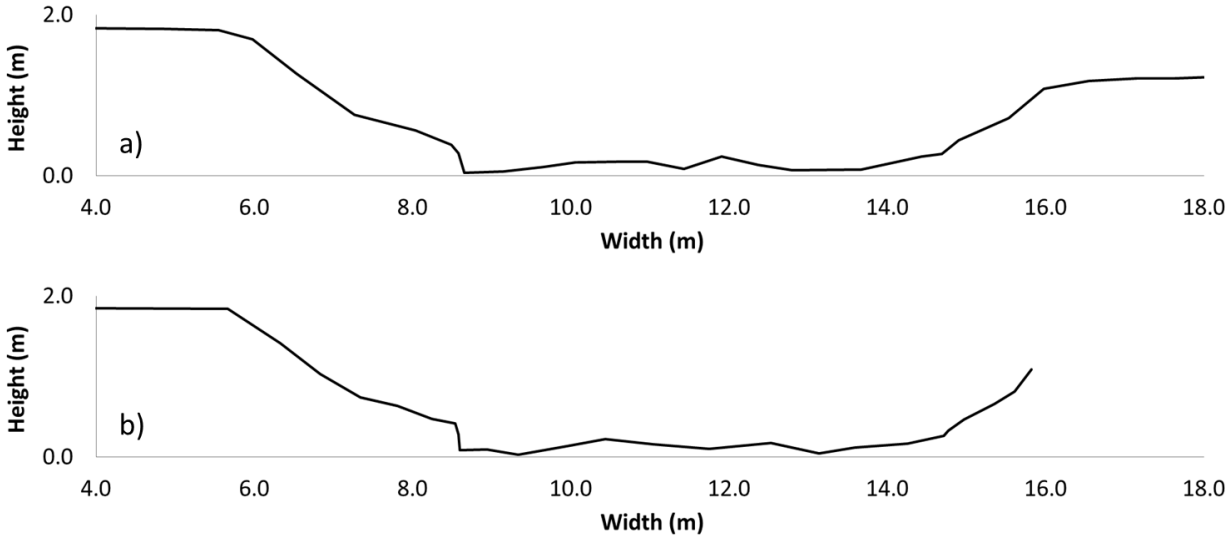

Figure 41. a) West Run experimental cross-section profile SL3000 deployment 3 pre-storm; b) West Run experimental cross-section profile SL3000 deployment 3 post-storm

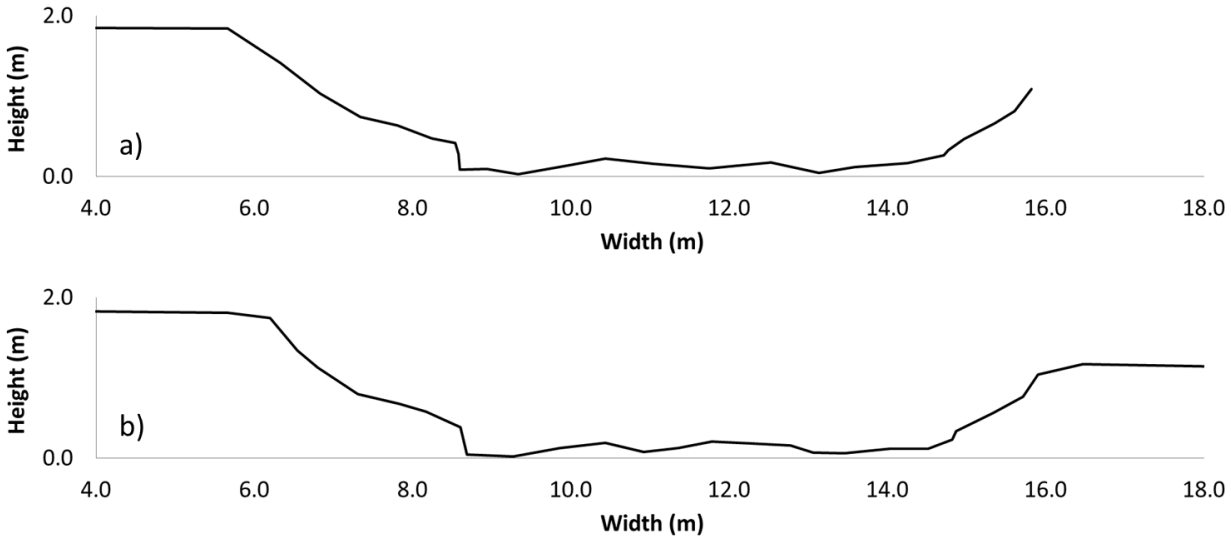

Figure 42. a) West Run experimental cross-section profile ADV deployment 1 pre-storm; b) West Run experimental cross-section profile ADV deployment 1 post-storm

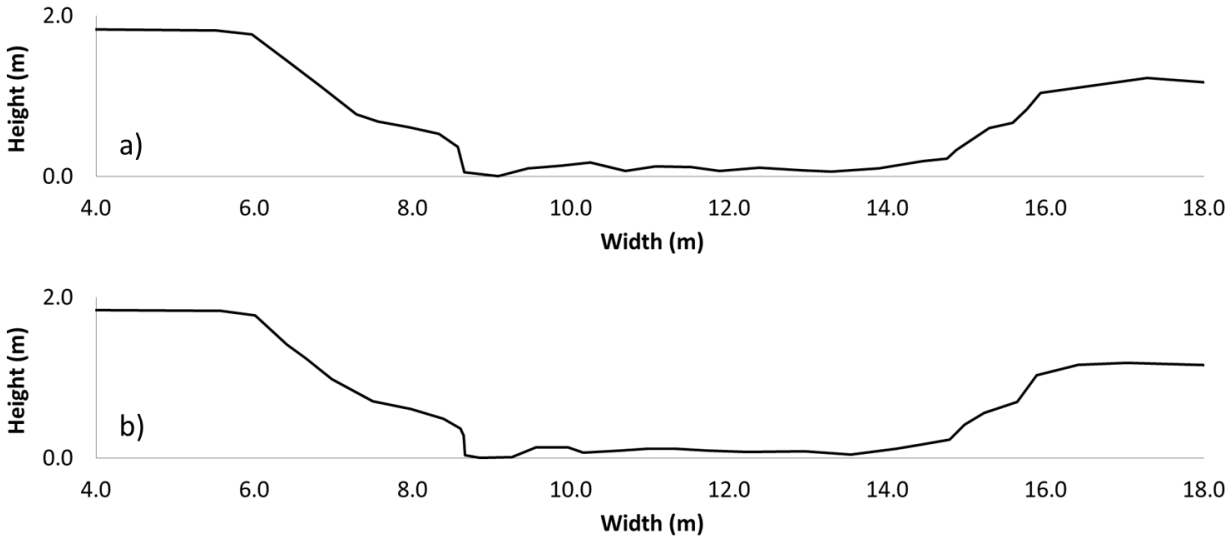

Figure 43. a) West Run experimental cross-section profile ADV deployment 2 pre-storm; b) West Run experimental cross-section profile ADV deployment 2 post-storm

Appendix D: Sontek 16-Mhz ADV Velocity Data

Sample	Time (min)	τ_{uv} (Pa)	τ_{uw} (Pa)	τ_{vw} (Pa)	RMS_u (cm/s)	RMS_v (cm/s)	RMS_w (cm/s)	TKE (N/m^2)	$\bar{u}$ (cm/s)	$\bar{v}$ (cm/s)	$\bar{w}$ (cm/s)	Stage (m)
10	0	1.05	0.04	0.08	6.3	4.5	4.5	4.0	4.4	0.0	-1.0	0.46
11	7	0.79	0.58	0.34	6.6	5.1	5.5	4.9	3.9	-0.2	-1.1	0.46
12	14	0.64	0.65	0.41	5.1	5.1	5.1	3.9	3.5	0.3	-1.0	0.46
13	21	0.31	0.41	0.28	5.5	4.6	4.9	3.8	3.0	0.1	-0.7	0.46
14	28	0.29	-0.01	0.35	4.8	4.5	4.3	3.1	2.4	-0.1	-1.1	0.46
15	35	0.82	-0.02	0.33	6.4	5.4	5.6	5.1	4.9	-0.8	-1.0	0.46
16	42	0.67	0.14	0.35	5.4	4.8	4.4	3.6	4.0	0.2	-1.3	0.46
17	49	0.71	0.59	0.20	6.2	5.1	5.3	4.6	4.8	-1.3	-1.0	0.46
18	56	0.55	0.24	0.09	5.3	4.4	4.8	3.6	3.4	0.5	-0.8	0.46
19	63	0.38	0.41	0.21	6.3	4.5	5.2	4.3	4.2	-0.3	-1.2	0.46
20	70	0.58	-0.18	0.37	5.7	4.9	5.1	4.1	3.5	-0.2	-1.5	0.46
21	77	0.60	0.01	0.17	5.5	4.9	5.2	4.1	4.0	-0.8	-0.3	0.46
22	84	0.45	-0.06	-0.06	4.7	4.3	4.7	3.2	3.3	-0.9	0.3	0.45
23	91	0.57	-0.03	0.11	5.2	4.6	5.0	3.7	4.1	-2.0	0.7	0.45
24	98	0.72	0.02	0.12	5.7	5.0	5.5	4.4	4.0	-1.5	-0.6	0.45
25	105	0.72	0.39	0.12	5.7	5.0	4.9	4.1	3.8	-1.4	-0.2	0.45
26	112	0.88	0.05	0.36	6.0	4.9	5.4	4.4	4.7	-1.7	-0.3	0.45
27	119	0.72	0.16	0.02	5.3	4.7	5.1	3.8	4.2	-1.5	-0.3	0.45
28	126	0.42	0.39	0.14	5.9	4.7	5.0	4.1	3.3	-0.2	-1.0	0.45
29	133	0.51	-0.10	0.15	6.5	5.2	5.5	4.9	4.8	-1.8	-0.3	0.45
30	140	0.62	-0.02	0.33	5.2	4.7	4.7	3.6	2.7	-0.9	-0.4	0.45
31	147	0.83	-0.14	0.46	5.6	5.2	5.1	4.2	3.3	-0.6	-1.1	0.45
32	154	0.55	0.18	-0.08	5.8	5.1	4.7	4.1	4.7	-1.1	-0.9	0.45
33	161	0.27	0.30	-0.05	5.6	4.8	5.3	4.1	4.3	-1.1	-0.5	0.45
34	168	0.86	0.49	-0.25	5.8	5.0	5.3	4.3	5.1	-1.3	0.1	0.45
35	175	0.78	0.00	0.06	5.0	4.4	4.6	3.3	3.9	-0.2	-1.1	0.45
36	182	1.31	-0.40	0.42	6.5	5.5	5.4	5.0	4.1	-1.4	0.0	0.45
37	189	0.49	0.40	0.26	5.7	4.5	5.0	3.9	4.6	-1.0	-0.5	0.45
38	196	1.06	0.09	0.05	6.0	5.3	5.2	4.6	5.0	-1.2	-0.2	0.45
39	203	0.70	-0.26	-0.01	5.9	5.2	5.0	4.4	4.1	-1.7	-0.5	0.44
40	210	0.56	0.17	0.10	5.2	4.4	4.2	3.2	2.5	-0.1	0.0	0.44
41	217	0.51	0.28	0.24	5.8	4.9	4.6	4.0	4.2	-0.3	-0.7	0.44
42	224	1.12	0.12	0.44	6.5	5.7	5.2	5.1	4.5	-1.4	-0.8	0.44
43	231	0.82	0.06	0.04	5.9	5.0	5.3	4.4	3.2	-0.5	-0.6	0.44
44	238	0.67	-0.32	0.08	5.5	5.1	5.0	4.1	3.5	-1.8	0.3	0.45
45	245	0.80	-0.37	0.11	5.6	4.7	4.5	3.7	3.4	-0.7	0.2	0.45

Sample	Time (min)	τ_{uv} (Pa)	τ_{uw} (Pa)	τ_{vw} (Pa)	RMS_u (cm/s)	RMS_v (cm/s)	RMS_w (cm/s)	TKE (N/m^2)	$\bar{u}$ (cm/s)	$\bar{v}$ (cm/s)	$\bar{w}$ (cm/s)	Stage (m)
46	252	1.15	-0.40	0.06	6.3	5.4	5.1	4.7	3.6	-0.3	0.2	0.45
47	259	1.21	-0.73	-0.20	6.6	5.0	5.9	5.1	5.1	-0.8	-0.6	0.45
48	266	0.79	-1.01	0.43	5.8	4.6	4.9	4.0	4.9	-0.3	-0.2	0.46
49	273	0.31	-0.69	-0.06	5.6	4.1	4.4	3.4	5.5	-0.6	0.6	0.46
50	280	1.01	-0.56	0.20	6.3	4.6	4.6	4.1	6.2	-0.6	1.2	0.46
51	287	0.34	-0.43	0.09	5.3	4.0	4.0	3.0	6.2	-1.0	1.1	0.46
52	294	0.36	-1.05	-0.06	5.8	4.1	4.4	3.5	5.6	-0.1	1.1	0.46
53	301	0.53	-0.73	0.17	5.8	4.1	4.3	3.4	6.1	-0.6	0.7	0.46
54	308	0.52	-0.63	-0.15	6.2	4.3	4.2	3.7	5.7	-1.2	0.6	0.46
55	315	0.87	-0.86	0.08	6.6	5.0	5.2	4.8	5.8	-1.1	0.5	0.46
56	322	0.68	-0.95	0.01	6.7	4.5	4.5	4.3	6.3	-0.3	0.5	0.46
57	329	1.01	-0.48	0.05	6.4	5.1	4.6	4.4	5.1	-0.7	0.0	0.45
58	336	1.07	-0.44	0.06	6.6	5.4	4.9	4.8	6.8	-0.8	0.5	0.45
59	343	0.87	-0.63	-0.23	6.7	5.3	5.4	5.1	5.7	0.0	-0.1	0.45
60	350	1.41	-0.70	0.18	7.2	6.0	5.3	5.8	8.2	-1.1	0.7	0.45
61	357	1.23	-0.84	-0.25	7.2	5.5	5.0	5.3	7.4	-1.2	0.5	0.45
62	364	0.52	-0.53	0.01	5.9	4.4	4.1	3.6	5.9	0.3	0.6	0.45
63	371	0.70	-0.51	0.22	5.8	4.8	4.3	3.7	6.7	-0.6	0.9	0.46
64	378	0.52	-0.33	0.18	5.5	4.6	5.5	4.1	5.1	-1.4	0.3	0.48
65	385	0.71	-0.80	0.30	5.8	5.2	5.5	4.6	4.5	-2.4	-0.6	0.49
66	392	1.82	-0.72	0.48	7.8	6.0	6.7	7.1	5.9	-2.4	0.2	0.49
67	399	0.62	0.09	0.07	6.6	6.1	6.6	6.2	5.3	-2.7	-1.1	0.49
68	406	0.45	-0.46	0.37	5.8	5.6	5.6	4.9	5.2	-1.7	-0.4	0.49
69	413	0.37	0.00	0.13	5.5	5.2	6.2	4.8	5.3	-3.4	0.8	0.49
70	420	0.39	-0.23	-0.10	5.7	5.6	6.3	5.1	4.2	-2.6	-1.0	0.48
71	427	0.65	-0.53	0.82	6.6	6.0	6.4	6.0	4.1	-3.0	-1.1	0.48
72	434	0.47	-0.17	0.01	6.3	5.4	5.8	5.1	4.7	-2.3	-0.8	0.48
73	441	0.83	-0.44	0.20	6.3	5.0	6.1	5.1	4.8	-3.0	-0.7	0.48
74	448	0.51	-0.28	0.07	6.8	5.9	7.0	6.6	5.9	-3.7	-0.1	0.48
75	455	0.67	-0.54	0.10	6.8	5.6	6.0	5.7	5.6	-3.1	-0.7	0.48
76	462	1.00	-0.61	0.63	6.4	5.8	6.4	5.8	6.4	-3.3	-0.2	0.49
77	469	0.72	-0.20	0.08	6.1	5.3	5.9	5.0	5.1	-4.1	0.2	0.50
78	476	0.56	-0.18	0.19	6.5	5.4	6.4	5.6	5.1	-3.9	-0.2	0.50
79	483	0.79	-0.35	0.10	6.1	5.8	5.6	5.1	5.6	-3.5	0.7	0.50
80	490	1.04	0.21	-0.12	6.8	5.3	5.9	5.4	6.4	-3.4	0.1	0.50
81	497	0.44	0.32	0.18	6.7	6.0	6.1	5.9	5.9	-3.3	0.2	0.50
82	504	0.74	-0.39	0.58	7.4	6.0	6.5	6.6	7.1	-3.8	1.4	0.50
83	511	0.83	-0.16	0.66	7.8	6.6	7.1	7.7	7.6	-4.3	0.4	0.50
84	518	1.00	-0.18	0.61	7.3	6.2	6.3	6.5	6.5	-3.5	-0.6	0.50
85	525	0.27	-0.56	0.56	6.4	5.3	6.1	5.3	6.2	-3.5	0.5	0.50
86	532	0.73	-0.09	0.84	7.0	5.8	6.1	6.0	6.0	-3.1	-0.3	0.50

Sample	Time (min)	τ_{uv} (Pa)	τ_{uw} (Pa)	τ_{vw} (Pa)	RMS_u (cm/s)	RMS_v (cm/s)	RMS_w (cm/s)	TKE (N/m^2)	$\bar{u}$ (cm/s)	$\bar{v}$ (cm/s)	$\bar{w}$ (cm/s)	Stage (m)
87	539	1.17	-0.01	0.01	7.2	6.3	6.8	6.9	8.1	-5.0	1.1	0.50
88	546	0.49	-0.39	0.15	5.9	5.1	5.7	4.7	6.7	-4.1	0.7	0.50
89	553	0.59	-0.24	0.56	6.1	5.6	5.9	5.2	4.7	-3.2	-0.2	0.50
90	560	0.83	0.02	0.38	6.6	5.6	6.2	5.7	5.2	-2.6	-0.6	0.50
91	567	1.04	-0.16	-0.03	7.4	5.9	6.4	6.5	5.8	-2.6	0.2	0.50
92	574	1.04	-0.16	0.12	6.4	6.1	6.6	6.1	5.1	-2.6	0.2	0.50
93	581	0.99	-0.61	0.70	6.6	5.5	5.7	5.3	5.6	-3.2	0.6	0.50
94	588	0.30	-0.37	0.50	6.5	5.2	6.2	5.4	6.2	-3.2	1.6	0.50
95	595	1.01	-0.34	0.65	7.2	6.5	6.8	7.0	5.7	-2.8	1.2	0.50
96	602	0.22	-0.21	0.17	6.6	5.8	6.6	6.0	4.8	-3.7	0.1	0.50
97	609	0.60	-0.55	-0.09	6.4	5.6	5.4	5.1	5.8	-2.9	1.4	0.49
98	616	0.68	-0.52	0.56	6.8	6.8	6.9	7.0	5.5	-3.5	0.2	0.50
99	623	0.65	-0.31	0.59	6.8	6.3	7.2	6.9	6.1	-3.4	0.0	0.50
100	630	0.68	-0.40	1.30	7.3	6.6	7.1	7.3	6.9	-4.7	-0.1	0.50
101	637	1.04	0.39	0.27	7.3	6.5	7.6	7.7	6.7	-4.6	0.7	0.50
102	644	1.15	0.22	0.32	7.6	6.3	6.8	7.1	7.4	-3.5	0.8	0.50
103	651	0.64	-0.31	0.62	6.2	5.4	6.6	5.6	7.2	-3.8	1.4	0.51
104	658	1.23	-0.58	0.77	7.0	6.1	6.3	6.3	7.1	-3.7	0.7	0.51
105	665	0.94	0.09	0.65	7.0	6.1	6.7	6.5	7.1	-4.3	-0.2	0.52
106	672	1.00	-0.12	0.47	6.7	5.8	5.5	5.4	5.9	-3.1	1.0	0.52
107	679	0.88	-0.47	0.62	6.4	5.5	5.7	5.2	6.9	-4.0	0.1	0.52
108	686	0.77	-0.40	0.47	6.1	5.1	5.1	4.5	6.2	-3.7	0.4	0.52
109	693	1.14	-0.47	0.67	6.2	5.6	6.0	5.3	7.7	-4.2	0.4	0.52
110	700	1.05	0.25	0.30	6.4	5.8	5.9	5.5	8.6	-5.1	-0.2	0.52
111	707	0.97	-0.53	0.63	7.3	6.6	6.1	6.7	7.6	-4.3	1.4	0.51
112	714	0.82	0.16	0.68	6.6	6.3	6.1	6.1	5.7	-4.2	0.7	0.51
113	721	0.54	-0.23	0.46	6.2	5.2	5.9	5.0	4.8	-2.0	-0.7	0.50
114	728	0.73	-0.22	0.63	6.5	6.2	6.3	6.1	5.4	-3.0	0.7	0.50
115	735	0.53	-0.08	-0.01	6.6	5.1	6.1	5.3	5.7	-3.6	0.2	0.50
116	742	0.42	-0.73	0.61	6.6	5.4	6.2	5.5	6.8	-4.8	0.7	0.51
117	749	1.03	-0.49	0.64	6.4	5.4	5.2	4.9	6.9	-3.4	0.2	0.51
118	756	0.63	-0.33	0.54	5.8	5.1	6.3	5.0	5.9	-3.2	-0.2	0.51
119	763	0.40	0.02	-0.07	6.3	5.5	5.7	5.2	6.7	-4.1	0.0	0.51
120	770	1.15	-0.60	0.41	6.8	5.5	5.7	5.5	6.7	-2.9	0.1	0.51
121	777	0.67	-0.05	0.28	7.9	5.6	6.1	6.5	6.5	-3.8	-0.4	0.51
122	784	0.55	-0.22	0.65	7.0	5.9	6.1	6.0	5.8	-4.2	0.8	0.51
123	791	0.66	-0.56	0.33	6.9	6.0	6.2	6.0	6.6	-3.9	0.9	0.50
124	798	0.49	-0.19	0.30	6.9	5.2	6.4	5.8	7.6	-4.9	1.3	0.50
125	805	1.03	-0.49	0.82	6.8	5.5	6.7	6.0	6.4	-4.9	1.6	0.50
126	812	0.40	-0.01	0.54	7.1	5.7	6.3	6.1	7.6	-3.8	0.0	0.50
127	819	0.75	-0.27	0.64	6.6	5.6	6.0	5.6	6.5	-4.3	1.2	0.49

Sample	Time (min)	τ_{uv} (Pa)	τ_{uw} (Pa)	τ_{vw} (Pa)	RMS_u (cm/s)	RMS_v (cm/s)	RMS_w (cm/s)	TKE (N/m^2)	$\bar{u}$ (cm/s)	$\bar{v}$ (cm/s)	$\bar{w}$ (cm/s)	Stage (m)
128	826	0.66	0.04	0.46	6.4	5.5	5.5	5.0	5.4	-2.9	-0.2	0.49
129	833	0.97	-0.25	0.48	6.8	5.5	5.5	5.4	5.6	-3.3	-0.3	0.49
130	840	1.18	0.30	0.72	6.3	6.3	6.7	6.2	7.3	-3.8	0.9	0.49
131	847	0.80	-0.61	0.96	6.7	5.6	6.7	6.1	5.8	-2.4	0.8	0.49
132	854	0.21	-0.60	0.23	6.2	5.1	5.9	5.0	6.0	-3.8	0.5	0.48
133	861	0.38	0.12	0.22	6.5	5.4	6.3	5.6	4.9	-2.8	0.3	0.48
134	868	1.06	-0.53	0.20	6.8	5.7	5.9	5.7	5.9	-2.5	0.4	0.48
135	875	1.05	-0.73	0.66	7.1	5.8	6.3	6.2	7.5	-3.3	0.3	0.48
136	882	1.13	-0.55	0.60	7.1	5.9	6.1	6.1	8.1	-3.7	1.2	0.48
137	889	1.21	-0.07	0.31	7.4	6.1	6.2	6.5	7.2	-3.1	0.9	0.48
138	896	1.88	-0.77	0.60	7.6	6.3	6.6	7.1	7.3	-3.7	0.5	0.48
139	903	1.06	-0.93	1.01	6.9	6.1	6.5	6.3	6.7	-3.7	1.6	0.48
140	910	0.83	-0.88	0.37	6.2	5.2	5.7	4.8	5.5	-2.5	0.5	0.47
141	917	0.60	-0.54	0.62	6.6	5.1	6.3	5.4	6.6	-3.5	0.5	0.47
142	924	0.94	-0.27	0.29	6.5	5.2	6.1	5.3	6.5	-2.5	0.9	0.47
143	931	0.83	-0.21	0.61	6.6	5.4	6.1	5.5	6.2	-3.3	0.5	0.47
144	938	0.59	0.10	0.08	6.6	5.1	5.3	4.9	5.6	-1.9	0.3	0.47
145	945	0.11	-0.40	0.31	5.9	5.2	5.8	4.8	5.1	-2.8	1.0	0.47
146	952	0.93	-0.50	0.64	5.8	5.2	5.2	4.4	5.2	-3.2	0.2	0.46
147	959	0.79	-0.67	0.30	6.2	5.8	5.8	5.3	4.1	-2.2	0.6	0.46
148	966	0.70	0.08	0.35	6.8	5.2	6.3	5.6	6.2	-3.1	0.4	0.46
149	973	0.57	0.05	0.39	5.6	5.0	5.1	4.1	4.1	-2.3	-0.5	0.46
150	980	1.01	-0.29	0.25	6.5	5.0	5.8	5.1	5.2	-2.3	0.4	0.46
151	987	0.94	-0.34	0.77	6.1	5.3	6.1	5.2	4.8	-2.6	0.5	0.46
152	994	0.75	-0.18	0.37	5.9	5.0	5.0	4.3	3.0	-2.2	-0.9	0.45
153	1001	0.57	-0.17	0.17	6.5	5.4	5.5	5.1	6.1	-2.4	0.1	0.45
154	1008	1.18	-0.25	0.89	6.3	6.0	5.9	5.5	4.8	-3.2	0.8	0.45
155	1015	0.15	-0.22	0.48	5.7	4.5	4.8	3.8	3.6	-3.0	0.7	0.45
156	1022	0.46	-0.09	0.74	5.6	4.8	5.2	4.1	3.8	-1.7	-0.4	0.45
157	1029	0.57	-0.52	0.53	6.4	5.1	5.9	5.1	4.6	-2.9	1.2	0.45
158	1036	0.69	-0.14	0.19	5.6	4.8	5.6	4.3	4.1	-2.3	0.1	0.45
159	1043	0.29	-0.02	0.03	5.8	5.1	5.8	4.7	4.0	-1.9	-0.4	0.45
160	1050	0.78	-0.06	0.39	5.5	4.6	5.3	4.0	3.6	-1.5	-0.8	0.45

Appendix E: Sontek SL3000 Velocity Data

Sample	Time (min)	RMS_u (cm/s)	RMS_v (cm/s)	TKE (N/m^2)	$\bar{u}$ (cm/s)	$\bar{v}$ (cm/s)	Stage (m)
1	0	15.6	5.2	13.5	21.4	0.5	NA
2	5	20.8	6.9	24.0	22.9	0.9	NA
3	10	15.6	5.2	13.5	20.9	0.3	NA
4	15	15.6	5.2	13.5	22.6	0.3	NA
5	20	12.1	3.5	8.0	21.1	1.1	NA
6	25	12.1	3.5	8.0	22.0	1.0	NA
7	30	12.1	3.5	8.0	22.5	0.5	NA
8	35	12.1	3.5	8.0	22.3	0.3	NA
9	40	12.1	3.5	8.0	23.0	0.8	NA
10	45	15.6	5.2	13.5	20.5	0.5	NA
11	50	12.1	3.5	8.0	21.8	0.7	NA
12	55	12.1	3.5	8.0	23.5	0.9	NA
13	60	12.1	3.5	8.0	20.9	1.4	NA
14	65	15.6	5.2	13.5	22.9	0.3	NA
15	70	12.1	3.5	8.0	22.9	0.5	NA
16	75	15.6	5.2	13.5	23.3	0.7	NA
17	80	15.6	5.2	13.5	21.9	0.7	NA
18	85	12.1	3.5	8.0	23.6	0.7	NA
19	90	17.3	6.9	17.4	21.4	0.4	NA
20	95	12.1	3.5	8.0	21.1	0.5	NA
21	100	12.1	3.5	8.0	19.9	1.2	NA
22	105	15.6	5.2	13.5	19.7	-0.2	NA
23	110	12.1	3.5	8.0	19.9	0.9	NA
24	115	12.1	3.5	8.0	19.5	0.7	NA
25	120	12.1	3.5	8.0	20.6	0.6	NA
26	125	12.1	3.5	8.0	34.2	-1.3	0.45
27	130	15.6	5.2	13.5	33.9	-1.3	0.47
28	135	12.1	3.5	8.0	39.5	-2.7	0.49
29	140	15.6	5.2	13.5	40.3	-1.1	0.49
30	145	17.3	6.9	17.4	36.8	-0.9	0.52
31	150	12.1	3.5	8.0	24.6	0.5	0.54
32	155	17.3	6.9	17.4	25.6	1.2	0.53
33	160	17.3	6.9	17.4	29.5	0.0	0.52
34	165	17.3	6.9	17.4	31.1	0.2	0.51
35	170	20.8	6.9	24.0	34.3	-0.9	0.51
36	175	19.1	6.9	20.6	31.8	-0.8	0.60
37	180	19.1	6.9	20.6	38.1	-1.9	0.63

Sample	Time (min)	RMS_u (cm/s)	RMS_v (cm/s)	TKE (N/m^2)	$\bar{u}$ (cm/s)	$\bar{v}$ (cm/s)	Stage (m)
38	185	20.8	6.9	24.0	44.4	-2.6	0.65
39	190	20.8	8.7	25.4	50.0	-4.7	0.67
40	195	20.8	8.7	25.4	55.0	-5.3	0.69
41	200	20.8	8.7	25.4	56.0	-4.4	0.69
42	205	20.8	8.7	25.4	61.7	-4.9	0.69
43	210	24.2	8.7	33.2	63.4	-5.1	0.70
44	215	20.8	6.9	24.0	67.7	-5.3	0.71
45	220	20.8	6.9	24.0	68.4	-6.0	0.72
46	225	24.2	8.7	33.2	69.3	-5.9	0.73
47	230	20.8	8.7	25.4	68.2	-6.8	0.73
48	235	24.2	8.7	33.2	68.2	-6.7	0.74
49	240	26.0	10.4	39.2	69.1	-5.1	0.74
50	245	22.5	8.7	29.1	68.1	-6.1	0.74
51	250	20.8	8.7	25.4	67.2	-4.9	0.74
52	255	20.8	8.7	25.4	70.0	-6.0	0.74
53	260	22.5	8.7	29.1	68.4	-5.3	0.74
54	265	20.8	8.7	25.4	69.4	-4.6	0.74
55	270	20.8	6.9	24.0	69.4	-5.6	0.74
56	275	20.8	6.9	24.0	66.8	-3.7	0.74
57	280	22.5	8.7	29.1	67.6	-5.2	0.74
58	285	22.5	8.7	29.1	64.4	-4.4	0.74
59	290	20.8	8.7	25.4	67.8	-5.2	0.74
60	295	19.1	6.9	20.6	68.5	-4.4	0.74
61	300	20.8	6.9	24.0	67.0	-5.6	0.74
62	305	20.8	6.9	24.0	69.2	-5.5	0.74
63	310	20.8	8.7	25.4	67.6	-4.5	0.73
64	315	20.8	8.7	25.4	63.0	-5.0	0.72
65	320	20.8	6.9	24.0	60.8	-3.8	0.71
66	325	19.1	6.9	20.6	57.2	-3.2	0.69
67	330	15.6	5.2	13.5	50.3	-4.4	0.68
68	335	17.3	6.9	17.4	48.9	-1.9	0.67
69	340	15.6	5.2	13.5	44.6	-2.5	0.66
70	345	19.1	6.9	20.6	42.9	-2.5	0.65
71	350	17.3	6.9	17.4	39.6	-1.8	0.64
72	355	17.3	6.9	17.4	39.3	-1.3	0.63
73	360	15.6	5.2	13.5	36.8	-0.9	0.63
74	365	17.3	6.9	17.4	35.4	-0.7	0.62
75	370	20.8	6.9	24.0	33.2	-0.3	0.61
76	375	15.6	5.2	13.5	32.6	-0.4	0.61
77	380	15.6	5.2	13.5	30.1	0.2	0.60
78	385	12.1	3.5	8.0	31.2	0.8	0.60

Sample	Time (min)	RMS_u (cm/s)	RMS_v (cm/s)	TKE (N/m^2)	$\bar{u}$ (cm/s)	$\bar{v}$ (cm/s)	Stage (m)
79	390	17.3	6.9	17.4	29.9	0.2	0.59
80	395	17.3	6.9	17.4	28.4	0.4	0.59
81	400	17.3	6.9	17.4	26.1	0.4	0.58
82	405	17.3	6.9	17.4	25.9	0.4	0.58
83	410	15.6	5.2	13.5	25.0	0.9	0.57
84	415	15.6	5.2	13.5	25.0	0.0	0.57
85	420	17.3	6.9	17.4	23.7	1.8	0.57
86	425	15.6	5.2	13.5	22.5	1.3	0.56
87	430	15.6	5.2	13.5	20.4	1.0	0.56
88	435	17.3	6.9	17.4	20.4	1.1	0.56
89	440	15.6	5.2	13.5	22.2	2.0	0.55
90	445	15.6	5.2	13.5	21.1	2.1	0.55
91	450	17.3	6.9	17.4	20.9	1.1	0.55
92	455	15.6	5.2	13.5	22.6	1.4	0.55
93	460	15.6	5.2	13.5	23.1	1.6	0.55
94	465	15.6	5.2	13.5	19.9	2.0	0.54
95	470	15.6	5.2	13.5	21.4	1.7	0.54
96	475	15.6	5.2	13.5	21.6	2.0	0.54
97	480	12.1	3.5	8.0	22.5	1.7	0.54
98	485	12.1	3.5	8.0	21.4	1.9	0.54
99	490	15.6	5.2	13.5	23.2	1.3	0.53
100	495	15.6	5.2	13.5	23.8	1.5	0.53
101	500	15.6	5.2	13.5	21.8	2.2	0.53